[UCI]I804:24011-200000263541

February, 2013

Thesis for Doctor degree

Isolation and Characterization of New Insulin-mimetic Compounds from Medicinal Plants

Chosun University Graduate School

Department of Pharmacy

Nguyen Phi Hung

Isolation and Characterization of New Insulin-mimetic Compounds from Medicinal Plants

February, 25th, 2013

Chosun University Graduate School

Department of Pharmacy

Nguyen Phi Hung

Isolation and Characterization of New Insulin-mimetic Compounds from Medicinal Plants

지도교수 오원근

이 논문을 약학 박사학위신청 논문으로 제출함

2012 년 10 월

조선대학교 대학원

약학과

응구엔피홍

This thesis is examined and approved for Nguyen Phi Hung's doctor degree

Chairman	Chosun Univ.	Dr. Woo Eun-Rhan	(印)
Member	Seoul Univ.	Dr. Kang Keon Wook	(印)
Member	KRIBB.	Dr. Lee Chul Ho	(印)
Member	Chosun Univ.	Dr. Oh Won Keun	(印)
Member	Chosun Univ.	Dr. Choi Hong Seok	(印)

December 2012

Chosun University Graduate School

CONTENTS

LIST OF SCHEMES

LIST OF TABLES

LIST OF FIGURES

LIST OF ABBREVIATIONS

$[\alpha]_D^{25}$: specific rotation measured by D line of sodium (589 nm) at temperature ^oC

IR: infrared spectroscopy spectrum

UV: ultraviolet absorption spectrum

CD: circular dichroism

NMR: Nuclear Magnetic Resonance

ppm: parts per min

^{1}H NMR: Proton Nuclear Magnetic Resonance spectroscopy

^{13}C NMR: Carbon Nuclear Magnetic Resonance spectroscopy

DEPT: Distortionless Enhancement by Polarization Transfer

COSY: Correlation Spectroscopy (good for determining basic connectivity via J-couplings through-bond)

TOCSY: Total Correlation Spectroscopy, same as COSY, but also able to generate cross peaks via intermediate spins (mix). Uses a spin lock that produces rf heating of the sample and hence requires many steady state scans (ds).

ROESY: Rotational Overhauser Effect SpectroscopY, same as NOESY, but works for all molecular weights. Has the disadvantage of producing more rf heating, hence it requires more steady state scans.

HMQC: Heteronuclear Multiple Quantum Correlation, allows one to pair NH or CH resonances. Often uses X-nucleus decoupling and hence gives rise to rf heating, requires reasonably well calibrated pulses and many steady state scans.

HSQC: Heteronuclear Single Quantum Correlation, provides the same information as HMQC, but gives narrower resonances for ^{1}H-^{13}C correlations. Also requires X-decoupling and hence a large number of steady state scans and is also more sensitive to pulse imperfections.

HMBC: Heteronuclear Multiple Bond Correlation, a variant of the HMQC pulse sequence that allows one to correlate X-nucleus shifts that are typical 2-4 bonds away from a proton.

NOESY: Nuclear Overhauser Effect SpectroscopY, allows one to see through-space effects, useful for investigating conformation and for determining

proximity of adjacent spin systems. Not so useful for MWs in the 1 kDa range due to problems arising from the NMR correlation time.

EI-MS: Electron Impact Mass Spectroscopy

ESI-MS: Electron Spray Ionization Mass Spectroscopy

HR-EI-MS: High Resolution Electro Impact Mass Spectroscopy

HR-ESI-MS: High Resolution Electron Spray Ionization Mass Spectroscopy

m/z: mass to charge ratio

TLC: Thin Layer Chromatography

HPLC: High Performance Liquid Chromatography

t_R**:** retention time

RP: Reverse Phase

NP: Normal Phase

OP-CC: Open Column Chromatography

DMSO: Dimethyl Sulfoxide

TFA: Trifluoroacetic acid

IC_{50}: 50% inhibition concentration

DMEM: dulbecco's modified eagle medium

HBSS: hanks' balanced salt solution

FBS: fetal bovine serum

CS: calf serum

PS: penicillin streptomycin

2-NBDG: 2-(N-(7-Nitrobenz-2-oxa-1,3-diazol-4-yl)amino)-2-deoxyglucose

W: water, H_2O

MeOH, (Me): methanol

BuOH, (Bu): buthanol, *n*-butyl alcohol

EtOH: ethyl alcohol

EtOAc, (EA): ethyl acetate

MeCN, (ACN): Acetonitrile

Ace (A): Acetone

CH_2Cl_2: methylene chloride

국문 초록

약용 식물자원으로부터 인슐린의 작용을 증가시키는 화합물의 분리 및 구조분석

응구엔 피 훙

지도교수: 오 원 근

약학대학

조선대학교 대학원

2형 당뇨병, 대사증후군, 고혈압, 고지혈증과 같은 비만 관련된 질병은 전세계에 걸쳐 주요한 질환 위험으로 나타나고 있다. 당뇨병과 인슐린 내성 증후군은 전세계 사망원인 중 수위를 나타내고 이다. 이러한 질환들은 순환계 합병증, 신장기능 이상, 망막손실 및 관절부위 이상과 같은 합병증의 위험을 증대시킨다. 당뇨병 중 2형 당뇨병이 가장 일반적이며 인간의 사망위험의 증가 및 위험도와 관련이 있다. 2형 당뇨병은 췌장에서의 인슐린 분비 저하 및 작용지점에서의 기능이상으로, 혈액에서의 당 농도 조절작용의 실패에 기인한 혈중 당 농도가 증가하는 특징을 갖는다.

탄수화물 식사 후 췌장으로부터 혈액으로 분비되는 호르몬인 인슐린은 당을 근육, 지방세포 및 심장으로 저장을 증가시켜 혈중의 당 농도를

조절한다. 그러나, 당뇨병 환자에게 있어서는 췌장으로부터 충분한 인슐린을 생산하지 못하거나 생산된 인슐린이 작용하지 못하는 특징을 갖는다. 즉, 혈액속의 당 농도를 조절하지 못하는 인슐린 내성이 2형 당뇨병 환자에게 있어서 가장 중요한 원인이다. 그리하여 인슐린 신호전달 과정에 작용하여 인슐린 작용을 개선시키는 천연물질 및 합성 저분자 물질의 개발이 시도되고 있다. 그러나, 현재까지 임상시도 되고 있는 약물은 심장에서의 부작용과 낮은 활성으로 인하여 인슐린과 같은 효율적인 약물의 개발은 성공하지 못하고 있다.

최근의 많은 증거는 heterotrimeric serine/threonine kinase의 일종인 AMPK 효소가 인슐린 작용을 증가시키는 것으로 알려지고 있다. AMPK 효소는 세포 및 신체 전반에 걸쳐 에너지 상태를 조절하는 주요한 작용을 한다. 활성화된 AMPK 효소는 ATP를 생산하는 대사통로를 활성화하고 ATP를 소모하는 대사계를 불활성화 시키는 것으로 알려져 있다. AMPK 효소는 많은 관련 하위 조절자들을 통제하여, 즉 근육에서의 glucose uptake를 촉진하고 간에서는 글루코스 생산을 억제하며, 말초 지방조직에서는 극소적인 지방 축적을 저해하여 신체 전체에 걸쳐 인슐린 민감도를 개선하는 것으로 알려지고 있다. 그러므로 AMPK 효소는 현재 비만과 당뇨를 치료하는 좋은 약물 목표로 각광받고 잇다.

약용식물로부터 항 당뇨물질을 개발하기 위한 계속적인 연구목표로 두 종류의 *Morinda* 속 식물인 (*M. longissima* and *M. citrifolia*)가 분화된 3T3-

L1 지방세포에서 강하게 glucose uptake를 증가시키는 것으로 관찰하였다. 이러한 약용식물로부터 화학적 구성성분을 크로마토그래픽적인 방법 (silica gel, RP-C_{18}, MPLC와 preparative HPLC system)을 사용하여 신규 화합물 9개 (10, 42, 47, 49, 51-53, 57와 59)를 포함하여 59개의 물질을 분리하였다. 분리한 화합물 각각의 화학구조는 분광학적인 방법 (^{1}H, ^{13}C, COSY, HSQC, HMBC, NOESY와 MS) 및 이화학적인 방법 (IR, UV, CD, and $[\alpha]_D$)으로 결정되었으며 기지물질은 또한 기존의 문헌값들과 비교를 통하여 확인하였다. 얻어진 물질들을 화합물의 골격에 따라 나누어 보면 21개의 안트라퀴논 (anthraquinones, 1-21), 2개의 코마린 (coumarinoids, 23 과 26), 12개의 페닐프로파노이드와 카페인산 (phenylpropanoid and caffeic acid derivatives, 22-35), 2개의 프라보노이드 (flavonol and flavonol glucoside, 40 와 41), 3개의 이리도이드 (iridoids, 36-38), 1개의 트리터페노이드 (triterpenoid, 39)와 18개의 리그난 및 네오리그난 (lignans and neolignans, 42-59)으로 구별될 수 있다.

분리된 모든 화합물 (1-59)의 분화된 3T3-L1 지방세포에서 glucose uptake 작용의 효과를 측정하였다. 최종농도 10 μM의 농도에서 몇몇 화합물들은 강한 2-NBDG 시약을 이용한 실험에서 glucose uptake를 증가시키는 것으로 확인되었다. 안트라퀴논 화합물 (1-21) 중에서는 화합물 2, 8, 그리고 10이 특히 강한 glucose uptake를 증가시켰으며 몇몇 다른 화합물은 보통의 증가효과를 보였다. 그리하여 우리는 화합물 2, 8 및 10번 화합물을 이용하여

세포내에서 형광물질의 존재를 측정하는 방법을 사용하여 2-NBDG의 화합물에 의한 효과를 보다 정밀하게 분석하였다. 노니로부터 분리된 화합물 (22-59)을 이용하여 2-NBDG의 glucose uptake 효능을 측정한 결과 7,9':7',9-diepoxylignan과 3',7-epoxy-8,4'-oxyneolignan이 가장 강한 활성을 보였으며, 주 화합물 가운데 화합물 39 (ursolic acid, at 20 μM)에서 양성 대조군인 rosiglitazone (400 μM)보다 강한 저해활성을 갖음을 또한 확인하였다.

계속적인 연구로 화합물들의 AMPK 효소 활성화 작용을 검토 하였다. 분화된 근육세포에서 AMPK (Thr^{172})에서의 인산화 증가활성을 화합물 최종농도 10 μM과 양성대조군인 AICAR (1 mM)로하여 측정한 결과 화합물 8이 강한 활성화 작용이 있으며, 화합물 10과 20은 중간 정도의 활성화 작용이 있음을 확인하였다. 분리된 리그난 계열의 화합물 중 9,7'α-epoxylignano-7α,9'-lactone (48)과 triterpenoid (39)과 가장 강한 활성을 보여 주었다. 이러한 결과는 분리돤 화합물 (2, 8, 10, 20, 39, 42, 44, 45와 48)의 높은 glucose uptake 활성이 AMPK 효소의 활성증가와 관련될 수 있음을 나타낸다.

결론적으로 우리의 결과는 *Morinda* 속 식물인 (*M. longissima*와 *M. citrifolia*) 로부터 분리된 화합물 중 안트라퀴논 (anthraquinones)과 ursolic acid, 7,9':7',9-diepoxylignans들 특히 9,7'α-epoxylignano-7α,9'-lactone이 2-NBDG uptake를 증가시키는 과정에서 중요한 화합물임을 밝혔다. 앞으로 이러한 화합물을 이용하여 추가적인 기전연구 및 효능평가가 필요한 것으로 사료된다.

ABSTRACT

Isolation and characterization of new insulin-mimetic compounds form medicinal plants

Nguyen Phi Hung

Advisor: Prof. Oh Won Keun

Department of Pharmacy

Graduate School of Chosun University

Obesity associated diseases like type 2 diabetes, the metabolic syndrome, hypertension, and atherogenic dyslipidemia represent major health risks around the world. Diabetes mellitus (DM) and/or insulin resistance (IR) are ranked in the top ten causes of mortality worldwide. Both disorders often lead to disability through vascular complications, renal failure, blindness, and limb amputation. Of which, type 2 diabetes mellitus (T2DM) is the most common, prevalent and fastest growing form of the disease and the principal cause of morbidity and mortality in human. It is often complicated by obesity and characterized by high levels of glucose in the bloodstream, resulting from impairment at insulin release and its action.

Insulin, a natural hormone which is secreted by the pancreatic β-cells into the bloodstream after the consumption of carbohydrate rich meals, causes skeletal muscle,

adipose, and heart, to increase their uptake of glucose for the production of ATP. In diabetes patients, however, either the pancreas cannot produces enough insulin for regulating blood glucose levels (Type 1), or the body cannot use insulin produced effectively (Type 2). Insulin resistance, resulting in loss of proper glucose homeostasis, is considered as the most important factor of type-2 diabetes and is generally due to defects in insulin-mediated signal transduction. Thus, a number of small molecular (including synthetic and natural products) materials affected in insulin signaling pathway are being investigated for improving insulin sensitivity and/or mimicking the action of insulin. However, clinical tests have shown that none of these compounds can replace insulin in the treatment of diabetes without causing adverse effects such as cardiac arrest.

Recent some evidences have emerged that AMPK, a heterotrimeric serine/threonine kinase, could be responsible for increasing insulin sensitivity and indirectly inhibit preadipocyte differentiation by improving insulin action. AMPK is well established as a key sensor and regulator of intracellular and whole-body energy metabolism. Activated AMPK re-establishes the proper energy balance in the cell by switching off the ATP-consuming anabolic pathways and switching on the ATP-generating catabolic pathways. Many downstream targets of AMPK have demonstrated the role of AMPK in glucose and lipid metabolism, such as stimulating glucose uptake in the muscle, suppressing hepatic glucose production in the liver, and reducing ectopic lipid accumulation for improving insulin sensitivity. Therefore, AMPK activators are considered as promising drugs for diabetes and obesity.

As part of our ongoing investigation for discovering new anti-diabetes agents from medicinal plants, we found that the total extracts of two *Morinda* species (*M. longissima*

and *M. citrifolia*) showed *in vitro* glucose uptake effects on 3T3-L1 adipocytes. Thus, phytochemical investigation of these medicinal plants using chromatographic methods (silica gel, RP-C_{18}, MPLC, and preparative HPLC system) led to the isolation of 59 natural products, comprising of 9 new compounds (**10**, **42**, **47**, **49**, **51-53**, **57**, and **59**) as active constituents. Their chemical structures were elucidated on the basis of spectroscopic (including ^{1}H, ^{13}C, COSY, HSQC, HMBC, NOESY, and MS) data interpretation and physicochemical (IR, UV, CD, and $[\alpha]_D$) data analyses, as well as comparison with those published in literatures. According to the structural skeleton, their structures were characterized to be 21 anthraquinones (**1-21**), 2 coumarinoids (**23** and **26**), 12 phenylpropanoid and caffeic acid derivatives (**22-35**), 2 flavonol and flavonol glucoside (**40** and **41**), 3 iridoids (**36-38**), one triterpenoid (**39**), and 18 lignans and neolignans (**42-59**). After structural elucidation, the isolates (**1-59**) were investigated for their stimulatory effects on glucose uptake in 3T3-L1 adipocytes. At the concentration of 10 μM, some of isolated compounds showed significant enhancing activity on glucose uptake with 2-NBDG reagent. Among the anthraquinones (**1-21**), compounds **2**, **8**, and **10** were found to possess stronger stimulatory effect at the combination of isolated compounds and insulin than insulin, a positive control. The others showed increasing effect to a level comparable with insulin. Thus, we further confirmed the transportation efficacy of 2-NBDG into the cells of compounds **2**, **8**, **10**, and **20** by measuring fluorescent signals induced after drug treatment. Comparing to control group, compounds **2**, **8**, and **10** showed higher levels of fluorescent signals from the adipocytes representing the inducement of 2-NBDG uptake into the cells. Among the compounds isolated from Noni (**22-59**), we found that the 7,9':7',9-diepoxylignan and 3',7-epoxy-8,4'-oxyneolignan possessed strongest activity, and

the most major compound **39** (ursolic acid, at 20 μM) showed stronger activity than rosiglitazone, the positive control used at 400 μM.

In progress, we investigated whether these 2-NBDG uptake inducers activate AMPK or not. In differentiated C2C12 cells, we observed increased phosphorylation of AMPK (Thr^{172}) by our compounds at the concentration of 10 μM to a level comparable with AICAR, a positive control used at 1 mM. Anthraquinones **8** showed strongest activation, followed by compounds **10** and **20**. Among the lignan type, 9,7'α-epoxylignano-7α,9'-lactone (**48**) and triterpenoid (**39**) showed strongest activation. These observation suggest that the AMPK signaling pathway is likely responsible for the improvement of glucose uptake by these compounds (**2**, **8**, **10**, **20**, **39**, **42**, **44**, **45**, and **48**). Taken together, our results indicated that anthraquinones, ursolic acid, and 7,9':7',9-diepoxylignans, especially the 9,7'α-epoxylignano-7α,9'-lactone, may be important for 2-NBDG uptake activity *in vitro*. Additionally, 2-NBDG uptake effects by members of anthraquinones and neolignans have not been previously reported. Further confirmation of the anti-diabetes effects of these natural products and evaluation of their potential *in vivo* efficacy in a diabetic model are necessary.

I. INTRODUCTION

1.1. Diabetes

Diabetes mellitus (DM) is one of the most prevalent and serious metabolic diseases and the principal cause of morbidity and mortality in human. It is characterized by high levels of glucose in the bloodstream, resulting from impairment in insulin release and its action. The diabetes epidemic has struck worldwide. More than 285 million people across the world suffer from diabetes, 90% of whom have Type II Diabetes. It is estimated that 438 million people will be inflicted with diabetes worldwide by the year 2030 (Fig. 1), profoundly increasing the need for treatment for type II diabetes.

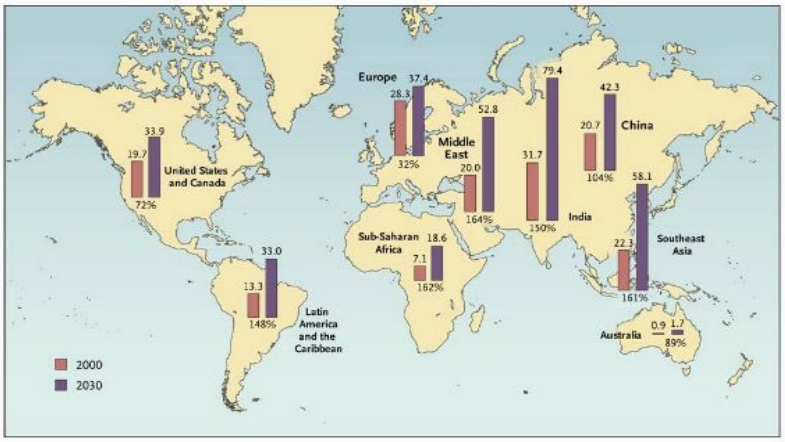

Figure 1: Worldwide prevalence of Diabetes 2000-2030

Diabetes may be divided into three main types (Table 1). First, type 1 diabetes (previously known as insulin-dependent diabetes) is an auto-immune disease where the body's immune system attacks and destroys the insulin-producing β cells in the pancreas,

and then the pancreas produces little or no insulin and the glucose stays in the blood instead, where it can cause serious damage to all the organ systems of the body. This type of diabetes, also known as juvenile-onset diabetes, accounts for 10-15% of all people with the disease.

Second, type-2 diabetes, known as non-insulin-dependent diabetes mellitus (NIDDM), is the most common form among three types of diabetes, affecting 85-90% of all people with the diseases. The disease is strongly genetic in origin but lifestyle factors such as excess weight, inactivity, high blood pressure and poor diet are major risk factors for its development. Hyperglycemia is one of the characteristic pathogenesis, and it is clear that control of hyperglycemia can attenuate the development of chronic complications such as retinopathy and nephropathy.[1] Therefore, therapy for type 2 diabetes relies mainly on several approaches to reduce the hyperglycemia itself: sulphonylureas (and related insulin secretagogues), which increase insulin release from pancreatic islets; metformin, which acts to reduce hepatic glucose production; peroxisome proliferator-activated receptor-γ (PPARγ) agonists (thiazolidinediones), which enhance insulin action; α-glucosidase inhibitors, with gut glucose absorption.[2]

Third, gestational diabetes (GD) occurs during pregnancy. Although it usually disappears after delivery, the mother will more likely develop type-2 diabetes later. Self-care and dietary changes are essential in treatment.

Table 1. Classification of diabetes

	Type 1 (IDDM)	Type 2 (NIDDM)
Distribution	< 10%	> 90%
Cause	Autoimmune disease	Insulin resistance (obese) Insulin secretion defect (nonobese)
Age	< 30 (mainly 11 - 14)	> 45
Clinical	Fast progress Hypoinsulinemia Ketonemia	Slow progress Hyperinsulinemia (obese) Normal insulin level (non-obese)
Treatment	Injection of insulin	Die, Glucose-lowing agent, linsulin

1.2. Insulin and insulin resistance

Insulin is a peptide hormone composed of 51 amino acids and has a molecular weight of 5,808 Da which is produced in the islets of Langerhans in the pancreas β-cells (Fig. 2). Insulin causes cells in the liver, muscle, and fat tissue to take up glucose from the blood, storing it as glycogen in the liver and muscle, and stopping use of fat as an energy source.

Insulin increases glucose uptake in muscle and adipose tissue, and inhibits hepatic glucose production, thus serving as the primary regulator of blood glucose concentration.[3] Also, insulin stimulates cell growth and differentiation, and it promotes the storage of substrates in fat, liver and muscle by stimulating lipogenesis, glycogen and protein synthesis, and by inhibiting lipolysis, glycogenesis, and protein breakdown.[4] By increasing the uptake of glucose by cells and reducing the concentration of glucose in the blood, insulin prevents or reduces the long-term complications of diabetes, including damage to the blood vessels, eyes, kidneys, and nerves.[4]

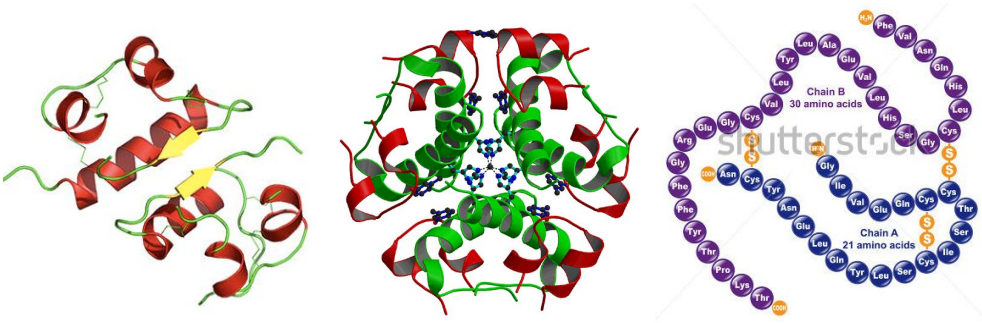

Figure 2: The primary amino acid structure of human insulin: Insulin dimer, hexamer, and simplified insulin. As is shown, insulin consists of two peptide chains which are connected by disulfide bonds

Insulin resistance is a physiological condition where the natural hormone insulin becomes less effective at lowering blood sugars. The resulting increase in blood glucose may raise levels outside the normal range and cause adverse health effects, depending on dietary conditions. At insulin resistance state, the glucose uptake in muscle and fat cells are reduced, whereas insulin resistance in liver cells results in reduced glycogen synthesis and storage and a failure to suppress glucose production and release into the blood. High plasma levels of insulin and glucose due to insulin resistance are a major component of the metabolic syndrome.

Up to recently, insulin is the only agent developed for the treatment of either type 1 or severe type-2 diabetes. A number of synthetic small molecules, such as zinc (II) complexes and vanadium compounds, have been shown to mimic the action of insulin in cell culture and animal models of diabetes. In addition, many natural products, such as antibiotics (e.g. anisomycin), fungal metabolites (e.g. L-783,281), plant extracts (e.g. leaf alcoholic extract from the tropical herbaceous perennial *Catharanthus roseus*) and animal constituents (e.g. dried chrysalis of the silkworm *Bombyx batryticatus*) also promote glucose uptake in cells. However, clinical tests have shown that none of these compounds or extracts can replace insulin in the treatment of diabetes. Thus, a need to search for new anti-diabetic agents that can mimic the effect of insulin is still remained.

1.3. Fluorescent-tagged glucose bioprobes (6-NBDG and 2-NBDG) and their use in monitoring glucose utilization

Glucose homeostasis is a fundamental aspect of life and its dysregulation is associated with important diseases such as cancer and diabetes. Glucose ($C_6H_{12}O_6$, also known as D-

glucose, dextrose, or grape sugar) is a monosaccharide and a pivotal carbohydrate in biology. It is the primary source of energy in organisms and an important metabolic intermediate.[5] Therefore, the ability to effectively monitor glucose homeostasis is crucially important in many aspects of biological research and medicine. Currently, research on anti-diabetic medicine have been focused on development and screening of compounds with potential insulin-mimetic effects to stimulate rate of cell glucose uptake. The first fluorescent-tagged glucose bioprobe, 6-deoxy-N-(7-nitrobenz-2-oxa-l,3-diazol-4-yl)-aminoglucose (6-NBDG), was developed in 1985 by Professor Howard Kutcha's laboratory in the University of Virginia. Hideaki Matsuoka s Laboratory at Tokyo University of Agriculture and Technology after eleven years on the development of 6-NBDG synthesized 2-(N-(7-nitrobenz-2-oxa-l,3-diazol-4-yl)amino)-2-deoxyglucose (2-NBDG).[6] A rapid, follow-up study validated the intracellular fate of 2-NBDG. In bacteria, 2-NBDG was shown to be phosphorylated after uptake, to produce fluorescent derivative (2-NBDG 6-phosphate), presumably by the glycolytic enzyme, hexokinase. 2-NBDG 6-phosphate was then converted back into 2-NBDG by the enzyme glucose 6-phosphatase. 2-NBDG was then rapidly degraded to non-fluorescent products by the glycolytic pathway. The cellular breakdown of 2-NBDG is a useful property, because 2-NBDG signal should indicate both the cellular glucose uptake rate and metabolic activity, although it should be noted that 2-NBDG may also accumulate as glycogen. Indeed, the usefulness and simplicity of 2-NBDG as a tracer for eukaryote cell viability was demonstrated in the same year.[7]

The proven usefulness of NBDG for diabetes, neurological and cancer research appears to be a factor in the subsequent development of alternative fluorescent-tagged

glucose bioprobes.

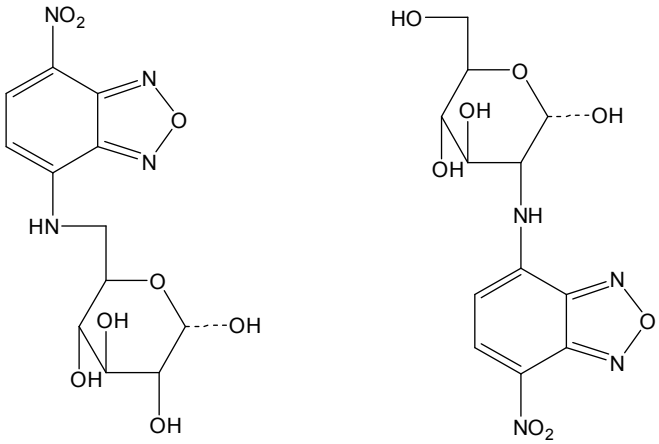

(A) 6-NBDG **(B) 2-NBDG**

Figure 3: Chemical structure of 6-NBDG and 2-NBDG

1.4. *Morinda citrifolia* and *Morinda longissima*

The genus *Morinda* (belong to Rubiaceae family) comprises approximately 80 species, distributed in all tropical regions of the world. These species may be trees, shrubs or vines bearing aggregated fruits (or syncarps) that can be fleshy or dry. The most popular species, *Morinda citrifolia*, commonly named "noni" has a long history of utilization throughout the Pacific Polynesia, South and Southeast Asia, Northeastern Australia and the Caribbean. It is deemed to be the second most important herb plant in the Hawaiian islands,[8] and has been used to treat a wide variety of ailments. While applications have been reported for all parts of the plant, the leaves have the most prevalent traditional use and the plant is usually used topically.[9] This contrasts with the current popular use where the fruit juice, and less commonly the leaves and roots, are primarily consumed orally. *Morinda citrifolia* L. is a

small evergreen tree or shrub, native to South Asia that currently grows throughout the tropics. The fruits of *M. citrifolia* are very distinct and easy to recognize. The white tubular flowers form in clusters on the young fruit. The syncarpous fruit grow to be about 5-10 cm long and turn from a greenish to a translucent yellowish-white colour when fully ripe. Responding to noni's ethnobotanical and popular use, a substantial number of biological and chemical studies have been performed on this species dating back more than 100 years. Many secondary metabolites of noni have been established. These include iridoid glycosides and triterpenoids which are the major constituents of the fruit, and a number of anthraquinones, which primarily accumulate in the roots, but have also been found in trace quantities in the fruit. Lignans, neolignans, and polypropanoid derivative are also reported as active constituents from the fruits. There are currently two recognized varieties of *M. citrifolia* (*M. citrifolia* var. *citrifolia* and *M. citrifolia* var. *bracteata*) and one cultivar (*M. citrifolia* cultivar Potteri). The most commonly found variety, *M. citrifolia* var. *citrifolia*, has the greatest economic importance. It is morphologically diverse with both large and small fruits and its leaves exhibit a wide range in size and shape, being variously described as elliptical, long and strap-like, and ovate or rounded. *M. citrifolia* var. *bracteata* has smaller fruits subtended by bracts and is found in countries between the Indian and Pacific Oceans.[10] In Vietnam, it has many different name belong to the local area where the tree located, such as Nhàu, Nhàu núi, Nhàu rừng, Ngao, or Grand Morinda. The root-bark has been used internally for hypertention, osteodynia, and lumbago. While the leaves have been used traditionally for treating furunculosis, and oedema, and the fruits are used for cough, coryza, and neuralgia. It is also used as supplier for stomachic and aperients.[11] The extract of these plant was used orally for fever, dysentery and diarrhea in remedies.

The second, *M. officinalis*, is another agelong herb and was considered to be an effective tonic for promoting overall health in traditional herbal medicines. *M. parvifolia* and *M. umbelllata* are two other popular species displayed analgesic, hemostatic, antibacterial, and antiphlogistic activities.[12]

Figure 4: Representative picture of Noni fruits, leave, and commercial noni products as tea, beverages and functional supplements

Among these species, *M. longissima* is closely related to *M. officinalis* and *M. citrifolia* in phytotaxonomy, which is distributed at the mountain area of North Vietnam. The root has been used traditional for detoxification, inflammation, blood influence, stomachic and aperients. Crude extract of the root of *M. longissima* has shown hepatoprotective effects with major principle as emodin.[13] However, phytochemical and pharmacological investigation associated with *M. longissima* have not been clarified.

1.5. AMP-activated protein kinase (AMPK)

AMPK was first described as an enzyme capable of phosphorylating and inactivating

hydroxymethylglutaryl-CoA (HMG-CoA) reductase and acetyl CoA carboxylase (ACC), key enzymes in the synthesis of cholesterol and fatty acids. It was later named as AMPK because its activity is highly dependent on the presence of 5′-AMP. The AMPK complex is a αβγ heterotrimer containing a catalytic α subunit (isoforms α1/α2) and regulatory subunits β (β1/β2) and γ (γ1/γ2/γ3) (Figure 4).[14] Homologues of these subunits are found in all eukaryotic species where genome sequences have been completed. The β subunit anchors both the α and γ subunits to form a regulatory core, where the C-terminal 70 residues of β interact via extensive hydrophobic contacts with the C-terminal 80 residues of α, and a short stretch of β-strand hydrogen bonding with residues 45–52 of γ (human isoform 1). The kinase domain at the N terminus of α is connected to the regulatory core via a linker region of approximately 60 residues. The β subunit is N-terminally myristoylated at Gly2 in both mammalian isoforms, and also contains a mid molecule carbohydrate-binding module (CBM) which is required for targeting the protein to glycogen (Glossary). Nucleotide sites (1 to 4) are numbered according to the CBS domain which contributes an Asp residue and hydrogen bonds to the ribose 20 and 30 hydroxyls (Figure 17D). Only three sites contribute to nucleotide regulation, and site 2 is unoccupied in all mammalian AMPK structures solved to date. Site 4 in mammalian AMPK γ has been assigned as an AMP non-exchangeable site. ATP, ADP and AMP are exchangeable at the other two sites (1 and 3), implicating them as key mediators of AMPK regulation.

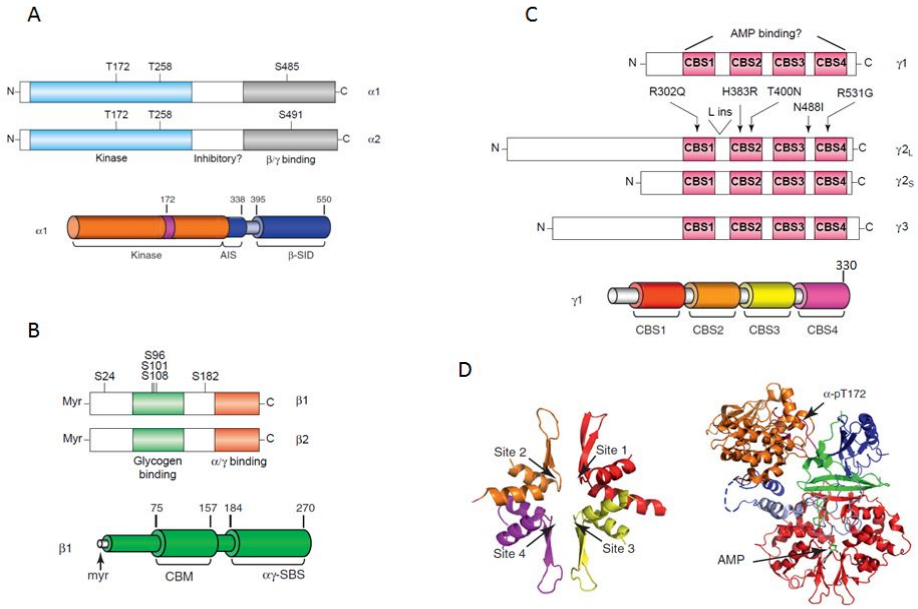

Figure 5: AMPK domains and subunit structures. Domain organization of AMPK subunits and AMPK is composed of three subunits (α, β, and γ); there are two isoforms of the α and β subunits, and three γ subunit isoforms. Residue numbering refers to human α1, β1, and γ1, isoforms. (**A**) The α subunit consists of an N-terminal kinase domain, an autoinhibitory sequence (AIS) and a β-subunit interacting domain (β-SID). The C-terminal domain of the α subunit binds to the β and γ subunits. Three phosphorylation sites have been identified as Thr^{172} (T172), Thr^{258} (T258) and Ser485 (α1)/491 (α2) (S485/S491). (**B**) The β subunit is N-terminally myristoylated (myr) and contains a mid-molecule carbohydrate-binding module (CBM) and C-terminal αγ subunit-binding sequence (SBS). The C-terminal domain of the β subunit is involved in binding of the α and γ subunits, and a putative glycogen-binding domain has been identified between residues 72–151 in β1. (**C**) The γ subunits contain four copies of a cystathionine-β-synthase (CBS) domain, paired (1+2 and 3+4) to form two Bateman modules, which appear to be involved in binding AMP. The location of the five missense mutations identified within γ2 that cause cardiac abnormalities, together with the missense mutation in γ3 that causes skeletal muscle

glycogen accumulation, are indicated by arrows. The mutation resulting in insertion of a leucine residue in γ2 is marked by a V. Two forms of γ2 protein are predicted, designated γ2L and γ2S. (**D**) Tetrad organization of CBS domains in the γ-subunit, colored as showing locations of nucleotide binding sites (black arrows). Structure of the mammalian AMPK regulatory core and kinase domain [PDB 2Y94: rat α1 (7–299)/(331–469)/(524–548), human β1 (198–272) (green), rat γ1 (23–326) (red)]; α-subunit regions are colored as in (a). AMP bound at γ site 3 is evident

1.5.1. Role of AMPK in energy metabolism and glucose homeostasis

AMPK activity is regulated by increases in the concentration of AMP (AMP: ATP ratio) through three separate mechanisms. AMP binds to the γ subunit, inducing a conformational change in the AMPK complex, which (1) allosterically activates the α catalytic subunits, (2) enhances phosphorylation of the Thr172 residue by upstream AMPK kinases AMPKK (known as LKB-1, CaMKK, TAK-1), and (3) inhibits the action of protein phosphatase 2C (PP2C) to dephosphorylate Thr172. These complex regulatory mechanisms allow AMPK activity to be exquisitely sensitive to small changes in intracellular AMP concentrations. Conditions that increase AMP:ATP ratio include exercise, starvation, diabetes mellitus, hypoxia, ischemia/reperfusion, oxidative stress, and heat shock (Fig. 5).[15] AMPK is also activated in conditions that do not cause a detectable increase in the AMP:ATP ratio, such as hyperosmolar stress and metformin treatment.

Binding of AMP to the γ subunit results in an allosteric activation and induces conformational changes exposing the α subunit to upstream kinases. Of these kinases, the

most important is considered to be the tumor suppressor LKB1. Different metabolic stresses that either inhibit ATP production such as hypoxia and hypoglycemia or increase ATP consumption (e.g., muscle contraction) lead to an activation of AMPK, which then turns on glucose uptake and various catabolic pathways (namely glycolysis and fatty acid oxidation) and switches off biosynthetic pathways (synthesis of glycogen, protein, and fatty acids). It thus activates pathways resulting in ATP production while turning off energy-consuming pathways both at a single cell and the whole-body level. Eventually, AMPK contributes to an increase in mitochondrial biogenesis in response to chronic energy depletion. AMPK is also involved in the regulation of food intake through its action on the expression of hypothalamic neuropeptides, with an activation of AMPK leading to increased food intake. Effects of AMPK activation further include modulation of cell cycle, tumor growth suppression, inhibition of proteosynthesis, stimulation of autophagy, ion channel regulation, and many other effects.[17] In line with its function as a cellular energy sensor, AMPK has been involved in the metabolic effects of hormones such as leptin, ghrelin, adiponectin, glucocorticoids, insulin, glucagon as well as cannabinoids, all these hormones being involved in regulation of energy metabolism. Although AMPK is apparently present in all tissues, its activation and mode of action seem to be regulated in a tissue-specific manner. For example, leptin activates AMPK in adipose tissue, skeleton muscle, and liver but inhibits it in hypothalamus, while adiponectin and anti-diabetic drugs primarily activate the AMPK in the peripheral tissues. The role of AMPK in energy metabolism has been most intensively studied in SM, heart, adipose tissue, liver, beta cells, and hypothalamus, that is, tissues that are highly sensitive to changes in energy balance and also actively involved in its regulation.

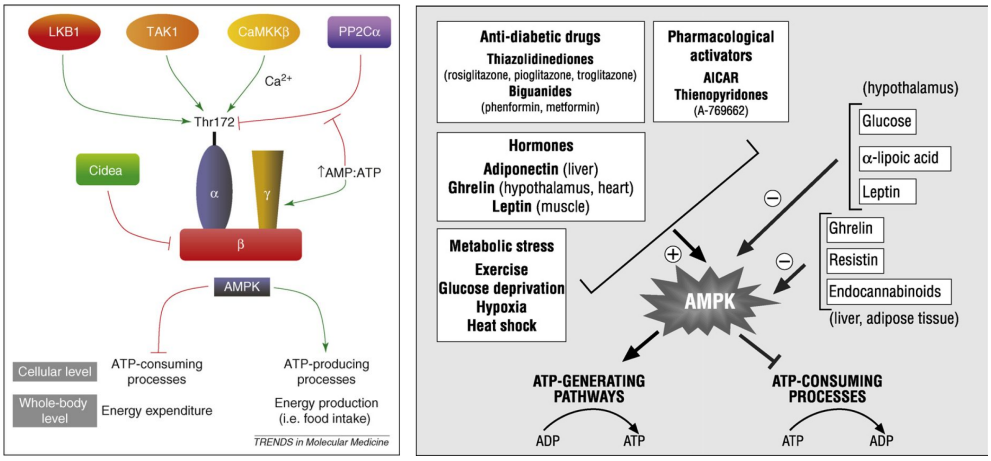

Figure 6: Regulation of AMP-activated protein kinase (AMPK): AMPK is activated in response to environmental or nutritional stress factors, which deplete intracellular ATP levels including heat shock, hypoxia, glucose deprivation or prolonged exercise. AMPK is activated as described above after an increase in AMP level, allosteric modifications and Thr172 phosphorylation via upstream AMPK kinases.[16]

The liver is one of the main metabolic tissues for controlling whole body glucose homeostasis. Hepatic AMPK has a central role in the metabolic adaptation to acute and chronic nutritional stress. AMPK influences hepatic lipid metabolism, where its activation leads to a reduction in lipogenesis and cholesterol synthesis and a simultaneous increase in fatty acid oxidation leading to a decreased hepatic lipid deposition.[17] Liver AMPK controls glucose homeostasis mainly through the inhibition of gluconeogenic gene expression and hepatic glucose production. Liver AMPK also decreases hepatic lipogenesis. AMPK phosphorylates and inactivates acetyl-CoA carboxylase 1 (ACC1) and 3-hydroxy-3-methylglutaryl-CoA reductase (HMG-CoA reductase), leading to inhibition of denovo

fatty acid and cholesterol synthesis.[18] Phosphorylation of ACC2 by AMPK, on the other hand, causes increases of fatty acid oxidation.

Both skeletal muscle and heart have wide fluctuations in energy demand from the extremes of rest and maximal exercise. Muscle AMPK is activated during contraction and may mediate multiple beneficial effects of exercise, which depletes ATP leading to an increase in the AMP/ATP ratio.[17] As in the liver, acute muscle AMPK activation increases fatty acid oxidation by decreasing malonyl-CoA concentrations through inhibiting ACC and activating MCD.[18] AMPK also increases SM glucose uptake by increasing the glucose transporter GLUT4 in the sarcolemma, a mechanism, which is distinct from the action of insulin that also stimulates GLUT4-mediated glucose uptake in muscle cells. AMPK was found to directly phosphorylate and thus activate PGC-1α, which has a crucial role in enhancing mitochondrial biogenesis in SM and brown adipose tissue (BAT). In parallel, AMPK increases cellular NAD(+) levels and enhances sirtuin 1 (SIRT1) activity, resulting in the deacetylation and activation of PGC-1α. Heart metabolism is also profoundly influenced by AMPK activation. GLUT4 translocation, glucose uptake, and fatty acid oxidation are stimulated AMPK is activated in the heart by exercise, by ischemia, and by the hormone ghrelin. The increased heart rate necessary to support increased energy needs of skeletal muscle during exercise, also requires increased oxidation of glucose and fatty acids. The utility of activation of AMPK during and following ischemia is not so straightforward, as increased fatty acid oxidation would result in increased oxygen requirements.[18]

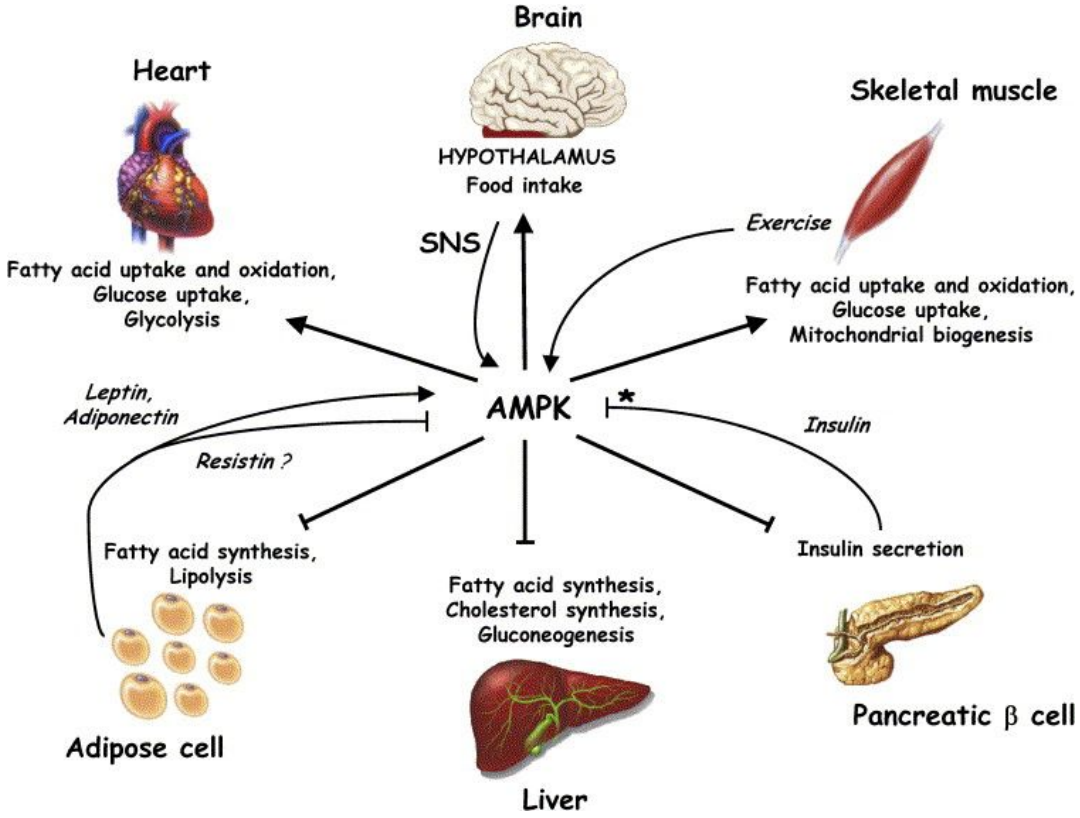

Figure 7: Roles of AMP-activated protein kinase (AMPK) in the control of whole-body energy homeostasis. Activation of AMPK in many tissues switches off ATP-consuming processes while switching on catabolic processes that generate ATP. The adipocyte-derived hormones leptin and adiponectin, as well as exercise, activate AMPK in skeletal muscle, stimulating fatty acid oxidation. Leptin's activation of AMPK in skeletal muscle involves the hypothalamic-sympathetic nervous system (SNS) axis. Adiponectin also activates AMPK in liver, increasing fatty acid oxidation and reducing gluconeogenesis, and in adipocytes, where the downstream biologic pathway has not been studied. Resistin inhibits AMPK in liver. AMPK inhibits insulin secretion from pancreatic β cells. *Insulin inhibits AMPK activation in ischemic heart and hypothalamus, whereas it has no effect on AMPK in skeletal muscle or adipocytes. In hypothalamus, AMPK activity plays a role in regulation of food intake and body weight.[17]

AMPK is likely involved in regulation of insulin secretion in the pancreatic beta cell. AMPK activation suppresses glucose-induced increases in glycolysis, mitochondrial oxidative metabolism, Ca^{2+} influx, and insulin secretion. AMPK activation also inhibits the effect of glucose on the promoter activities of L-PK and preproinsulin (PPI).[15] AMPK activation may also have adverse effects in pancreatic β cells by inducing β-cell apoptosis, as shown in MIN6 β cells. Accumulation of triacylglycerol in β cells causes reduced insulin secretion and β-cell apoptosis, which is considered an important mechanism of β-cell loss in type 2 diabetes mellitus.

A very exciting milestone in the AMPK field was the discovery that AMPK is involved in regulation of food intake. Activated AMPK in the hypothalamus increases in response to fasting and decreases in response to refeeding.[18] Orexigenic peptides (ghrelin, agouti-related peptide) stimulate an increase in AMPK activity and anorexigenic peptides (leptin) and lipids (α-lipoic acid) decrease AMPK activity in this region of the hypothalamus. Thus, changes in hypothalamic neuropeptides expression may simply explain how AMPK regulates food intake.

Adipose tissue has the function of converting excess carbohydrates and fatty acids into triglycerides and then releasing fatty acids and glycerol in times of nutrient paucity or increased energy need. AMPK activity has been reported to increase in epididymal fat pads in response to fasting, exercise, and cold exposure. This activation is accompanied by inactivation of ACC, activation of malonyl-CoA decarboxylase, and decrease in malonyl-CoA. Glycero-phosphate acyl transferase (GPAT), the enzyme responsible for triglyceride synthesis, is also inhibited by AMPK phosphorylation.[18] AMPK is activated in adipocytes

by beta-adrenergic agonists. Treatment of adipocytes with AICAR or induction of expression of constitutively active AMPK results in phosphorylation and inactivation of ACC and a decrease in lipolytic rate. A recent study showed stimulation of glucose uptake and GLUT4 translocation to the plasma membrane of 3T3-L1 adipocytes by both AICAR and dinitrophenol. Secretion of adipokines by fat cells may also be regulated by AMPK. TNF and interleukin 6 secretion decrease and adiponectin secretion by fat cells increases in response to incubation of adipocytes with AICAR.[18]

1.5.2. Activation of AMPK by indirect activators

A number of hormones and pharmacological agents have been reported to activate AMPK *in vivo* or upon treatment of cells and/or tissues (Fig. 8). While the detailed modes of action by which these agents activate AMPK are not fully delineated, they act in an indirect manner. Changes in mitochondrial coupling and cellular energy state could account for, at least in part, the mechanisms leading to cellular AMPK activation. Studies using these agents have aided our understanding of the role of AMPK in the regulation of cellular processes and whole-body energy homeostasis.

Metformin is an anti-hyperglycemic agent with effects on suppressing hepatic glucose output by activating AMPK in hepatocytes, reducing ACC activity and inducing fatty acid oxidation. Correlative results were also observed with respect to metformin increasing AMPK activity in skeletal muscle of subjects with type-2 diabetes.[19] TZDs are activators of PPARγ and function as insulin sensitizers. TZDs significantly increased phosphorylation of AMPK and ACC in rat muscle, paralleled by a transient increase in the

AMP/ATP ratio. However, the major effect of TZDs is likely to be on the release of adiponectin by adipocytes, leading to activation of AMPK in liver to reduce glucose production.[20] Whereas leptin selectively stimulates phosphorylation and activation of the α2 catalytic subunit of AMPK in skeletal muscle. In addition to AMPK phosphorylation, leptin also induced PPARα gene transcription in C2C12 cells.[21]

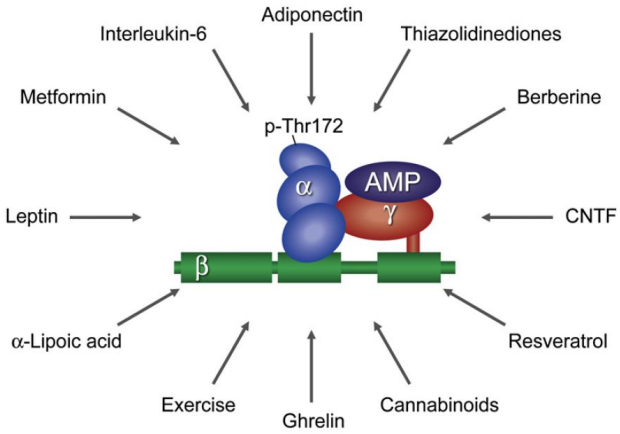

Figure 8: Activation of AMPK by indirect activators: Exercise and the agents listed have been shown to modulate the activity of AMPK

Both endocannabinoids and ghrelin are potent appetite stimulators that increase AMPK activity in the hypothalamus and the heart while inhibiting AMPK in liver and adipose tissue, which may contribute to the well known effects of endocannabinoids and ghrelin on the metabolism of peripheral tissues, including the reduction in infact size in the myocardium, the enlargement in adipose tissue, and changes in carbohydrate and lipid metabolism.[22] IL-6 is produced and released by skeletal myocytes in response to contraction. Basal IL-6 release from soleus was increased in AMPKα2 and AMPKα1

knockout mice, respectively, suggesting AMPK participates in the regulation of IL-6 release from oxidative muscle. IL-6 also rapidly and markedly increased AMPK activity in myotubes, enhancing fatty acid oxidation as well as basal and insulin-stimulated glucose uptake. Berberine caused inhibition of mitochondrial function that increases the AMP/ATP ratio, which could explain the activation of the AMPK pathway by berberine as well as its beneficial effects in the treatment of diabetes and obesity in animal models.[23] *α*-Lipoic acid (*α*-LA) is a cofactor of mitochondrial enzymes that play key roles in catalyzing the decarboxylation of *α*-keto acids. *α*-LA decreased hypothalamic AMPK activity and caused profound weight loss in rodents by reducing food intake and enhancing energy expenditure. In peripheral tissues, *α*-LA activated AMPK in skeletal muscle as well as endothelial cells. However, *α*-LA-stimulated glucose oxidation in rat hearts was independent of AMPK activation.[24]

1.5.3. Activation of AMPK by direct activators

As can be inferred from the discussions above, direct activators of AMPK that act without increasing cellular AMP/ATP ratios are being pursued as novel therapeutics. By definition, a direct activator should bind directly to the three subunits (α, β, or γ) of the AMPK enzyme. A-769662 is a recently identified thienopyridine family of AMPK activators. It acts by directly stimulation on partially purified liver AMPK and inhibition of fatty acid synthesis in primary hepatocytes.[25a] Similar to AMP, A-769662 activates AMPK both allosterically and by inhibiting dephosphorylation of AMPK on Thr172.[25] Based on a previous report that inactive mammalian AMPKα1 catalytic subunit contains an auto-inhibitory domain, screening of a chemical library with inactive human α1 (residues 1–

394) led to the identification of a novel small molecule activator, PT1, which allosterically activated AMPKα1 (1–394), α1 (1–335), α2 (1–398), and α1β1γ1 in vitro and promoted phosphorylation of AMPK and ACC in L6 myotubes and HeLa cells without an increase in cellular AMP/ATP ratio.[26] Studies revealed that PT1 may interact with AMPKα1 near the auto-inhibitory domain and directly relieve auto-inhibition.

Given the aforementioned critical actions of AMPK on glucose and lipid metabolism and the encouraging data from indirect as well as direct activators of AMPK in preclinical setting, targeting AMPK activation appears to be an attractive therapeutic strategy for the treatment of T2DM and related metabolic disorders.

II. MATERIALS AND METHODS

2.1. Materials

2.1.1. Chemical, reagent, and chromatography

Column chromatography was conducted on silica gel (63-200 μm particle size) and RP-18 (75-150 μm particle size) from Merck. TLC was carried out with silica gel 60 F_{254} plates from Merck. HPLC was carried out using a Gilson System 321 pump equipped with a model UV/VIS-155 UV detectors and an Optima Pak C_{18} column (10 × 250 mm, 10 μm particle size, RS Tech Korea). Baker analyzed HPLC solvents Acetonitrile (MeCN) and Methanol (MeOH) were purchased from Mallinckrodt Baker, Inc. USA. Deuterated solvent for NMR analysis Me_2CO-d_6, D_2O, Chloroform, and Methanol-d_4 were purchased from CIL (Cambridge Isotope Lab., USA).

2.1.2. General experimental procedures

The optical rotations were determined on an Autopol IV A7040–12 automatic polarimeter using a 100 mm glass microcell. The ultraviolet (UV) spectra were obtained in MeOH using an Optizen 3220UV spectrophotometer. The CD spectra were recorded in MeOH on a JASCO J-710 spectropolarimeter (CD/ORD spectropolarimeter). ^{1}H nuclear magnetic resonance (NMR, 300 MHz) and ^{13}C NMR (75 MHz) spectra were recorded on an YH300-OXFORD NMR spectrometer. The ^{1}H NMR (500 and 600 MHz) and ^{13}C NMR (125 and 150 MHz) spectra were measured on Unity INOVA 500 and 600 FT–NMR spectrometer with TMS as the internal standard at Korea Basic Science Institute (KBSI, Gwangju Center, Korea). Electron ionization (EI)-mass spectroscopy (MS) and high-

resolution EI-MS spectra were recorded on a Micromass ESI–Tof II (Micromass, Wythenshawe, UK) mass spectrometer. Column chromatography was carried out using silica gel 60 (40–63 and 63–200 µm particle size) and RP-18 (75–150 µm particle size) from Merck. Precoated TLC silica gel 60 F_{254} plates from Merck were used for thin-layer chromatography. The spots were visualized using UV light or 10% sulfuric acid. The HPLC runs were carried out using a Gilson System LC-321 pump with an UV/vis–155 UV detectors, and an Optima Pak C18 column (10 × 250 mm, 10 µm particle size). J sphere ODS-H80 (20 × 150 mm, 4 µm particle size) RS Tech, Korea, and Shodex-C18M-10E (10 × 250 mm, 10 µm particle size), and/or YMC-Pak ODS-AM (6.0 × 150 mm, 5 µm particle size) for semi-preparative runs.

2.1.3. Plant material

2.1.3.1. *Morinda longissima*

The root of *Morinda longissima* was collected from Cao Bang province, Northern Vietnam in spring, 2007. The voucher specimen was identified by Bs Ngo Van Trai, Department of Botany at Vietnam Institute of Medicinal Materials, 1A-Quang Trung, Ha Noi, Vietnam.

1.3.2. *Morinda citrifolia* (Noni)

The dried powder of *Morinda citrifolia* (Noni) was purchased at Korean Food Institute, Republic of Korea. The sample was botanically authenticated by Prof. Oh Won Keun, and its voucher specimen has been deposited at the Department of Pharmacy, Chosun University, 375-Seoseuk dong, Dong-gu, Gwangju, Republic of Korea.

2.2. Methods

2.2.1. Isolation of compounds from *Morinda longissima*

The root of *Morinda longissima* (1 kg, dried material) was extracted with EtOAc (5 L × 3 time) at 50 ^{o}C, using sonication. After removing the solvent under reduced pressure, the residue (45 g) was chromatographed on a silica gel column (10 × 60 cm; 63–200 μm particle size, Merck) using a stepwise gradient of *n*-hexane/ethyl acetate (20:1 to 1:20) to yield for combined fractions according to their TLC profiles. Among them, fraction 1 (ML-1) and fraction 3 (ML-3) were found to be the most active fractions. Thus, fraction 1 (ML-1, ~10.5 g) was further subjected onto an open silica gel (SiO_2) column chromatography (6.0 × 60 cm; 40–63 μm particle size), eluted with *n*-hexane/acetone (from 20:1 to 1:5) to afford four sub-fractions (ML-1.1 to ML-1.4) and compound **6** (2.0 mg). Purification of sub-fraction ML-1.1 (153 mg) by an open silica gel column chromatography (2.0 × 80 cm, 40–63 μm particle size), using an isocratic solvent system of chloroform/methanol (25:1), afforded compounds **1** (5.9 mg) and **2** (4.6 mg), respectively. Similarly, compounds **3** (8.2 mg) and **7** (53.6 mg) were also purified from subfraction ML-1.2 (213 mg) using an open SiO_2 (40–63 μm particle size) column chromatography (2.5 × 80 cm), eluted with an isocratic solvent system of chloroform/methanol (20:1). Subfraction ML-1.3 was also purified by an open silica gel column chromatography (2.0 × 80 cm, 40–63 μm particle size), using an isocratic solvent system of chloroform/methanol (20:1) to afford compounds **4** (22.6 mg) and **5** (34.5 mg). Further purification of subfraction ML-1.4 by semi-preparative Gilson HPLC [using an isocratic solvent system of 79% MeOH in H_2O (flow rate 2 mL/min) over 40 min; UV

detections at 205 and 254 nm; RS Tech Optima Pak C_{18} column (10 × 250 mm, 10 μm particle size), resulted in the isolation of compounds **20** (5.0 mg; t_R = 28.1 min) and **21** (4.0 mg; t_R = 35.5 min), respectively.

Fraction 3 (ML-3, ~14 g) was also subjected to a silica gel column chromatography (6.0 × 60 cm; 63–200 μm particle size) and eluted with a stepwise gradient solvent system of *n*-hexane/acetone (from 15:1 to 1:5) to afford compound **8** (25.6 mg) and six sub-fractions (ML-3.1 to ML-3.6). Further purification of subfraction ML-3.2 by semi-preparative Gilson HPLC [using Shodex C18M-10E column (10 × 250 mm, 10 μm particle size); mobile phase MeOH/H_2O (85:15), isocratic; flow rate 2 mL/min; UV-detections at 205 and 254 nm], resulted in the isolation of compounds **9** (1.8 mg; t_R = 17.8 min), **10** (10.5 mg, t_R = 20.5 min), and **11** (12.1 mg, t_R = 23.9 min), respectively. Similarly, subfraction 3 (ML-3.3, 1500 mg) was also purified by Gilson HPLC system with same column, using an isocratic solvent system of 80% MeOH in H_2O containing 0.1% formic acid, over 30 min, gave compounds **13** (4.2 mg, t_R = 24.5 min), **15** (98.5 mg, t_R = 27.1 min), and **16** (6.5 mg, t_R = 19.5 min), respectively. Compounds **12** (2.5 mg), **14** (5.6 mg) and **18** (62 mg) were isolated from sub-fraction ML-3.4 by semi-preparative Gilson HPLC systems [using J.sphere ODS-H80 column (20 × 150 mm, 4 μm particle size); mobile phase MeOH in water (MeOH:H_2O = 75:25) for 35 min; flow rate 3 mL/min; UV-detection at 205 and 254 nm]. Finally, compound **17** (12.9 mg) and compound **19** (550 mg) were isolated by repeated column chromatography over an RP-C18 (3.5 × 60 cm; 150 μm particle size, Merck) using a gradient solvent system of MeOH/H_2O from 2:3 to 3:2, each 3 L.

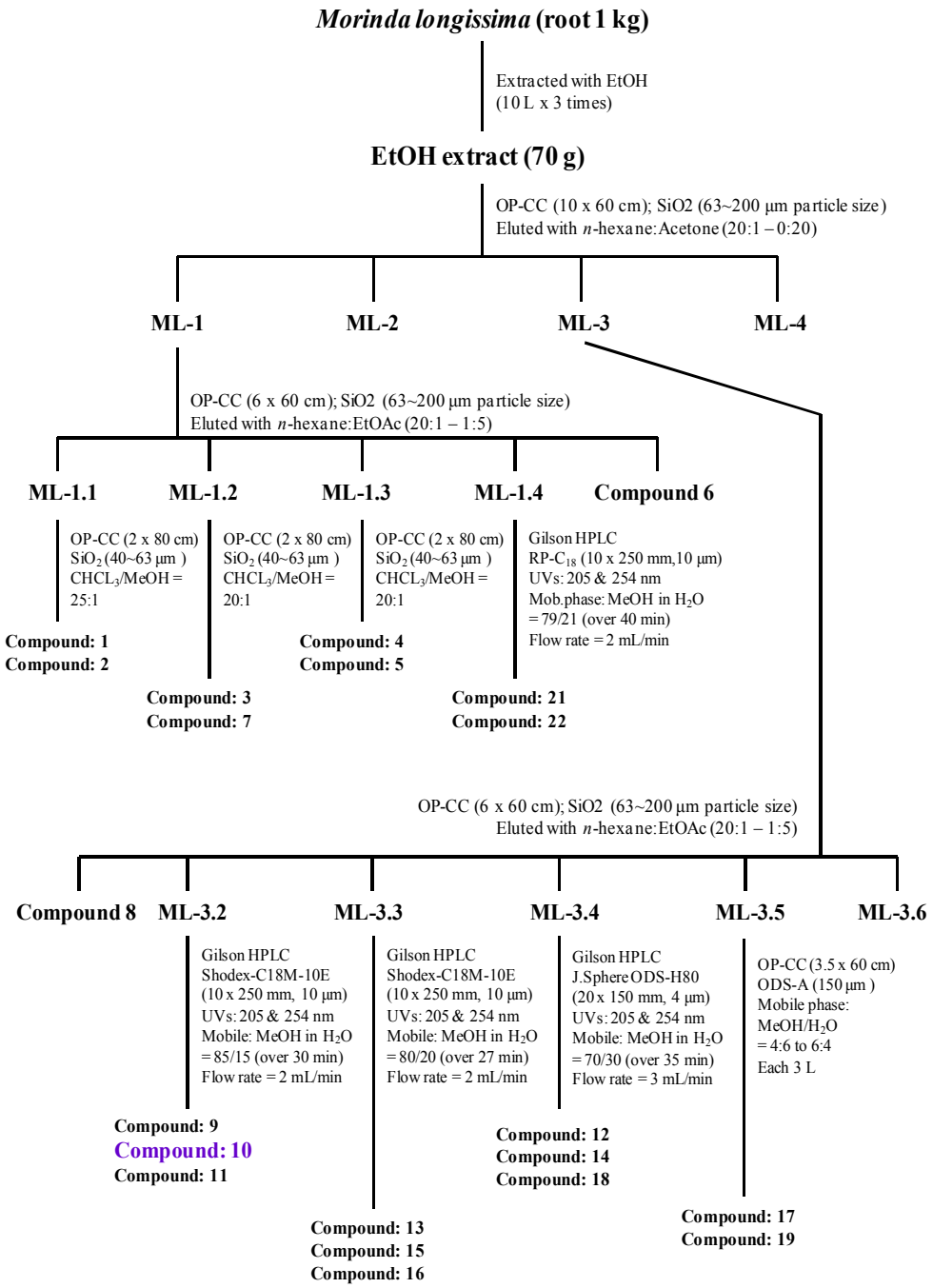

Scheme 1. The isolation scheme of isolated anthraquinones (**1-22**) from the EtOH-soluble extract of the root of *Morinda longissima*.

2.2.2. Isolation of compounds from fermented *Morinda citrifolia*

The fermented noni powder (*Morinda citrifolia*) (Noni, 1.58 kg) was extracted with MeOH (5 L × 3 time) at room temperature using sonication for 5 h. After removing the solvent under reduced pressure, the residue (155 g) was successively partitioned with EtOAc (1.5 L × 4 time). The EtOAc-soluble fraction was then filtrated and concentrated to give a darkness residue (94.6 g). A part of this (90 g) was chromatographed on an open silica gel column (10 × 60 cm; 63–200 μm particle size, Merck) using a stepwise gradient of *n*-hexane/acetone (20:1 to 1:20) yielded compound **39** (1g, eluted with H:A = 15:1) and six combined fractions (MC-1 to MC-6) according to their TLC profiles. Fraction 3 (MC-3, ~5 g) was further subjected onto an open reverse phase (RP) column chromatography (5.0 × 60 cm; 75 μm particle size), eluted with MeOH:H_2O (from 1:1 to 3:1, each 2.5 L) resulted in the isolation of compounds **22** (7.4 mg), **23** (17.6 mg), and **24** (5.5 mg). Similarly, fraction 4 (MC-4, ~10 g) was also subjected onto an open RP column chromatography (5.0 × 60 cm; RP-C18, 75 μm particle size), eluted with MeOH:H_2O (from 4:6 to 6:1, each 3 L) afforded subfractions MC-4.1, MC-4.2, compound **26** (158 mg), subfraction MC-4.4 and compound **27** (10.4 mg). Further purification of sub-fraction MC-4.2 by semi-preparative Gilson HPLC [using an isocratic solvent system of 15% MeOH in H_2O (flow rate 2 mL/min) over 40 min; UV detections at 205 and 254 nm; RS Tech Optima Pak C_{18} column (10 × 250 mm, 10 μm particle size), resulted in the isolation of compounds **31** (100 mg; t_R = 28.6 min) and **25** (14.8 mg; t_R = 39.0 min), respectively. The same application, compounds **30** (27.1 mg; t_R = 32.1 min), **30** (8.5 mg; t_R = 40.0 min), and **28** (4.3 mg; t_R = 46.4 min) were also purified from subfraction MC-4.4 by the same Gilson

HPLC systems using an isocratic solvent system of 12% MeCN in H_2O + 0.1% formic acid (flow rate 2 mL/min) over 50 min.

Fraction 5 (MC-5, ~15 g) was fractionated using MPLC systems (EYELA ceramic pump VSP-1200, Japan) with an plastic column (6.0 × 20 cm); RP-C8 (75 μm particle size), eluted with MeOH:H_2O (from 1:10 to 10:1, each 2.5 L) to give five subfractions (MC-5.1 to MC-5.5) and compound **40** (15.8 mg). Subfraction MC-5.1 was further purified by Gilson HPLC system [using an isocratic solvent system of 23% MeOH in H_2O + 0.1% formic acid (flow rate 2 mL/min) over 35 min; UV detections at 205 and 254 nm; RS Tech Optima Pak C_{18} column (10 × 250 mm, 10 μm particle size), resulted in the isolation of compounds **32** (8 mg; t_R = 18.6 min), **33** (5.3 mg; t_R = 21.5), and **34** (4.8 mg; t_R = 32.1 min), respectively. The same application, subfraction MC-5.2 was also purified by Gilson HPLC system [using an isocratic solvent system of 48% MeOH in H_2O + 0.1% formic acid (flow rate 2 mL/min) over 35 min; UV detections at 205 and 254 nm; RS Tech Optima Pak C_{18} column (10 × 250 mm, 10 μm particle size), resulted in the isolation of compounds **43** (155 mg; t_R = 20.1 min), **44** (7.3 mg; t_R = 24.8), and **45** (30 mg; t_R = 29.2 min), respectively. With the same system, subfraction MC-5.3 was purified by HPLC using 24% of MeCN in H_2O + 0.1% formic acid, flow rate was set at 2 mL/min, over 45 min, resulted in the isolation of compounds **42** (4.0 mg; t_R = 25.9 min), **51** (2.9 mg; t_R = 34.8 min), **52** (1.5 mg; t_R = 37.5 min), and **53** (3.3 mg; t_R = 39.6 min), respectively. The same application, compound **45** (3.7 mg; t_R = 20.1 min) and **54** (16.0 mg; t_R = 30.0 min) were isolated from subfraction MC-5.4, compound **46** (7.8 mg; t_R = 22.2 min) and **35** (2.7 mg; t_R = 25.9 min) were purified from subfraction MC-5.5 by eluting with isocratic solvent system of 50% and 60% of MeOH in H_2O + 0.1% formic acid (flow rate 2 mL/min) over 35 and 30 min,

respectively.

Fraction 6 (MC-6, ~20 g) was also fractionated by using MPLC systems (EYELA ceramic pump VSP-1200, Japan) with an plastic column (6.0 × 20 cm); RP-C8 (75 μm particle size), eluted with MeOH:H_2O (from 1:15 to 1:1, each 3 L) afforded five subfractions (MC-6.1 to MC-6.5) according to their TLC profiles, and compound **56** (20 mg) and compound **41** (15 mg). Subfraction MC-6.2 was further purified by Gilson HPLC system with an RS Tech Optima Pak C_{18} column (10 × 250 mm, 10 μm particle size), eluted with an isocratic solvent system of 10% MeOH in H_2O + 0.1% formic acid (flow rate 2 mL/min) over 30 min, UV detections at 205 and 254 nm, resulted in the isolation of compounds **37** (2.2 mg; t_R = 19.8 min), **37** (222 mg; t_R = 23.1 min), and compound **38** (12.9 mg; t_R = 26.7 min), respectively. Purification of subfraction MC-6.3 by Gilson HPLC system using an Optima Pak C_{18} column (10 × 250 mm, 10 μm particle size), eluted with an isocratic solvent system of 20% MeCN in H_2O + 0.1% formic acid (flow rate 2 mL/min) over 50 min, UV detections at 205 and 254 nm, resulted in the isolation of compounds **55** (2.1 mg; t_R = 20.1 min), **47** (2.3 mg; t_R = 27.4), **48** (35.5 mg; t_R = 33.4), and **49** (20.8 mg; t_R = 37.6 min), respectively. Similarly, compounds **57** (4.5 mg; t_R = 22.2 min), **58** (150 mg; t_R = 24.3 min), and **59** (14 mg; t_R = 28.5 min) were purified from subfraction MC-6.4 by Gilson HPLC system using an Optima Pak C_{18} column (10 × 250 mm, 10 μm particle size), eluted with an isocratic solvent system of 26% ACN in H_2O + 0.1% formic acid (flow rate 2 mL/min) over 40 min, respectively.

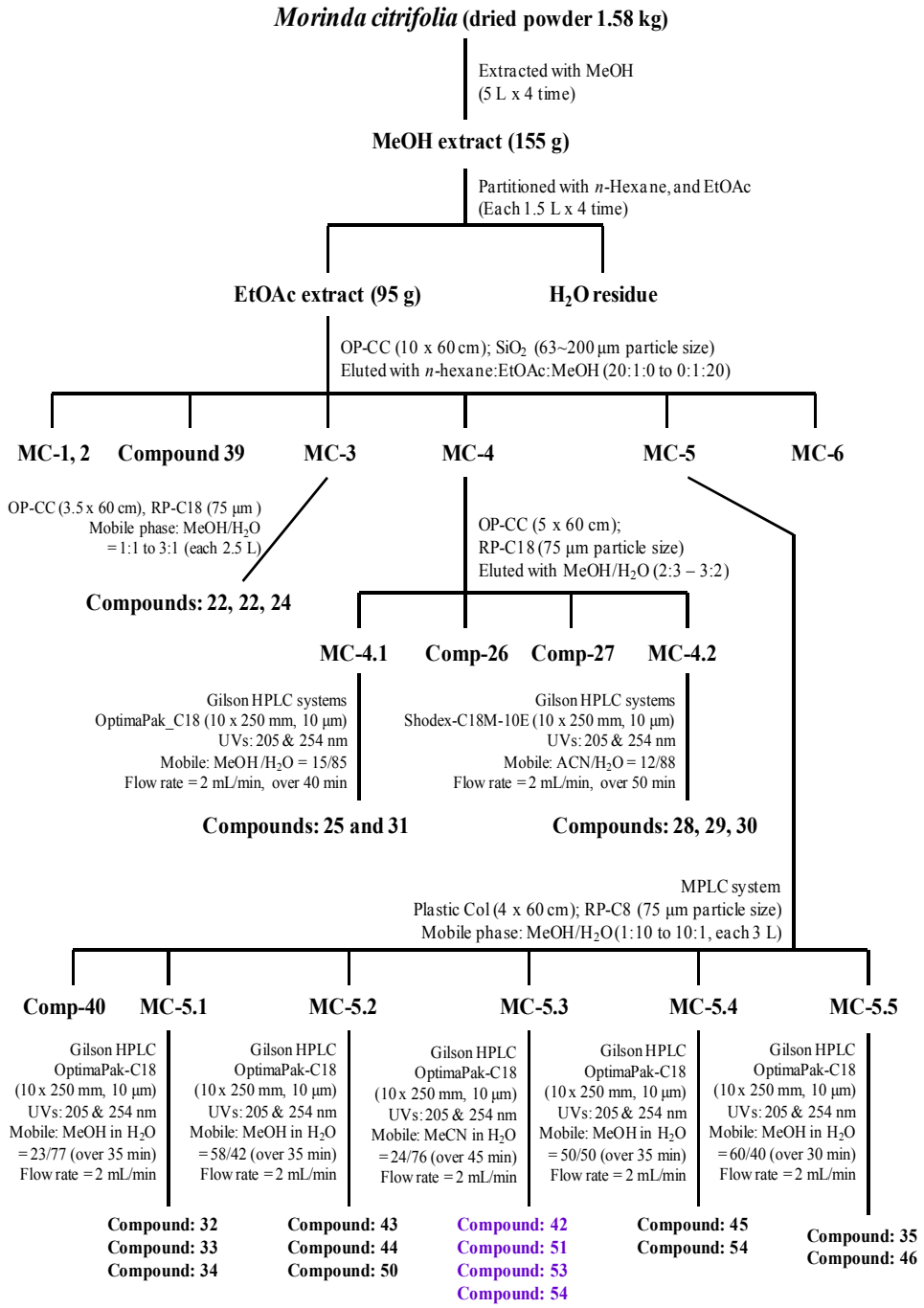

Scheme 2. The isolation scheme of compounds (**23-60**) from the MeOH extract of the dried fermented powder of *Morinda citrifolia* (Noni).

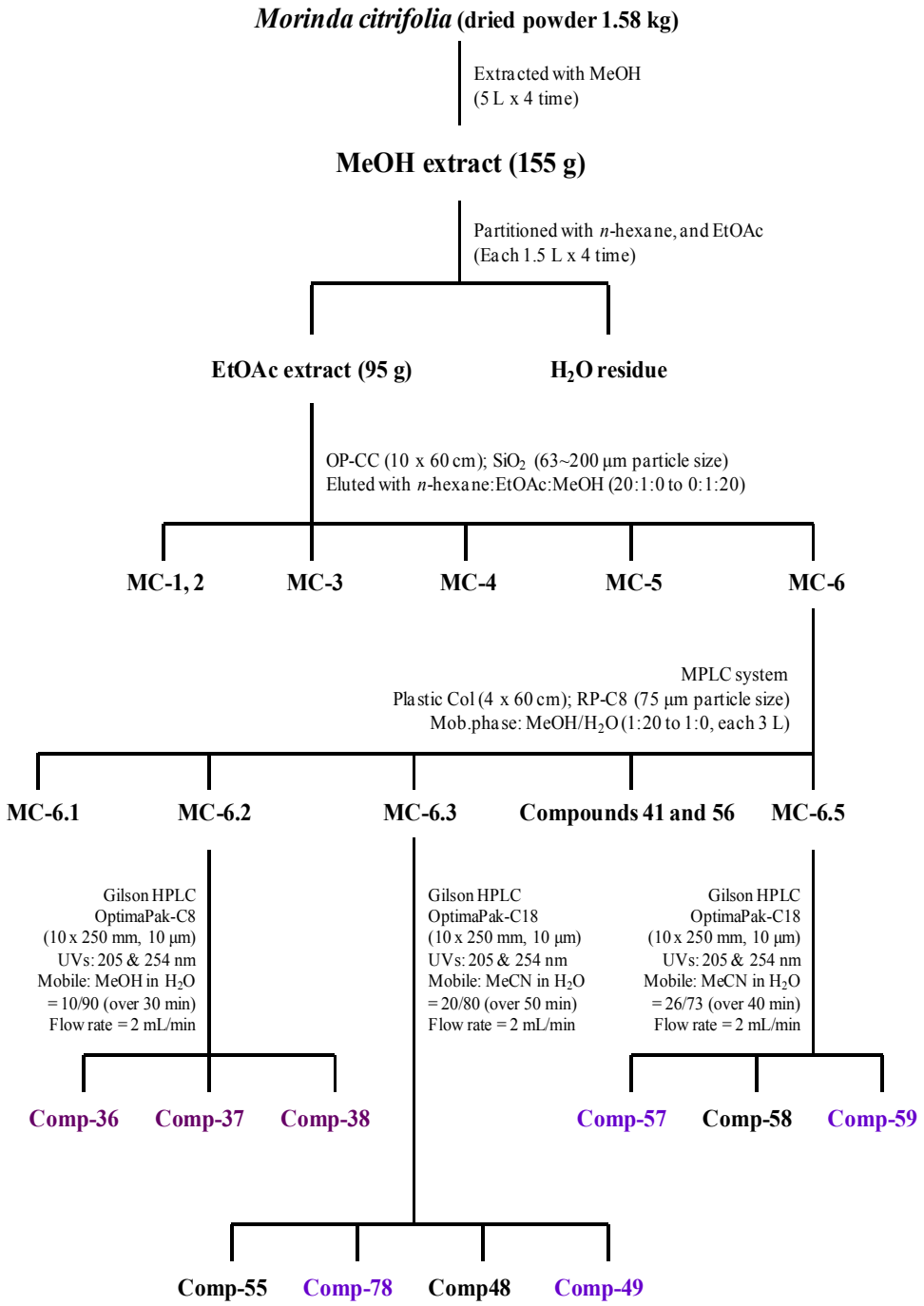

Scheme 3. The isolation scheme of compounds (**23-60**) from the MeOH extract of the dried fermented powder of *Morinda citrifolia* (Noni).

2.2.3. Cell culture and induction of 3T3-L1 adipocytes

3T3-L1 pre-adipocytes were maintained for 48 h in Dulbecco's Modified Eagle's Medium (DMEM) supplemented with 10% calf serum (CS), and pen/strep (50 unit/mL penicillin and 50 μg/mL streptomycin), an atmosphere of 95% air and 5% CO_2 at 37 ^{o}C. To induce adipogenesis, the media was changed to DMEM supplemented with 10% fetal bovine serum (FBS), 0.5 mM 3-isobutyl-1-methyl-xanthine, 2 μg/ml dexamethasone, 1 μg/mL insulin, 1 μM rosiglitazone, and pen/strep and further cultured for 48 h. Every 2 days thereafter, the cells were incubated with fresh DMEM supplemented with 10% FBS, 1 μM rosiglitazone, 1 μg/mL insulin, and pen/strep. 3T3-L1 adipocytes were used for experiments 7 days after the induction of differentiation.

2.2.4. 2-NBDG assay for measuring glucose uptake

NBDG assay was performed as previously described with some modifications.[27] Briefly, differentiated 3T3-L1 adipocytes (3×10^4 cells/well) were seeded in a 24-well tissue culture plate (BD Falcon, NJ, USA) and cultured in glucose-free culture media supplemented with 10% FBS and pen/strep for treating NBDG with or without compounds of interest. Compounds were treated at a concentration of 10 μM. 2 μg/mL of insulin served as a positive control. After 90 min, cells were rinsed with 1 mL of PBS prior to measuring fluorescent signals (Excitation 450 nm and Emission 535 nm) using the VICTOR™ X3 Multilabel Plate Reader fluorescent reader (PerkinElmer).

2.2.5. Cell culture and differentiation of myoblasts

Mouse C2C12 skeletal myoblasts were maintained in DMEM supplemented with 10% fetal bovine serum in an atmosphere containing 95% air and 5% CO_2 at 37 ^{o}C. To prepare for each assay, the cells were seeded in 12-well plates at 10^5 cells/well in 2 mL of growth medium. The differentiation of C2C12 myoblasts was induced by replacing the growth medium with DMEM containing 5% horse serum when the cells were confluent. The medium was changed every 48 h until the formation of myotubes was observed. The cells were used in the experiments after differentiation.

2.2.6. AMPK Assay (Immunoblot analysis)

The C2C12 myotubes were incubated with the appropriate concentration of the compounds for 30 min and then lysed in an EBC lysis buffer [50 mM Tris-HCl (pH 7.6), 120 mM NaCl, 1 mM EDTA (pH 8.0), 0.5% nonidet-P40 (NP-40), and 50 mM NaF]. The cell debris was removed by centrifugation at 12,000 rpm for 15 min, at 4 ^{o}C. The protein concentrations in the cell lysates were determined using a Bio-rad protein assay kit. Approximately 30 μg of proteins from the total cell extracts was subjected to western blot analysis using anti-phosphospecific AMPKα Thr^{172} and anti-phosphospecific ACC Ser^{79}. The β-actin protein levels were used as a control fJor equal protein loading. The immunoreactive antigen was then recognized using a horseradish peroxidase-labeled anti-rabbit IgG and an enhanced chemiluminescence detection kit.[28]

III. RESULTS AND DISCUSSION

3.1. Structural determination of isolated compounds (1-21) from *Morinda longissima*.

3.1.1. Structural characterization of 9,10-anthraquinones

Repeated column chromatography (silica gel, RP-18, and semi-preparative HPLC) of the EtOAc-soluble extract of the root of *M. longissima* resulted in the isolation of 21 anthraquinone derivatives (**1-21**), including a novel named as modasima A (**10**). The known compounds were determined by detailed analyses of their spectroscopic (^{1}H and ^{13}C NMR) data and comparison of their physicochemical properties with those reported in literature. Thus, chemical structures of the known anthraquinones were characterized to be 1-hydroxy-anthraquinone (**1**),[29] tectoquinone (**2**),[30] rubiadin-dimethyl ether (**3**),[30] 1-hydroxy-2-methyl-9,10-anthraquinone (**4**),[30] rubiadin-3-methyl ether (**5**),[30] 1,2-dihydroxy-3-methoxy-anthraquinone (**6**),[30] 1,3-dimethoxy-2-methoxymethylanthraquinone (**7**),[30] 1-methoxy-2 ,2 -dimethyldioxine-(5 ,6 :2,3)-anthraquinone (**8**),[31] lucidin-ω-butyl ether (**9**),[31] rubiadin (**11**),[32] 3-hydroxy-2-methylanthraquinone (**12**),[30, 32] 1-methoxy-3-hydroxy-2-methoxymethylanthraquinone (**13**),[30, 32] 2-methoxy-3-methyl-anthraquinone (**14**),[33] damnacanthol-ω-ethyl ether (**15**),[34] lucidin-ω-methyl ether (**16**),[34] 1-methoxy-2,3-dihydroxy-anthraquinone (**17**),[30, 34] rubiadin-1-methyl ether (**18**),[30, 34] damnacanthol (**19**),[30, 34] 1-hydroxy-6methoxy-2methyl-9,10-anthracenedione (**20**),[12] and soranjidiol (**21**).[30, 34] The new compound was determined by fully studies of 1D, 2D (HSQC, COSY, HMBC, and NOESY) NMR spectroscopic data, and physicochemical (IR, UV, $[\alpha]_D$) data analyses.

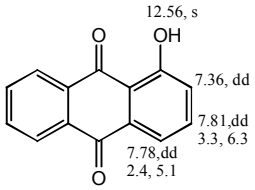

1

1-hydroxy-anthraquinone

Chemical Formula: $C_{14}H_8O_3$
Exact Mass: 224.0473
Molecular Weight: 224.2115

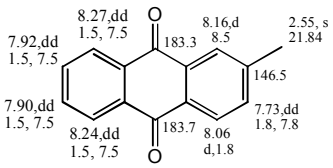

2

tectoquinone

Chemical Formula: $C_{15}H_{10}O_2$
Exact Mass: 222.0681
Molecular Weight: 222.2387

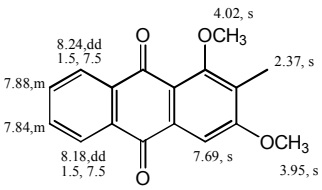

3

rubiadin-dimethyl ether

Chemical Formula: $C_{17}H_{14}O_4$
Exact Mass: 282.0892
Molecular Weight: 282.2907

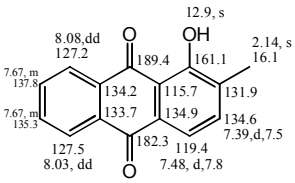

4

1-hydroxy-2-methyl-9,10-anthraquinone

Chemical Formula: $C_{15}H_{10}O_3$
Exact Mass: 238.0630
Molecular Weight: 238.2381

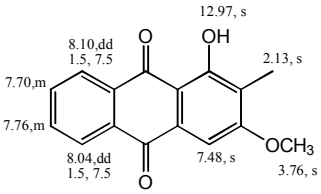

5

Rubiadin-3-methyl ether

Chemical Formula: $C_{16}H_{12}O_4$
Exact Mass: 268.0736
Molecular Weight: 268.2641

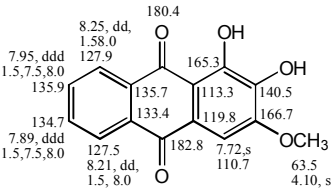

6

1,2-dihydroxy-3-methoxy-anthraquinone

Chemical Formula: $C_{15}H_{10}O_5$
Exact Mass: 270.0528
Molecular Weight: 270.2369

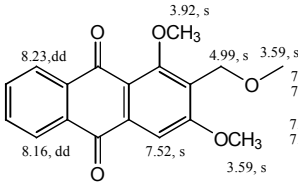

7

1,3-dimethoxy-2-methoxy methylanthraquinone

Chemical Formula: $C_{18}H_{16}O_5$
Exact Mass: 312.0998
Molecular Weight: 312.3166

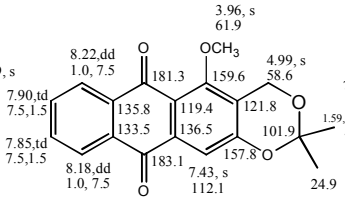

8

1-methoxy-2',2'-dimethyldioxine-(5',6':2,3)anthraquinone

Chemical Formula: $C_{19}H_{16}O_5$
Exact Mass: 324.0998
Molecular Weight: 324.3273

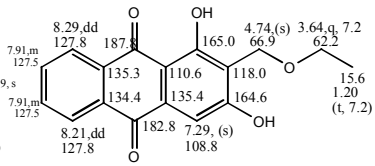

9

lucidin-w-butyl ether

Chemical Formula: $C_{17}H_{14}O_5$
Exact Mass: 298.0841
Molecular Weight: 298.2901

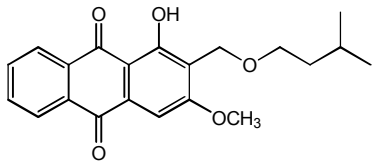

10

Modasima A

Chemical Formula: $C_{21}H_{22}O_5$
Exact Mass: 354.1467
Molecular Weight: 354.3964

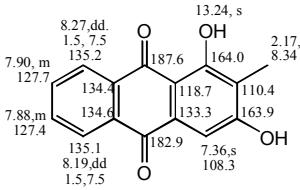

11

Rubiadin

Chemical Formula: $C_{15}H_{10}O_4$
Exact Mass: 254.0579
Molecular Weight: 254.2375

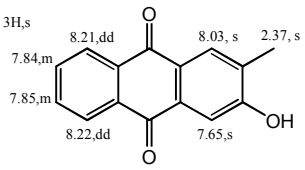

12

3-hydroxy-2-methylanthraquinone

Chemical Formula: $C_{15}H_{10}O_3$
Exact Mass: 238.0630
Molecular Weight: 238.2381

Figure 9: Chemical structure of isolated compounds **1-12** from *Morinda longissima*

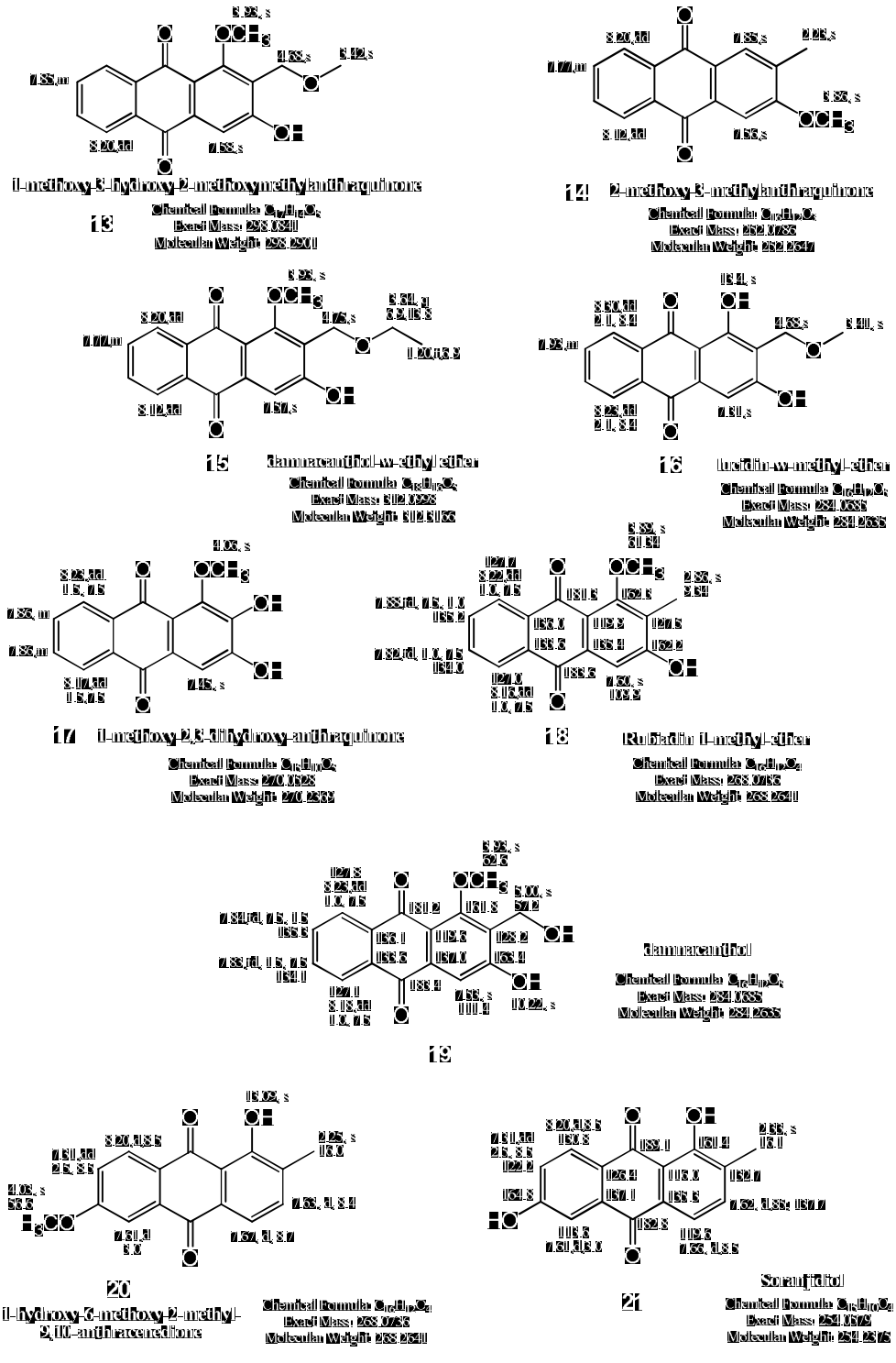

Figure 10: Chemical structure of isolated compounds **13-21** from *Morinda longissima*

3.1.2. Structural determination of new anthraquinone 10

Compound **10** was isolated as yellowish amorphous powder. A molecular formula of $C_{21}H_{22}O_5$ was determined for this compound from the molecular ion peak at *m/z* 354.1465 $[M]^+$ (calcd. for $C_{21}H_{22}O_5$, 354.1467), obtained by HREIMS.

The IR spectrum of compound **10** suggested the presence of a hydroxy group at 3395 cm^{-1}, 2923 (C─C), 1670-1631 (C=O), 1594, 1364-1256, and 1124 cm^{-1}. The UV spectrum showed absorption maxima at 240, 274, 316, and 371 nm and the ^{13}C NMR gave two quaternary carbonyl resonances at δ_C 181.4 and 183.9, suggesting a structure of 9,10-anthraquinone.[32b, 35]

The ^1H NMR spectrum in the aromatic region showed two broad doublets at δ_H 8.17 and 8.23 (each 1H, br, d, J = 7.6 Hz), integrating for two H-atoms at C-5 and C-8, and two broad triplets at δ_H 7.86 (br, t, J = 7.6 Hz, H-6), 8.23 (br, t, J = 7.6 Hz, H-7), indicating a typical A_2B_2 system of a 1,2-disubstituted aromatic ring. The above data together with a proton *singlet* observed at δ_H 7.59 indicated that **10** was an anthraquinone possessing a tri-substituted C-ring. The phenolic OH-C(1) appeared at 13.19 ppm in the ^1H NMR measured in chloroform (Data not shown) was the result of a H-bond with the C(9)=O group. This is indicated that the hydroxy group was located at the *peri* position to the C-9 carbonyl group.[35] One methoxy group was also observed [δ_H 3.94 (3H, s) and δ_C 63.5]. Other ^1H NMR signals were of a 2H-singlet of hydroxymethyl protons at δ_H 4.76 and an isopentyloxy group [δ_H 3.63 (2H, t, J = 6.8 Hz), 1.51 (1H, q, J = 6.4 Hz), 1.72 (1H, m), and 0.90 (6H, d, J = 6.4 Hz)], it was further supported by ^1H-^1H COSY, and HMBC

experiments (Figure 10).

The connectivity of this group to C-2 through the hydroxymethyl group (C-1') was confirmed using an HMBC experiment, showing correlations between H-2' (δ_H 3.63) and C-1' (δ_C 64.0), and from H-1' (δ_H 4.76) to C-1 (δ_C 163.9), C-2 (δ_C 126.8), and C-3 (δ_C 163.5).

Only one cross-cross peak correlation between the methoxy protons (δ_H 3.94) and C-3 (δ_C 163.5) was observed, indicating that the methoxy group was attached to C-3. The aromatic singlet proton at C-4 (δ_H 7.59) showed HMBC correlations with carbons at C-10 (δ_C 183.9), C-13, C-14, and C-2, C-3 (Figure 10), further supported this conclusion. From the above data obtained, compound **10** was thus determined to be 1-hydroxy-2-((isopentyloxy)methyl)-3-methoxy-9,10-anthraquinone, and named modasima A.

Compound 10 (modasima A): Yellowish amorphous powder; IR (KBr): ν_{max} 3395, 2923, 1670, 1631, 1594, 1364-1256, 1124, and 713 cm^{-1}; UV (*c* 0.025, MeOH) λ_{max} nm: 210, 240, 274, 316, 371 nm; HREIMS *m/z* 354.1465 $[M]^+$, (calcd. $C_{21}H_{22}O_5$, 354.1467).

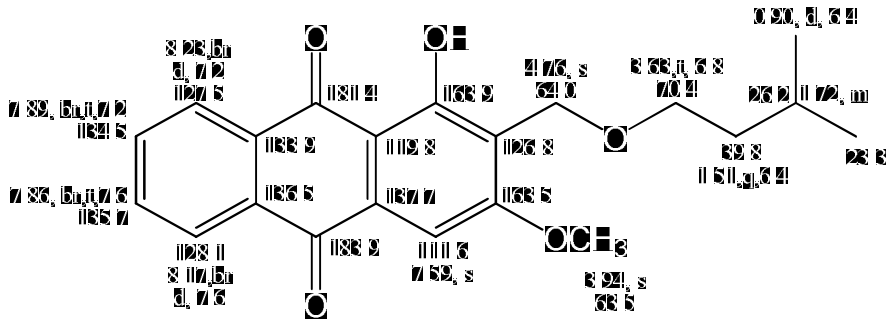

^{1}H & ^{13}C NMR data of compound 10

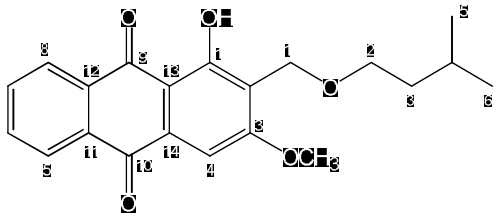

Chemical structure of compound 10

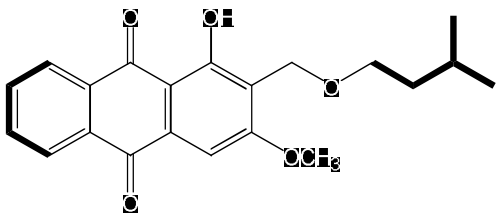

(1H – 1H) COSY correlations of compound 10

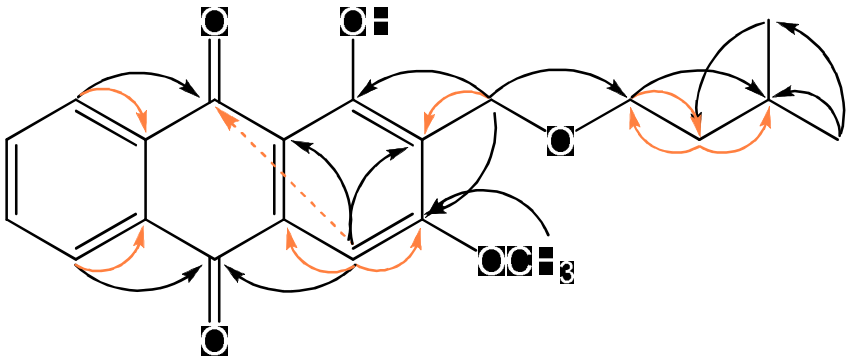

HMBC correlations of compound 10 (^{1}H – ^{13}C)

= large cross peak signal assignable for 3 bond correlation

= medium/ or small signal assignable for 2 or 4 bond correlation

Figure 11: Chemical structure, 1D NMR, COSY, and HMBC correlation of compound **10**

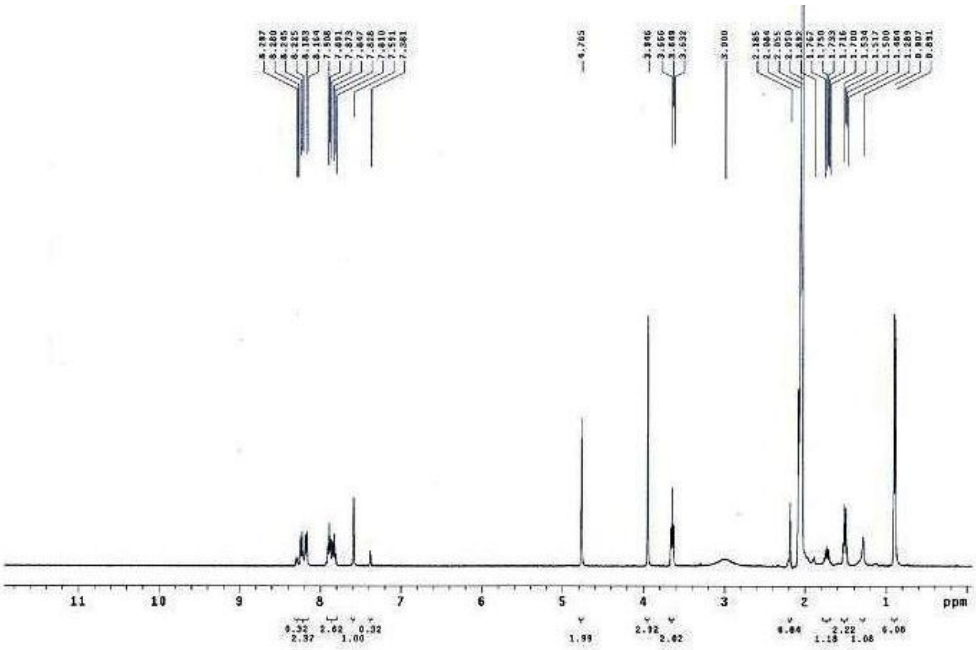

Figure 12: ^{1}H-NMR spectrum of compound **10** (400 MHz, acetone-d_6)

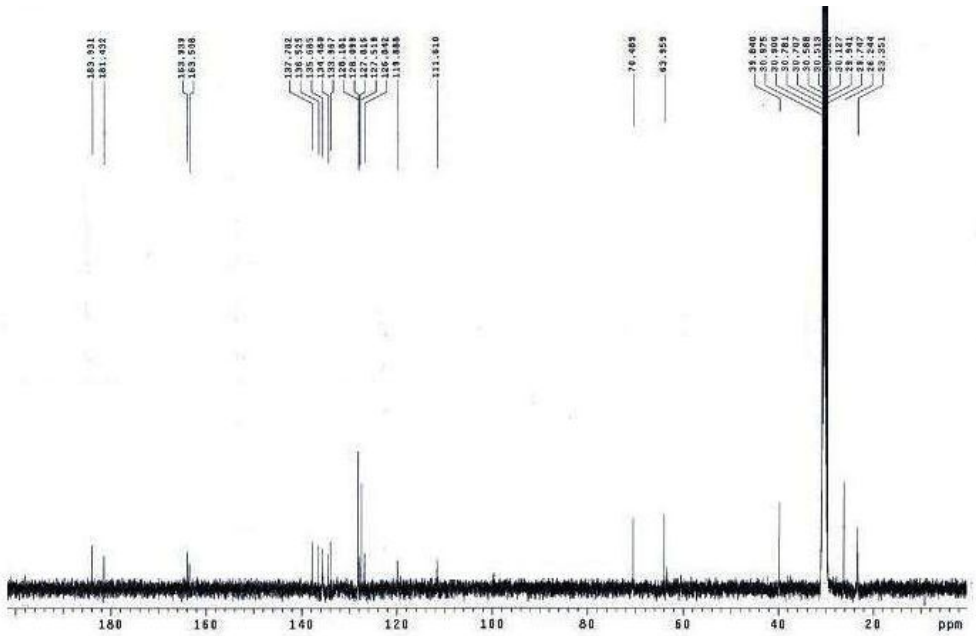

Figure 13: ^{13}C-NMR spectrum of compound **10** (100 MHz, acetone-d_6)

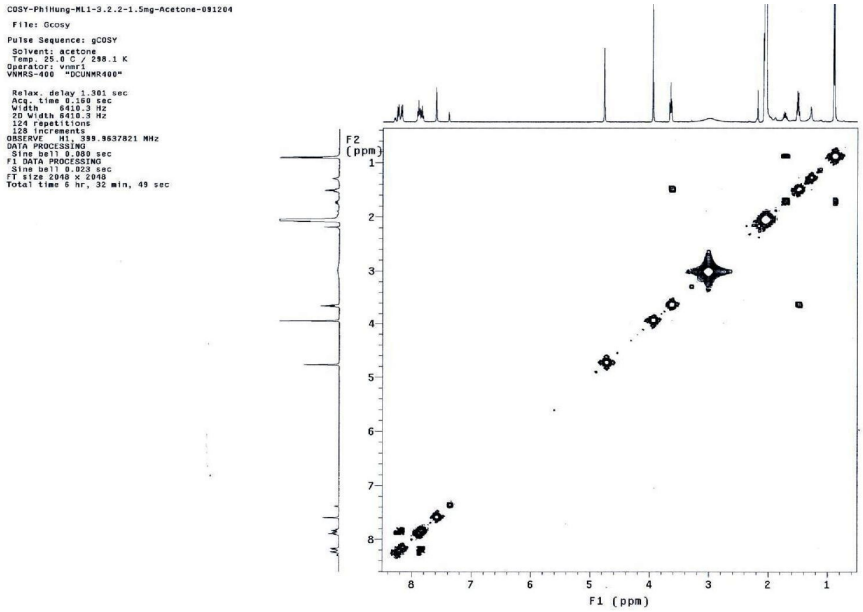

Figure 14: COSY spectrum of compound **10** (400 MHz, acetone-d_6)

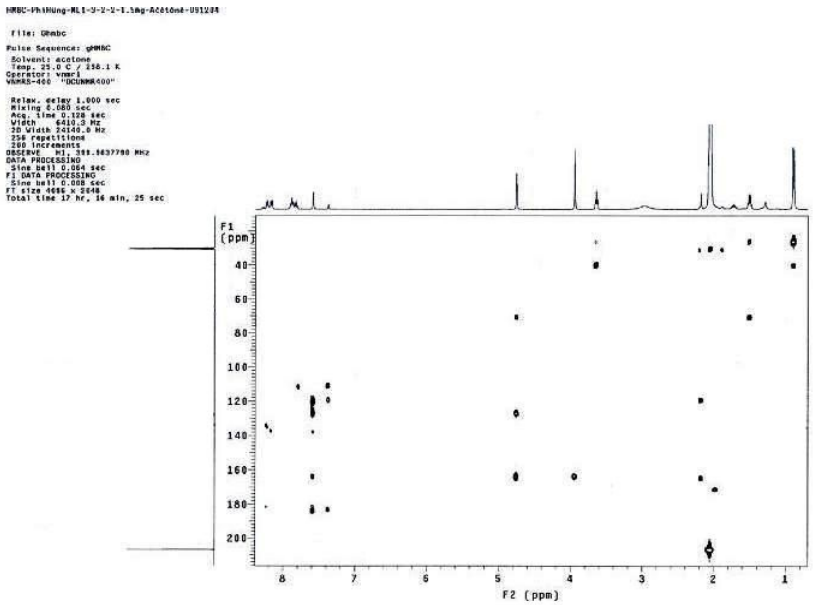

Figure 15: HMBC spectrum of compound **10** (400 MHz, acetone-d_6)

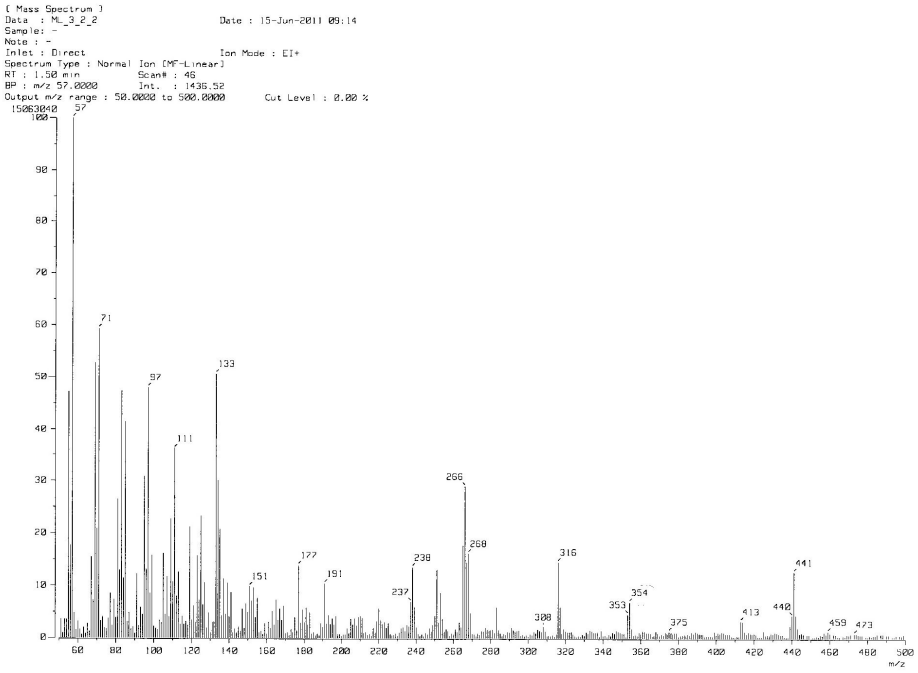

[Elemental Composition] Page: 1

Data : ML_3_2_2 Date : 28-Jun-2011 08:46
Sample: -
Note : -
Inlet : Direct Ion Mode : EI+
RT : 1.97 min Scan#: 60
Elements : C 100/1, H 100/1, O 10/1
Mass Tolerance : 1mmu
Unsaturation (U.S.) : 0.0 - 30.0

Observed m/z	Int%	Err[ppm / mmu]	U.S.	Composition
354.1465	34.7	-0.7 / -0.2	11.0	C 21 H 22 O 5

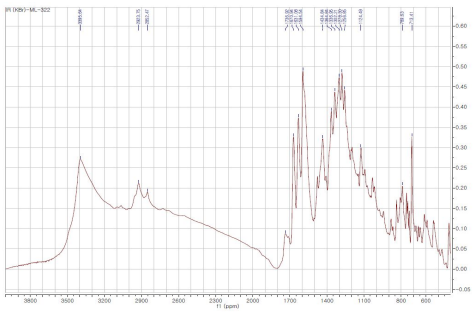

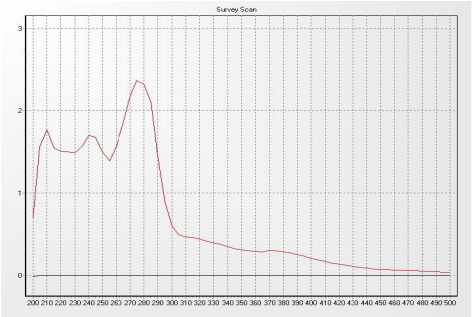

Fig. 16: HR-EI-MS, IR (KBr, left) and UV (c = 0.025, MeOH) spectra of compound **10**

3.2. Structural determination of compounds isolated from *Morinda citrifolia*

Repeated column chromatography (open silica gel, RP-18, and semi-preparative MPLC and HPLC systems) of the EtOAc-soluble fraction of the MeOH extract of *M. citrifolia* (Noni) resulted in the isolation of 38 natural products, consisting of two coumarins (**23**, **26**), five phenyl propanoids (**22**, **24**, **25**, **26**, and **35**), eight caffeic acid derivatives (**28-34**), three iridoids (**36-38**), a triterpenoid (**39**), two flavonoids (**40-41**), and 18 lignans (**42-59**). Of which, 8 compounds were isolated as new natural lignans and neolignans (**42**, **47**, **49**, **51-53**, **57**, and **59**) by interpretation of their 1D NMR (^{1}H and ^{13}C) and 2D NMR (COSY, HSQC, HMBC, NOESY, and MS) data, together with analyses of the physicochemical (including IR, UV, $[\alpha]_D$, and CD) data.

The other known compounds were elucidated and classified according to their structural skeletons by detailed analyses of their spectroscopic (^{1}H, ^{13}C NMR, and MS) data and comparison of their physicochemical properties with those reported in literature. Thus, chemical structures of the known compounds were characterized to be scoparone (**23**),[36] scopoletin (**26**),[36] 3-(2-hydroxy-4,5-dimethoxyphenyl)propanoic acid (**22**),[36] 3-(4-hydroxy-2,5-dimethoxyphenyl)propionic acid (**24**),[58] methyl 3-(2-hydroxy-4,5-dimethoxyphenyl)propionate (**25**),[58] methyl 3-(2,4-dihydroxy-5-methoxyphenyl)propionate (**27**),[37] caffeic acid (**28**),[38] 3-hydroxy-6-methoxybenzoic acid (**29**),[38] 4-hydroxy-3-methoxybenzoic acid or vanillic acid (**30**),[38] 4-hydroxy-6-(hydroxymethyl)-2H-pyran-2-one (**31**),[39] 3,4-dihydroxybenzoic acid or protocatechuic acid (**32**),[38] 2-oxo-2H-pyran-6-carbaldehyde (**33**),[37] 4-hydroxybenzoic acid (**34**),[38] 3-methoxycaffeic acid (**35**),[38] loganic acid (**36**),[40] Asperulosidic acid (**37**),[40] loganin (**38**),[40] ursolic acid (**39**),[41] quercetin (**40**),[42] quercetin-3-O-β-D-glucose (**41**),[42] 3,3-bisdemethylpinoresinol (**43**),[43] pinoresinol (**44**),[43] lirioresinol B (**45**),[43] lirioresinol B dimethyl ether (**46**),[43] (+)-3,4,3 ,4 -tetrahydroxy-

9,7 α-epoxylignano-7α,9 -lactone (**48**),[43] americanin A (**50**),[44] arteminorin D (**54**),[45] morindolin (**55**),[44] rel-(7α,8β)-3-methoxy-4 ,7-epoxy-8,3 -oxyneolignan-4,9,9 -triol (**56**),[45] and americanoic acid A (**58**).[45]

3.2.1. Structural determination of phenylpropanoids 22, 24, 25, and 27

Compound **22**, **24**, **25**, and **27** were obtained as a brown yellowish vicious state. The ^{1}H and ^{13}C NMR spectra of these compounds were identical, presenting signals for two methoxyl groups at δ_H 3.78-3.81 (each 3H, s), two aromatic protons at δ_H 6.31-6.85 (each 1H, s), and two conjoint methylenes at δ_H 2.56-2.95 (each 2H, t, J = 7.2~7.5 Hz). The ^{13}C NMR spectra displayed 11 carbon resonances ascribable to 2 methoxyl groups (δ_C 51.6-57.2), 2 methylenes (δ_C 25.8-26.3 and 35.1~35.6), 2 methines (δ_C 105.1, and 115.9), and 5 quaternary carbons (δ_C 117.9~118.1 and 141.9~150.2). These observations indicated the structure of a α,β-saturated phenylpropanoid.[36] Detailed analysis of HMBC spectra of these compounds established that the two methoxy groups in **22** were attached at C-4 and C-5, respectively. While, one of the methoxy groups was placed at C-5 and the other was linked at C-2 in compound **24**. Similarly, compound **27** possessed two methoxyl groups; one of them was placed at C-5, the other was found to be linked at C-9 suggesting a methyl ester group. While compound **25** possessed three methoxyl groups, of which, two were assignable to C-4 and C-5, the third one was attached at C-9. Thus chemical structures of these compounds were determined to be methyl 3-(2,4-dihydroxy-5-methoxyphenyl)propionate (**22**),[36] 3-(4-hydroxy-2,5-dimethoxyphenyl)propionic acid (**24**),[36] 3-(2-hydroxy-4,5-dimethoxyphenyl)propionate (**25**),[37] and 3-(2,4-dihydroxy-5-methoxyphenyl)propionate (**27**).[37] Compounds **24** and **25** were isolated for the first time as new natural products even though they were synthesized previously.

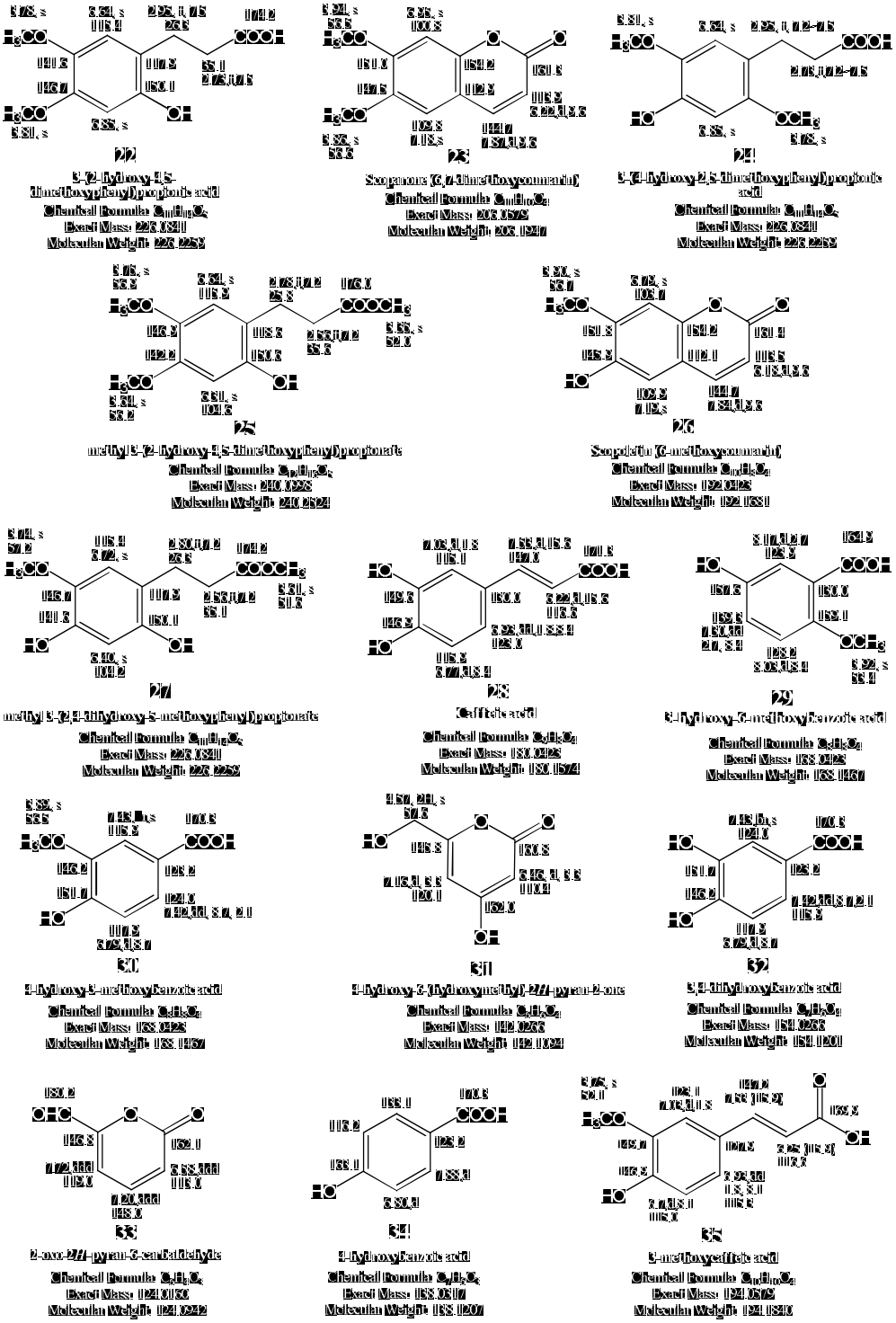

Figure 17: Chemical structure of isolated compounds **22-35** from *Morinda citrifolia*

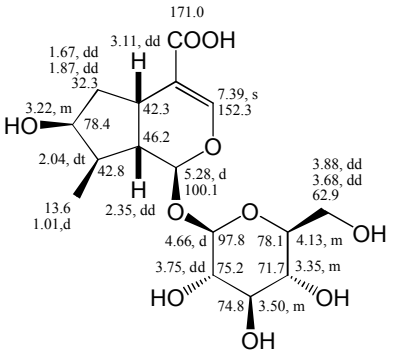

36

Loganic acid

Chemical Formula: $C_{16}H_{24}O_{10}$
Exact Mass: 376.1369
Molecular Weight: 376.3558

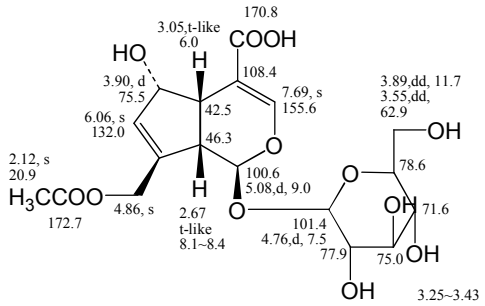

37

Asperulosidic acid

Chemical Formula: $C_{18}H_{24}O_{12}$
Exact Mass: 432.1268
Molecular Weight: 432.3760

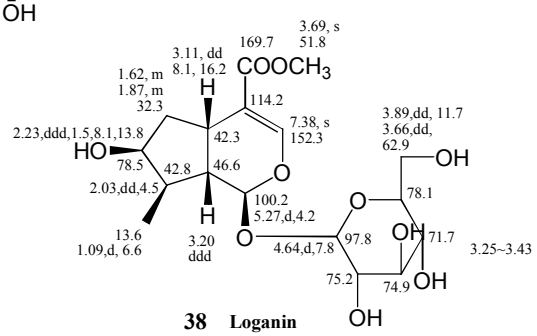

38 Loganin

Chemical Formula: $C_{17}H_{26}O_{10}$
Exact Mass: 390.1526
Molecular Weight: 390.3823

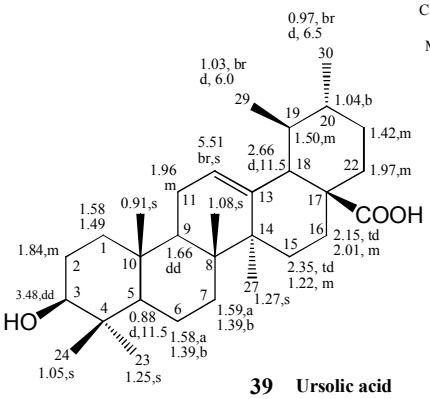

39 Ursolic acid

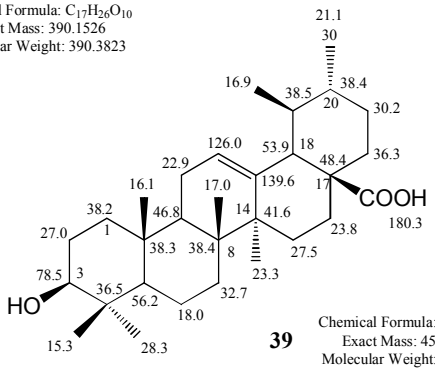

39

Chemical Formula: $C_{30}H_{48}O_3$
Exact Mass: 456.3603
Molecular Weight: 456.7003

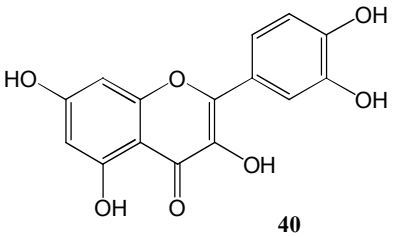

40

Quercetin

Chemical Formula: $C_{15}H_{10}O_7$
Exact Mass: 302.0427
Molecular Weight: 302.2357

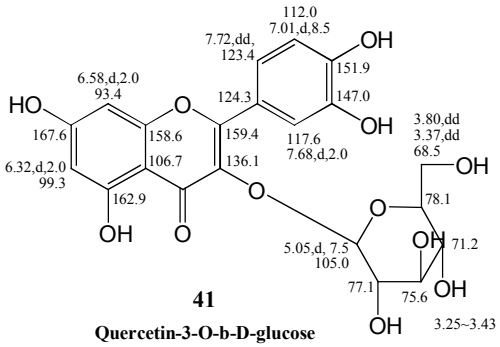

41

Quercetin-3-O-b-D-glucose

Chemical Formula: $C_{21}H_{20}O_{12}$
Exact Mass: 464.0955
Molecular Weight: 464.3763

Figure 18: Chemical structure of isolated compounds **36-41** from *Morinda citrifolia*

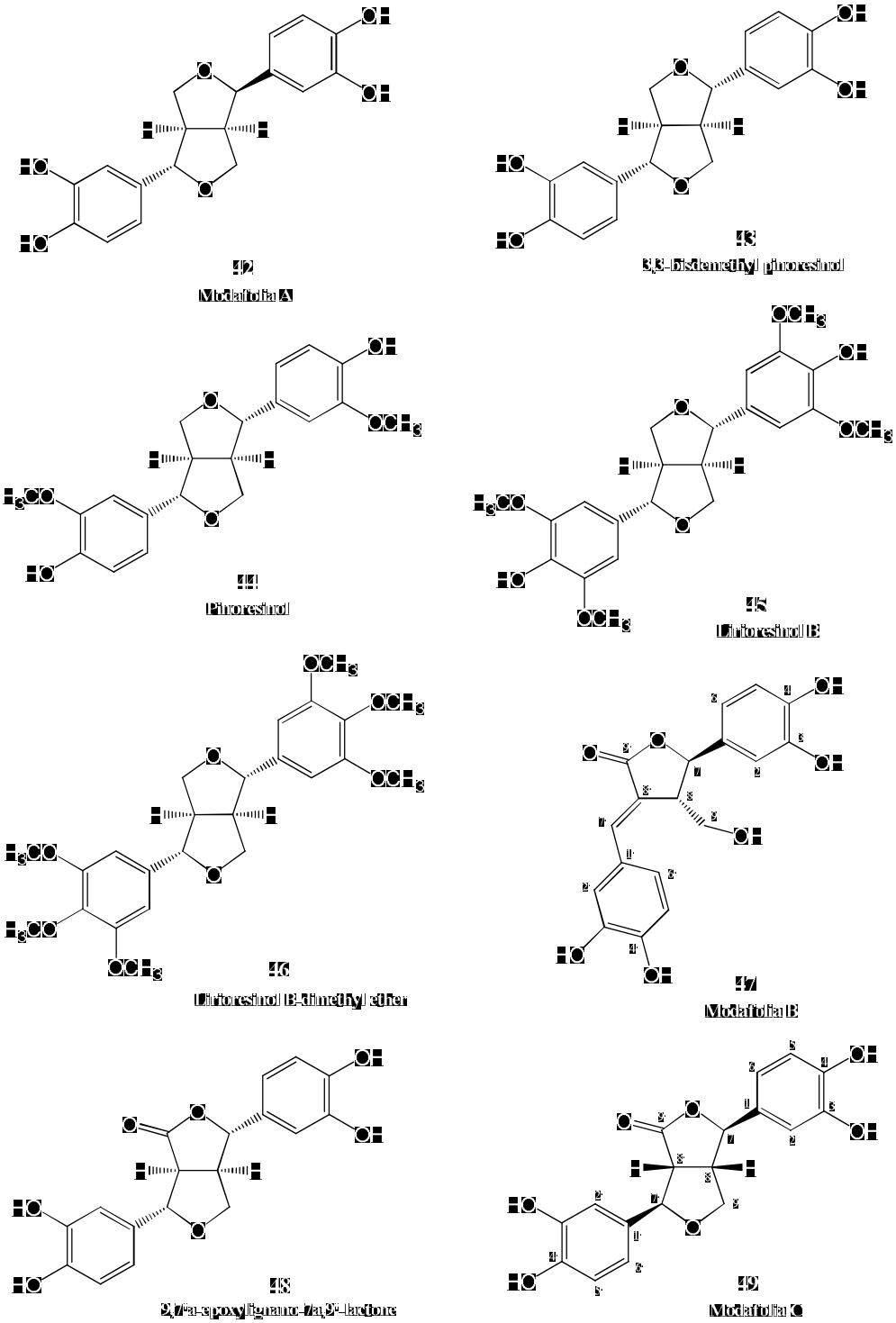

Figure 19: Chemical structure of isolated compounds **42-49** from *Morinda citrifolia*

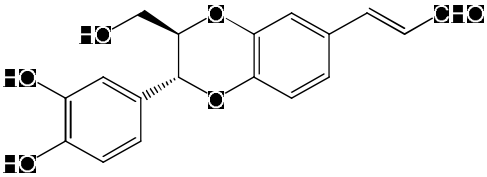

50

Americanin A

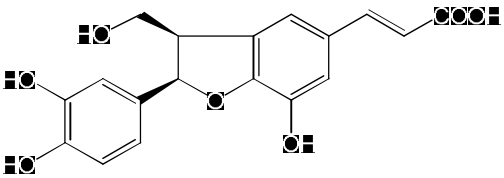

55

Morinfolin

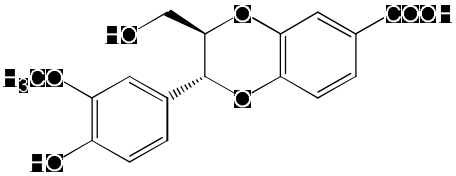

51

Molafolia D

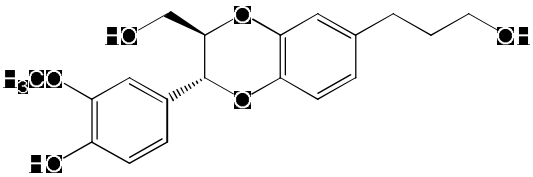

56

Rel-(7a,8b)-3-methoxy-4,7-epoxy-3,3'-oxyneolignan-4,9,9'-triol

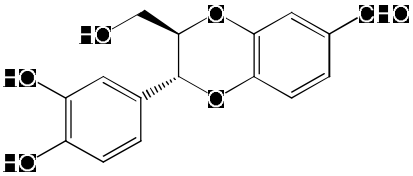

52

Molafolia B

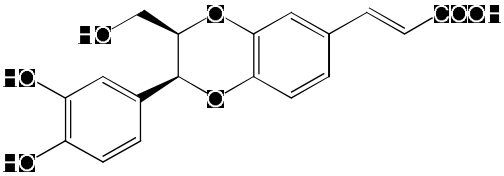

57

Molafolia C

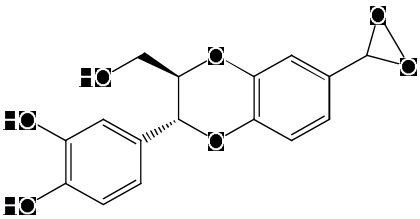

53

Molafolia D

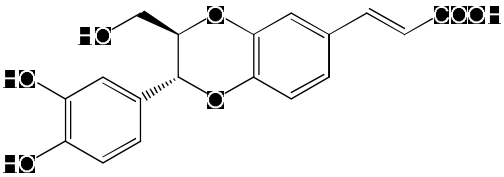

58

Americanoic acid A

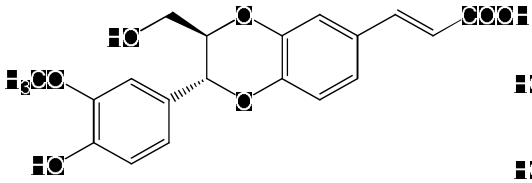

54

Artemlignin D

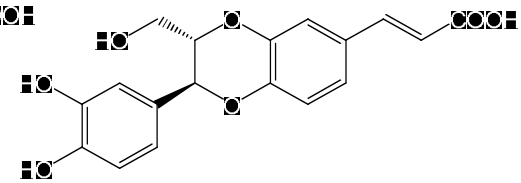

59

Molafolia E

Figure 20: Chemical structure of isolated compounds **50-59** from *Morinda citrifolia*

3.2.2. Structural determination of new compound 42, and compounds 43-46.

Compound **42** was obtained as a brown vicious state with absorption bands at 3406 (OH), 2927(C–C), 1606, 1468, 1374, 1279, 1142, and 1062 cm^{-1} in the IR spectrum. The HR-EI-MS of compound **42** showed a molecular ion peak at *m/z* 330.1103 $[M]^+$ (calcd. $C_{18}H_{18}O_6$, 330.1103) analogous to that of 3,3 -bisdemethylpinoresinol (**43**),[43] a known constituent was also isolated in this study. However, the ^1H NMR spectrum of compound **42** was not consistent with that of 3,3 -bisdemethylpinoresinol (**43**), but showed characteristic signals for two sets of aromatic ABX-spin systems at δ_H 6.73 (1H, d, J = 8.1 Hz), 6.69 (1H, dd, J = 8.1, 1.8 Hz), 6.80 (1H, d, J = 1.8 Hz) for the ring A, and at δ_H 6.74 (1H, d, J = 8.1 Hz), 6.67 (1H, dd, J = 8.1, 1.2 Hz), 6.81 (1H, d, J = 1.2 Hz) for the second ring B. Two oxymethines at δ_H 4.79 (d, J = 6.0 Hz, H-7) and 4.32 (d, J = 6.0 Hz, H-7) with corresponding carbons at δ_C 83.6 and 89.5, respectively. In addition, two aliphatic nonsubstituted oxymethines at δ_H 3.33 (1H, m, H-8) and 2.89 (1H, m, H-8), and two oxymethylenes at δ_H 4.04 (1H, d, J = 9.0 Hz, H-9ax) and 3.81 (1H, dd, J = 6.0, 9.0 Hz, H-9eq)/δ_C 72.0, and at δ_H 3.30 (1H, dd, J = 8.4, 16.8 Hz, H-9ax) and 3.76 (1H, t-like, J = 8.4 Hz, H-9 eq)/δ_C 70.7 were also found in its ^1H and ^{13}C NMR spectra.

Furthermore, ^{13}C NMR spectrum of **42** showed six aromatic quaternary carbons, four of them were oxygenated [δ_C 146.3 (C3/4), 146.6 (C-3), and 145.5 (C-4)], the other two was belong to C-1 (131.5) and C-1 (134.0), this observation demonstrated the asymmetry of the molecule, and were as expected for an equatorial quaiacyl at C-1 and axial guaiacyl at C-1 . All of this data resembled structure identical with epipinoresinol.[43] However, two methoxy groups in epipinoresinol were disappeared in compound **42**.

Study about 2D NMR experiments of compound **42** illustrated that total HSQC, COSY, and HMBC correlations were all matched for structure (Fig. 21). To allow additional analyses of the ^{1}H NMR spectrum and the stereochemistry of the compound, NOESY experiment was carried out and total correlations were shown in the figure 22. When H-9ax (4.04, d, J = 9.0 Hz) was fixed as axial proton (α),[43] which gave correlation with H-7 (4.32, axial proton), and H-7 with H-9 ax. In contrast, H-7 (4.79) showed the correlations with H-9eq (3.81, dd, J = 6.0, 9.0 Hz) and H-8 (3.33, m), while H-8 (2.89, m) showed correlation with H-9eq (3.81, dd, J = 6.0, 9.0 Hz). These observations clearly established the axial- and equatorial- relationship for proton H-7 and H-7 , respectively. By this means, the geometry of each proton may be fixed for the furofuran system (as shown in figure 21 and 22). An optical rotation value of +11.13 (c = 0.227) was obtained for compound **42** in MeOH solvent. Thus, chemical structure of compound **42** was identified to be (+)-(7α,7 β,8α,8 β)-3,3 ,4,4 -tetrahydroxy-7,9 :7 ,9-diepoxylignane, a new natural product from noni and named modafolia A.

Compounds **43** to **46** were also isolated from this noni powder as brown yellowish viscous state. The ^{1}H NMR data of **43** showed signal for one aromatic ABX-spin system, one aliphatic oxymethine (δ_H 4.62), one oxygenated-non-methine (δ_H 3.08), and one oxymethylene (δ_H 4.20, 3.79). Its ^{13}C NMR spectrum displayed 9 carbon signals which could be assignable for a phenyl propanoid. However, its EI-MS gave a molecular ion peak at *m/z* 330, indicating a symmetric structure of **43**. Comparison of the ^{1}H and ^{13}C NMR spectroscopic data of **43** with those published in literature led to the identify that compound **43** was 3,3-bisdemethylpinoresinol.[43] The specific optical rotation value of

compound **43** was $[\alpha]_D^{25}$: –2.208 (c = 0.227, MeOH). Similarly, compound **44** was characterized as pinoresinol[43] with two methoxy group at C-3 and C-3 .

Compounds **45** and **46** were also appeared as symmetry with methoxy moiety (δ_H 4.04 and 3.81, s with δ_C 56.7), however, the ^{1}H NMR spectra showed aliphatic oxymethine, methylene, and non-oxygenated methine, and only one siglet aromatic proton at δ_H 6.87~6.68. EI-MS spectra gave molecular ion peak at *m/z* 418 for **45**, and 446 for **46**, indicating that **45** and **46** possessed four and five methoxy groups in their structure, respectively. Thus, compounds **45** and **46** were characterized as lirioresinol B and lirioresinol B dimethyl ether, respectively.

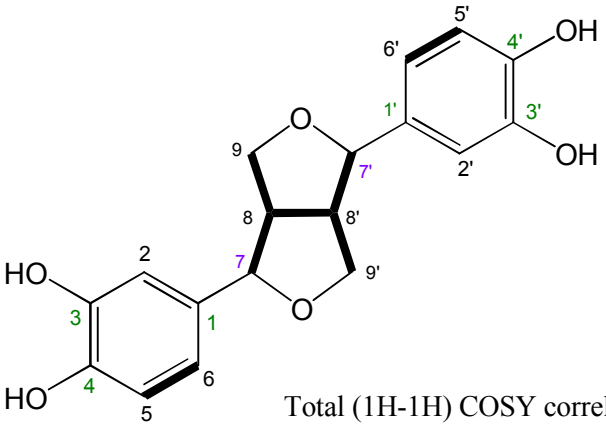

Total (1H-1H) COSY correlations

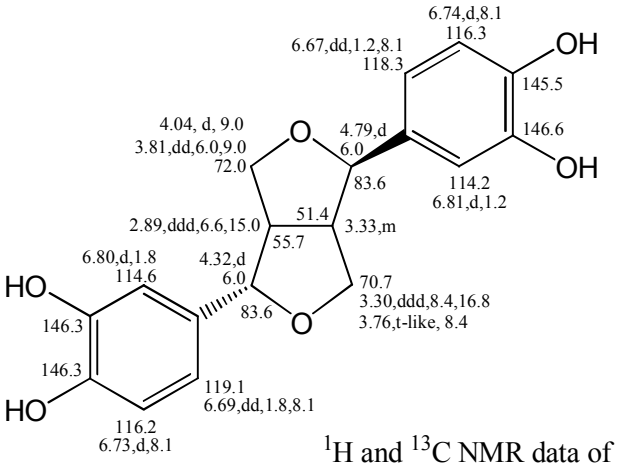

^{1}H and ^{13}C NMR data of compound **43**

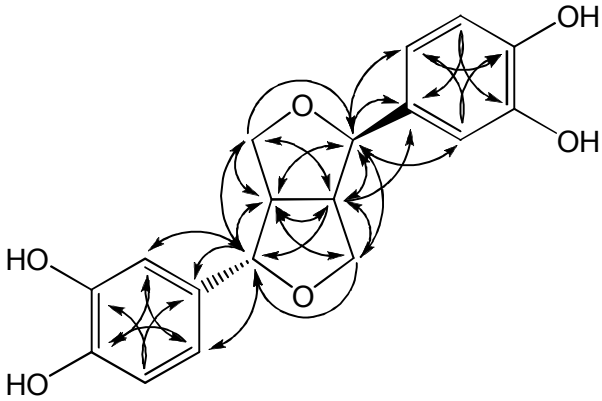

Total (1H-13C) HMBC correlations

Figure 21: ^{1}H, ^{13}C, total COSY, and HMBC correlations data of compounds **42**

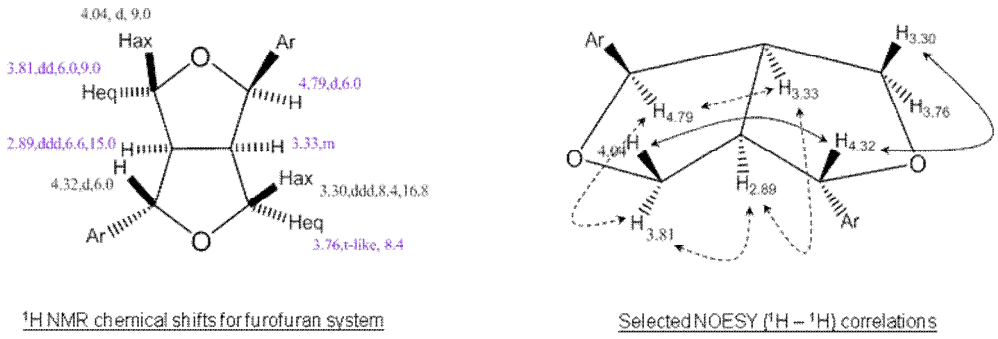

Figure 22: Key NOESY (^{1}H – ^{1}H, dotted line) correlations of compound **42**

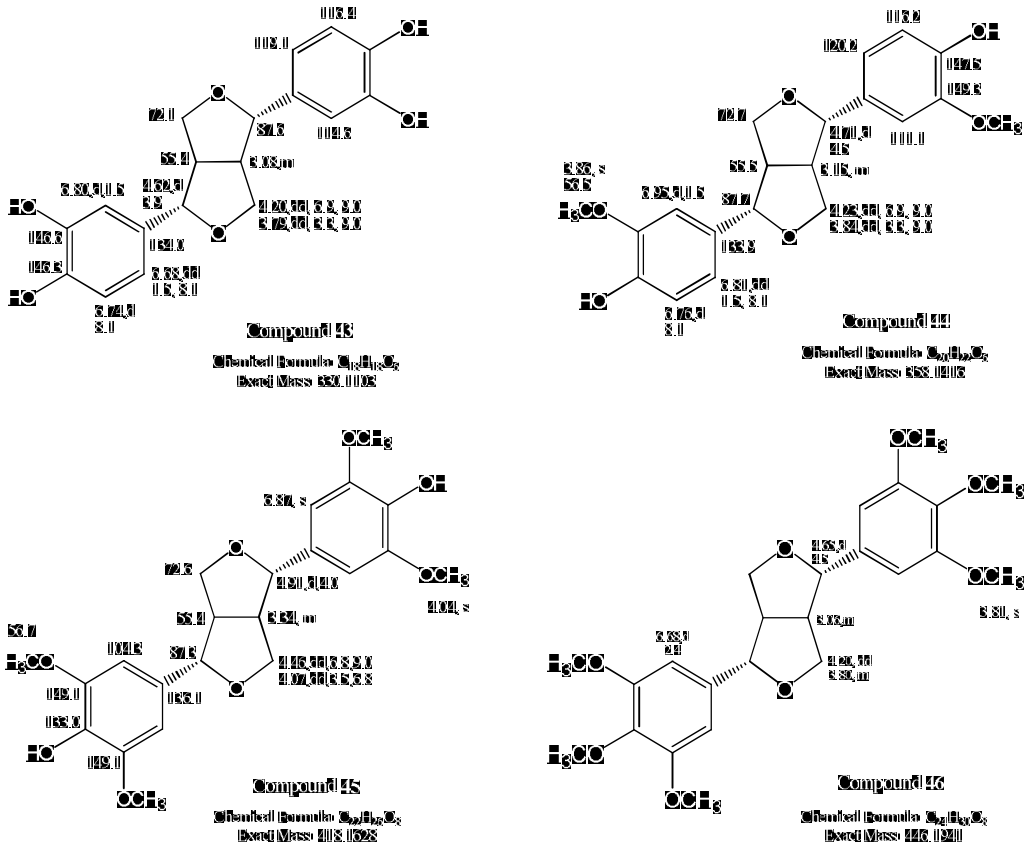

Figure 23: Chemical structure, ^{1}H and ^{13}C NMR data of compounds **43** to **46**

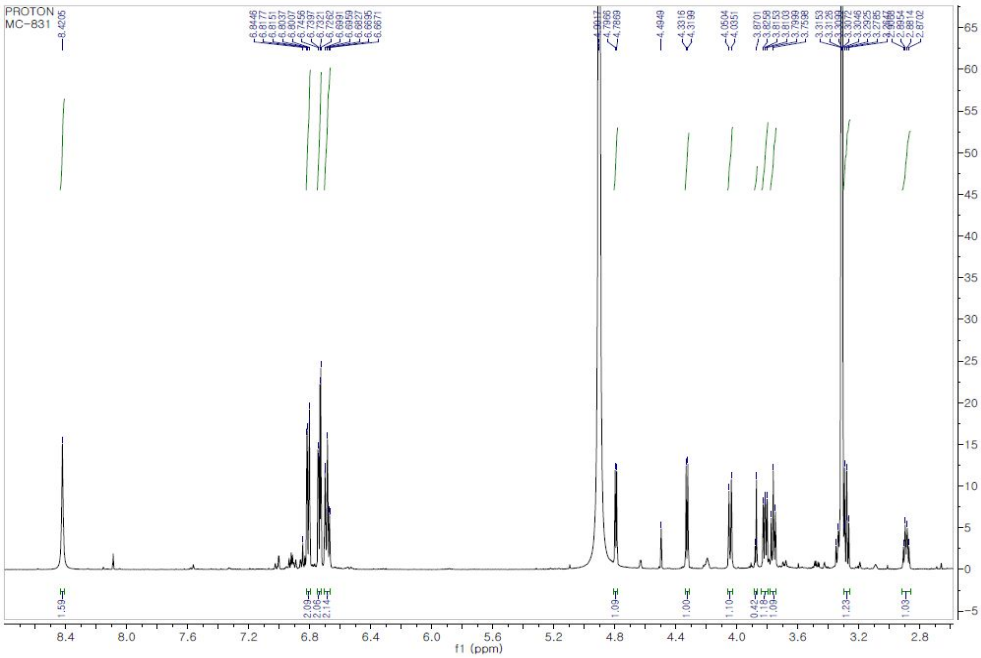

Figure 24: ^{1}H-NMR spectrum of compound **42** (600 MHz, MeOH-d_4)

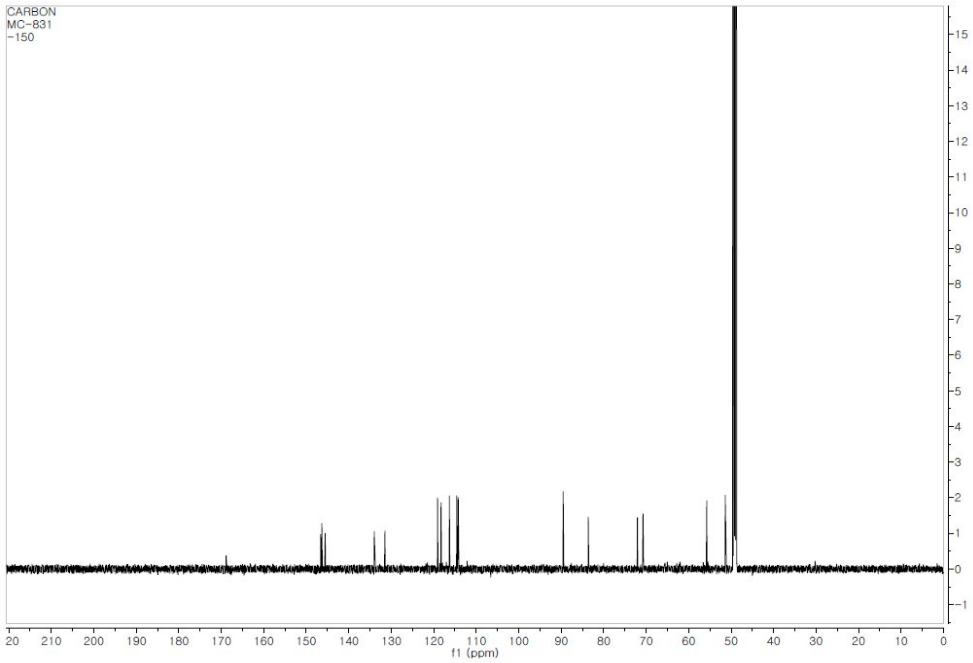

Figure 25: ^{13}C-NMR spectrum of compound **42** (150 MHz, MeOH-d_4)

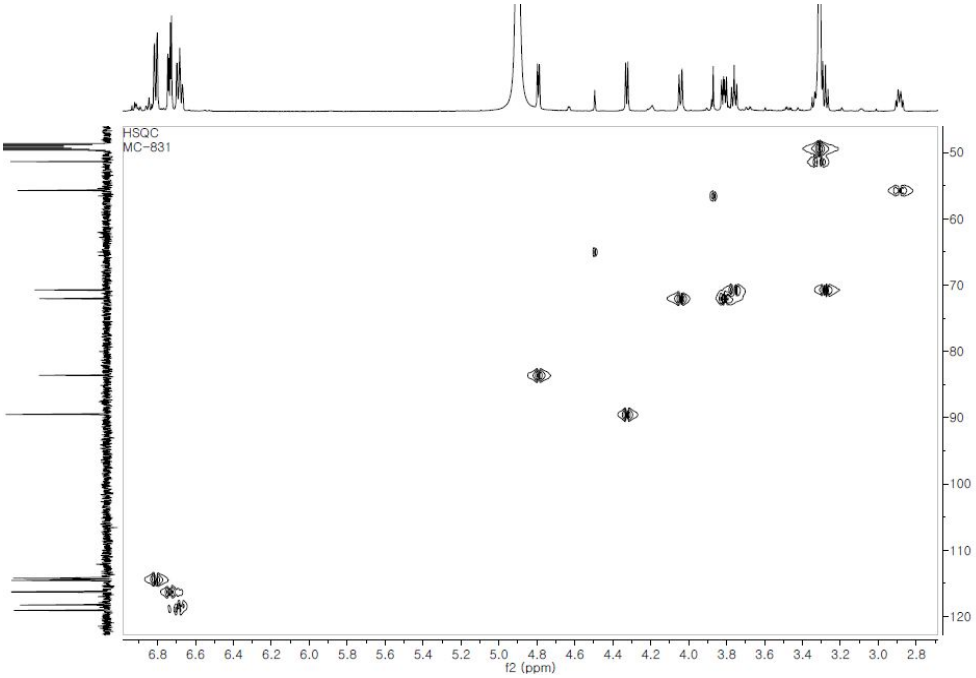

Figure 26: HSQC spectrum of compound **42** (600 MHz, MeOH-d_4)

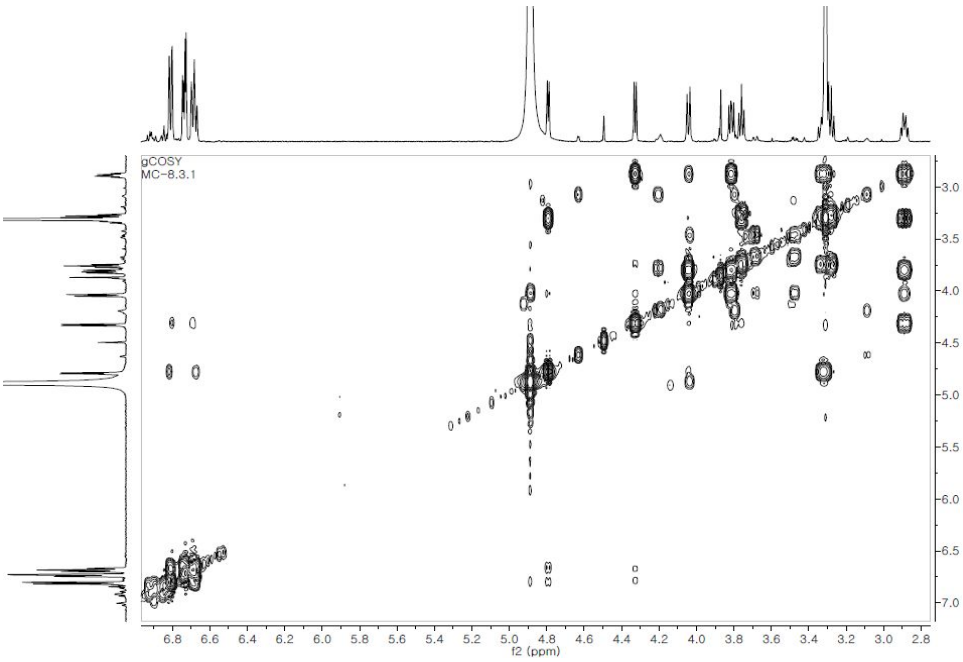

Figure 27: COSY spectrum of compound **42** (600 MHz, MeOH-d_4)

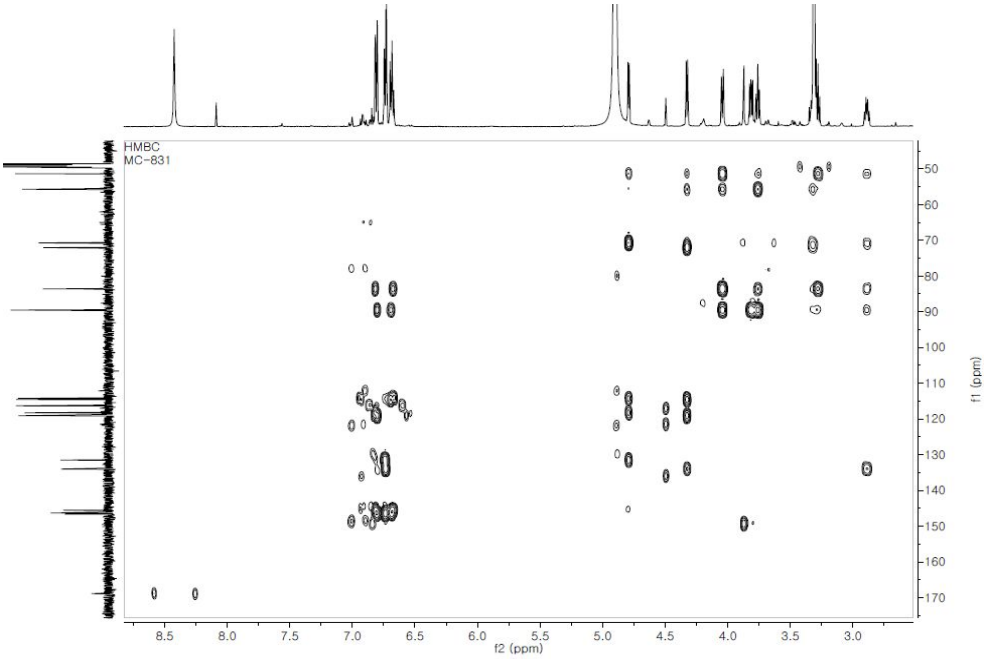

Figure 28: HMBC spectrum of compound **42** (600 MHz, MeOH-d_4)

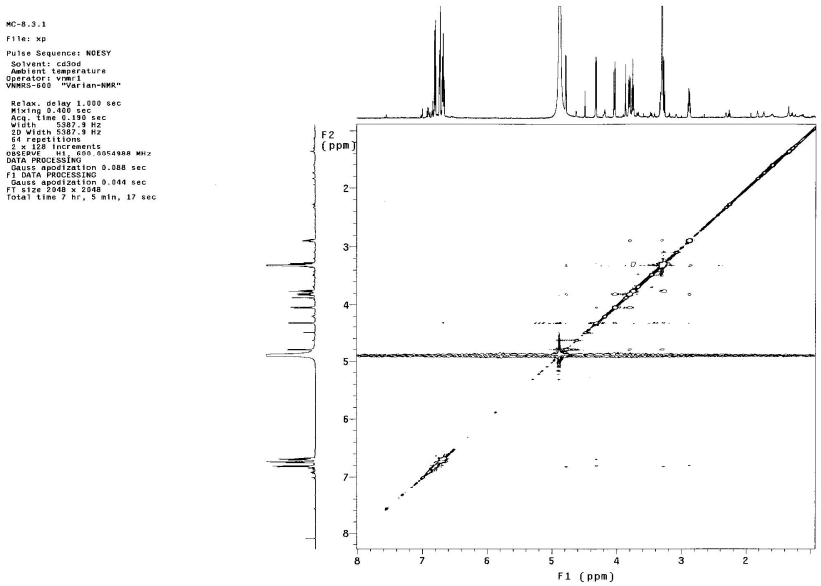

Figure 29: NOESY spectrum of compound **42** (600 MHz, MeOH-d_4)

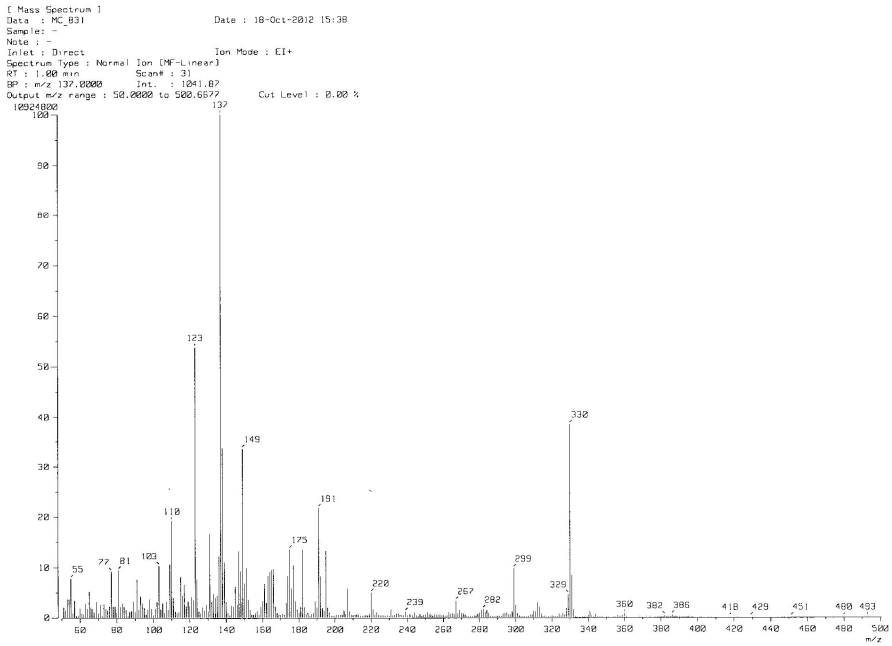

[Elemental Composition] Page: 1

Data : MC_831 Date : 01-Nov-2012 09:53
Sample: -
Note : -
Inlet : Direct Ion Mode : EI+
RT : 0.80 min Scan#: 17
Elements : C 100/1, H 100/1, O 10/1
Mass Tolerance : 3mmu
Unsaturation (U.S.) : 0.0 - 30.0

Observed m/z	Int%	Err[ppm / mmu]	U.S.	Composition
330.1103	42.1	-0.2 / -0.1	10.0	C 18 H 18 O 6

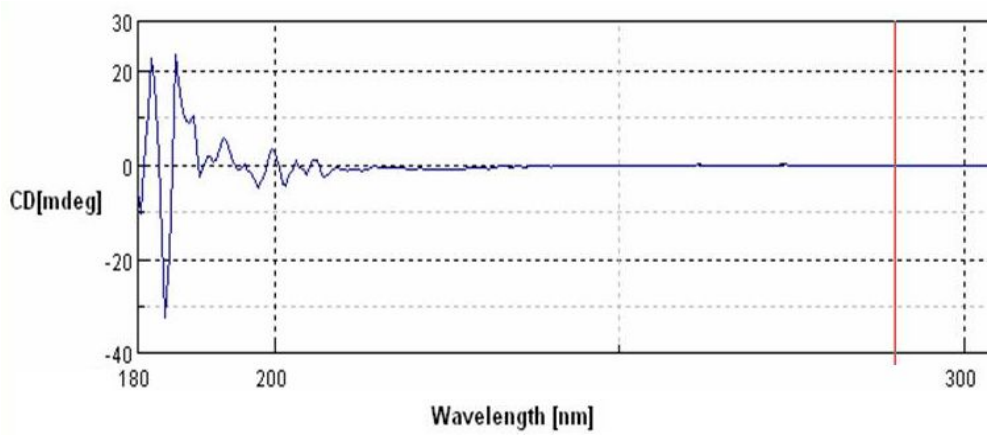

Figure 30: EI-MS and HR-EI-MS and CD spectra of compound **42**

3.2.3. Structural determination of new compound 47

Compound **47** was obtained as a yellowish amorphous state, The $[\alpha]_D^{25}$: –5.62 (c = 0.107, MeOH) was obtained from Autopol IV spectrometer. The molecular formula of **47** was determined as $C_{18}H_{16}O_7$ from a molecular ion peak at *m/z* 344.0898 $[M]^+$ (calcd for $C_{18}H_{16}O_7$, 344.0896) in the HR-EI-MS. Its UV spectrum showed absorption bands at λ_{max} 208, 233, and 284 nm.

The ^{1}H NMR spectrum displayed two sets of ABX-type aromatic spin systems at δ_H 6.83 (1H, d, J = 8.4 Hz, H-5), 7.02 (1H, dd, J = 1.8, 8.4 Hz, H-6), and 7.08 (1H, d, J = 1.8 Hz, H-2), as well as at δ_H 6.75 (1H, d, J = 8.1 Hz, H-5), 6.64 (1H, dd, J = 1.8, 8.1 Hz, H-6), and 6.72 (1H, d, J = 1.8 Hz, H-2). A singlet aromatic proton (δ_H 7.47), an oxygenated aliphatic proton (δ_H 5.52, 1H, d, 4.2 Hz), and a non-oxygen-substituted aliphatic proton were observed.

In the ^{13}C NMR spectra (see Figure 50), 18 carbon signals could be found, including four oxygensubstituted aromatic carbons, two carbon-substituted aromatic carbons, six C–H aromatic carbons, two unsaturated carbons, and two saturated carbons. All of these data resembled those of Phellinsin A,[46] however, an additional oxymethylene signals were presented [δ_H 3.89 (1H, dd, J = 9.0, 16.8 Hz) and 3.63 (1H, dd, J = 8.4, 16.8 Hz) in the ^{1}H NMR spectrum of **47**. According to this observation, the ^{13}C NMR spectrum showed only one carbonyl carbon (δ_C 175.2, C-9), the other carboxylic carbon (C-9) in Phellinsin A was shifted to upfield (62.6, C-9) in **47**. This data indicated that a methylene hydroxy moiety was presented at C-8. COSY and HMBC correlations further supported this conclusion.

By according to the chemical shift of H-7 (δ_H 7.47), the configuration at C-7 and C-8 should be *E* form, on the other hand, if the plane constitution were *Z*, the chemical shift should shift to upfield.[48] This conclusion could be confirmed by its NOESY NMR spectra. Compared with Phellinsin A, the coupling constant of H-7 /H-8 of compound **47** ($J_{7\ 8}$ = 4.2 Hz) was similar from that of Phellinsin A, a minus optical rotation value –5.62°, combined with the CD data, the relative configuration at C-7 and C-8 was deduced to be *trans* (7β,8α).[48-49] According to the above analysis, the structure of compound **47** was elucidated as (7β,8α)-3,3 ,4,4 ,9-pentahydroxy-7 -en-7,9 -lactone, and named as modafolia B.

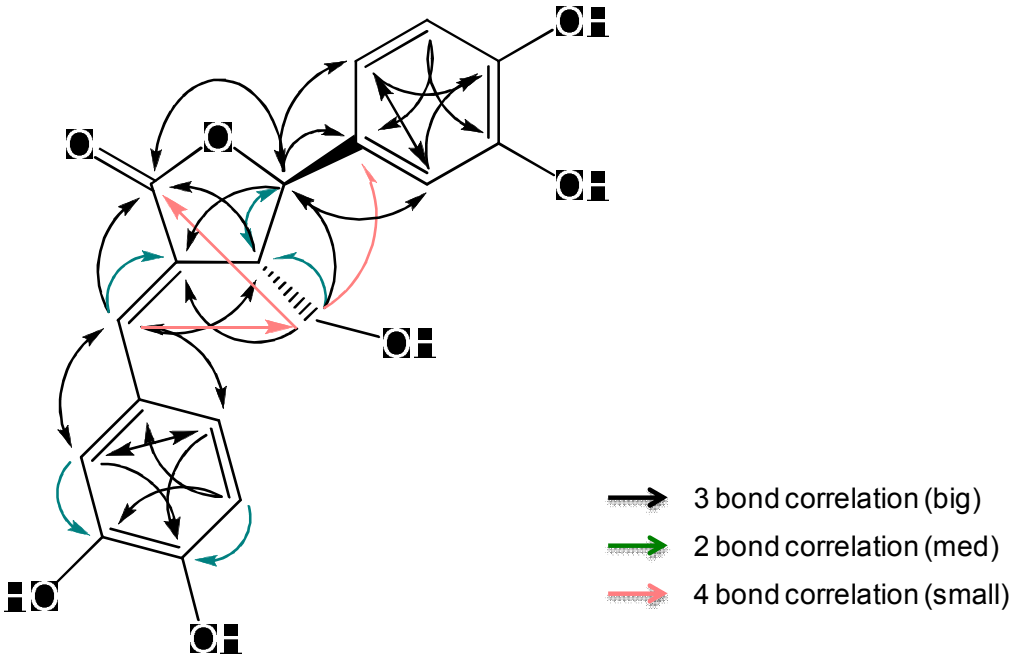

Figure 31: Total HMBC correlations found for compound **47**

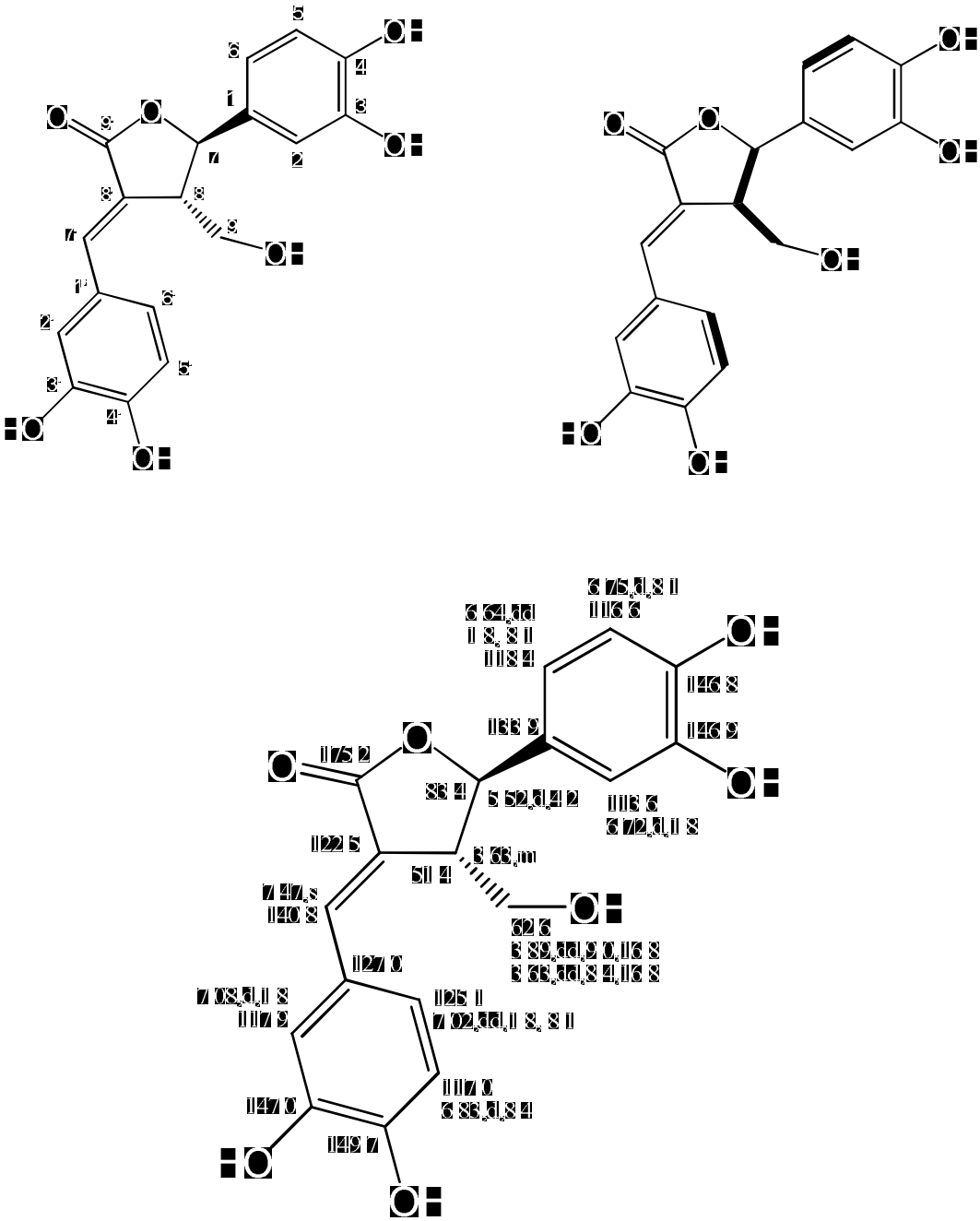

^{1}H and ^{13}C NMR data of compound 47

Figure 32: Chemical structure, 1D-NMR spectroscopic data and COSY of compound **47**

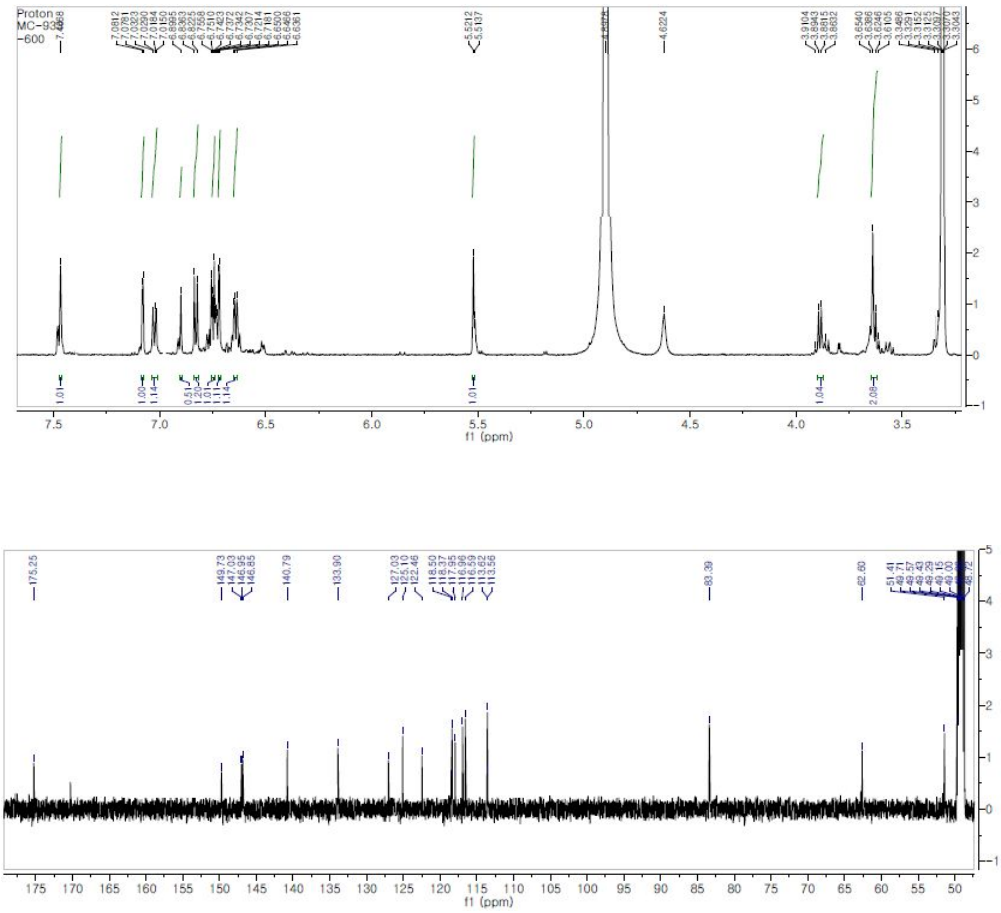

Figure 33: ^{1}H and ^{13}C-NMR spectra of compound **47** (600/150 MHz, MeOH-d_4)

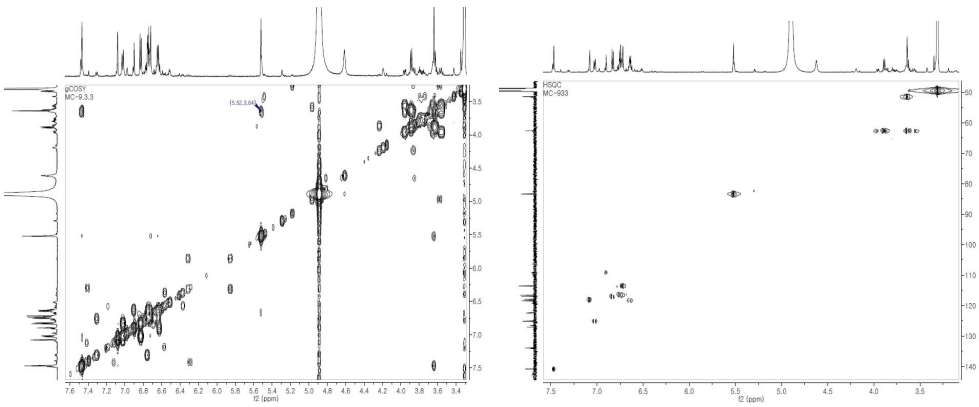

Figure 34: COSY and HSQC NMR spectra of compound **47** (600 MHz, MeOH-d_4)

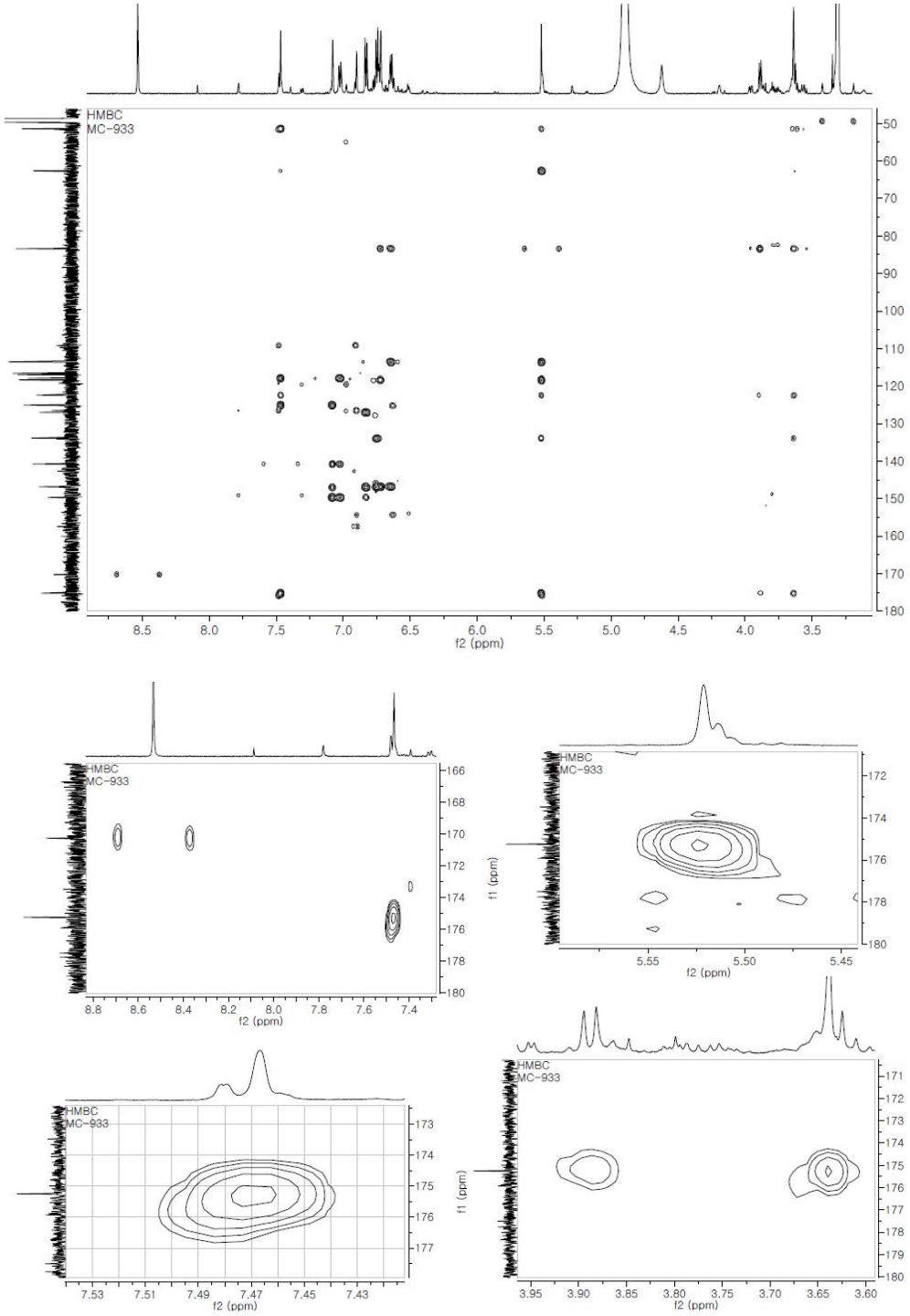

Figure 35: HMBC spectrum of compound **47** (600 MHz, MeOH-d_4)

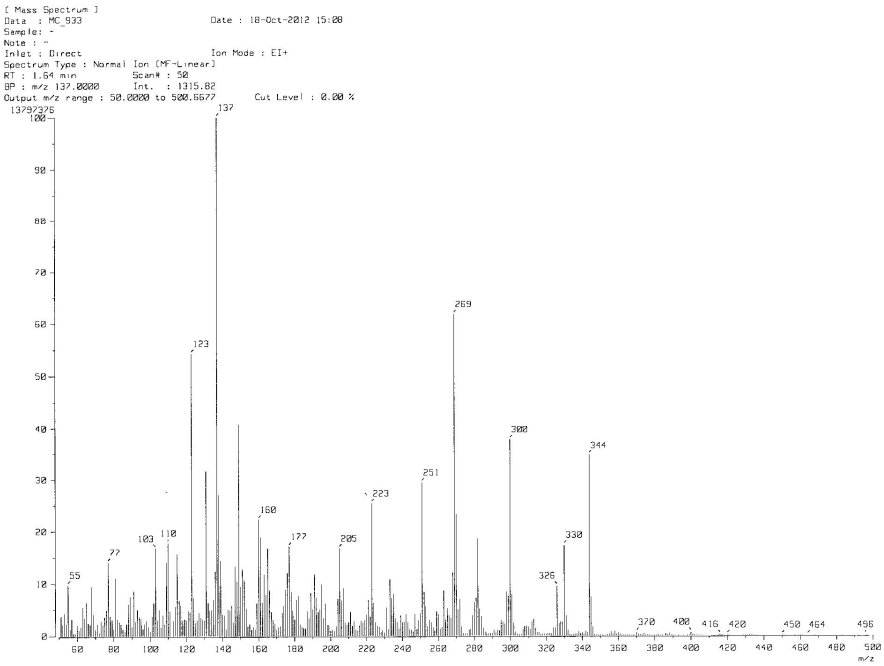

[Elemental Composition] Page: 1

Data : MC_933 Date : 01-Nov-2012 09:27
Sample: -
Note : -
Inlet : Direct Ion Mode : EI+
RT : 0.95 min Scan#: 20
Elements : C 100/1, H 100/1, O 10/1
Mass Tolerance : 3mmu
Unsaturation (U.S.) : 0.0 - 30.0

Observed m/z	Int%	Err[ppm / mmu]	U.S.	Composition
344.0898	100.0	+0.5 / +0.2	11.0	C 18 H 16 O 7

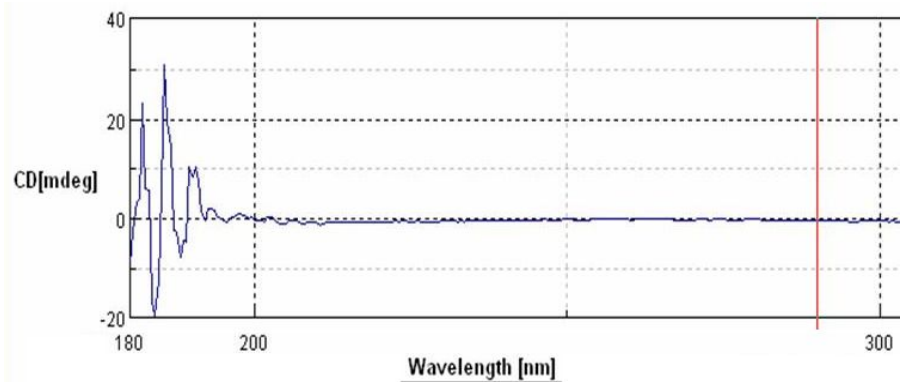

Figure 36: EI-MS and HR-EI-MS and CD spectra of compound **47**

3.2.4. Structural determination of compound 48 and new compound 49

Compound **48** and **49** were purified as light brown resinous semisolid from same fraction by using HPLC with UV detections at 205 and 254 nm, the retention time were 33.4 min and 37.6 min, respectively. The IR spectra of both compounds suggested the presence of OH functional groups at 3421 cm^{-1}, 2927 (C–C), 1630 (C=O), and C–O stretching vibrations at 1081–1033 cm^{-1}. Their UV spectra showed absorption bands at λ_{max} 206-210, 230-234, 280-290 nm.

Compound **48** gave a molecular ion peak at *m/z* 344.0898 in the HR-EI-MS. The molecular formula of compound **49** was also determined as $C_{18}H_{16}O_7$ from a molecular ion peak at *m/z* 344.0894 $[M]^+$ (calcd for $C_{18}H_{16}O_7$, 344.0896) in its HR-EI-MS. The ^1H NMR displayed two sets of aromatic ABX-type spin systems at δ_H 6.75 (1H, d, J = 8.4 Hz, H-5), 6.70 (1H, dd, J = 8.4, 1.8 Hz, H-6), and 6.82 (1H, d, J = 1.8 Hz, H-2), as well as at δ_H 6.78 (1H, d, J = 7.8 Hz, H-5), 6.68 (1H, dd, J = 7.8, 1.8 Hz, H-6), and 6.77 (1H, d, J = 1.8 Hz, H-2). In addition, an oxymethylene signal at δ_H 4.25 (1H, dd, J = 7.2, 9.6 Hz) and 3.97 (1H, dd, J = 4.2, 9.6 Hz), two oxymethine signals at δ_H 5.30 (1H, d, J = 3.6 Hz, H-7), 5.16 (1H, d, J = 3.6, Hz, H-7), and two non-oxymethines at δ_H 3.27 (1H, m, H-8), and 3.57 (1H, dd, J = 3.6, 9.0 Hz, H-8) were presented.

The COSY spectrum of both compounds revealed the presence of the moiety of -CH_2-CH(CH)-CH-CH-, which corresponds to positions C-7, -8, -9, -7 , and -8 in a dioxabicyclo[3.3.0]octane skeleton.[43, 48] The ^{13}C NMR spectra indicated the presence of 18 carbons, including an ester carbonyl group (δ_C 179.9), two oxymethine groups (δ_C 87.2 and 85.2), two non-oxymethine groups (δ_C 51.0 and 54.5), and 12 aromatic carbons in the

range δ_C 114.0 to 147.1 which assignable to two bezenyl ring.

HMBC experiments of compound **48** and **49** (Fig. 36) revealed that the following correlations between: H-7/C-2, C-6, C-9, C-8 , and C-9 ; H-8/C-1, C-7 , and C-9 ; H-9/C-7 and C-8 ; H-7 /C-8, C-9, C-2 , C-6 , C-8 , and C-9 ; H-8 /C-7, C-9, and C-1 . The relative configuration of compound **48** and **49** were established by the analysis of four diastereomers A-D (Figure 56). The stereochemical constraints posed by aryl substitution are indicated clearly in appropriated molecular models. Severe crowding between the carbonyl at C-9 and the endo-aryl substituent at C-7 cannot be eliminated in isomers C and D. Therefore, isomers **A** and **B** are more probable structures than **C** and **D** (Fig. 37).

The NOESY spectrum of compound **48** exhibited correlations between H-8 and H-8 , H-7 and H-9ax, and H-8 and H-9eq, which indicated that these protons are on the same face of the molecule and confirmed the relative configuration proposed as shown below. While, the NOESY spectrum of compound **49** displayed correlations between H-8 and H-8 , H-7 and H-9eq, H-8 and H-9ax, and H-7 and H-9eq, H-7 and H-2, H-7 and H-2 , these indicated that two benzenyl rings and H-8, H-8 are on the same β-orientation.

Specific optical rotation value of **48** $[\alpha]_D^{25}$: -17.54 (c = 0.667, MeOH) and **49** $[\alpha]_D^{25}$: -5.78 (c = 0.667, MeOH) were further supported for these different orientation. On the basis of the abovementioned data, compound **48** was identified as a previously reported lignan, (+)-3,4,3 ,4 -tetrahydroxy-9,7 -epoxylignano-7,9 -lactone,[43] and compound **49** was a new lignan, ( )-(7β,7 β,8β,8 β)-3,4,3 ,4 -tetrahydroxy-9,7 β-epoxylignano-7β,9 -lactone, and named modafolia C.

Compound 49 (modafolia C): Light brown resinous semisolid; IR (KBr): v_{max} 3421 (OH), 2927 (C–C), 1630 (C=O), and C–O stretching vibrations at 1081–1033 cm^{-1}. UV (*c* 0.025, MeOH) λ_{max} nm: 206-210, 230-234, 280-290 cm^{-1}; $[\alpha]_D^{25}$: -5.78 (c = 0.667, MeOH); HR-EI-MS *m*/*z* 344.0894 $[Ma]^+$, (calcd $C_{18}H_{16}O_7$, 344.0896).

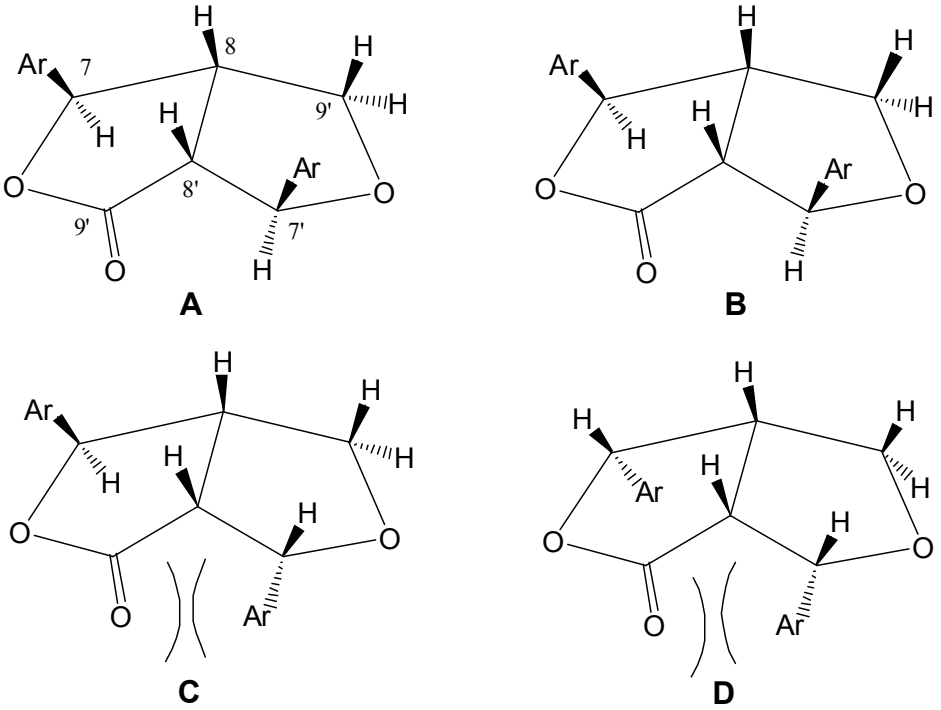

Figure 37: Four diastereomers **A** to **D** diagnosed for compound **48** and compound **49**

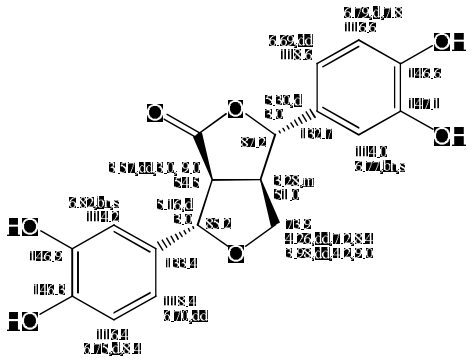

^{1}H and ^{13}C NMR data of compound **48**

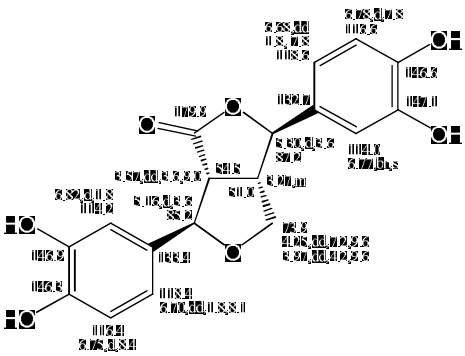

^{1}H and ^{13}C NMR data of compound **49**

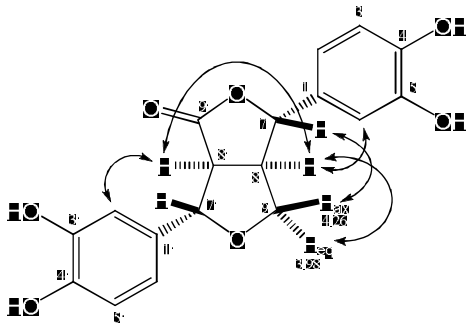

NOESY (^{1}H-^{1}H) correlations of compound **48**

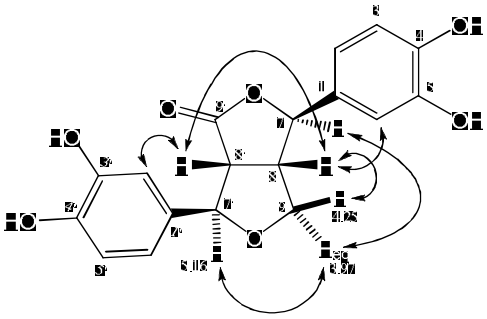

NOESY (^{1}H-^{1}H) correlations of compound **49**

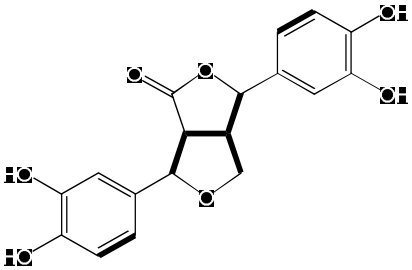

COSY (^{1}H-^{1}H) correlations of compound **49**

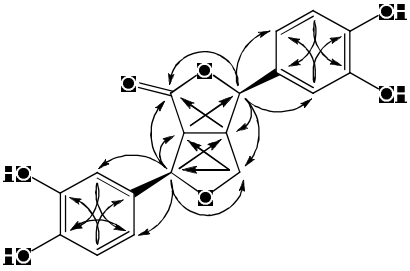

Total HMBC (^{1}H-^{13}C) correlations of compound **49**

Figure 38: 1D NMR, COSY, HMBC, and NOESY data of compounds **48** and **49**

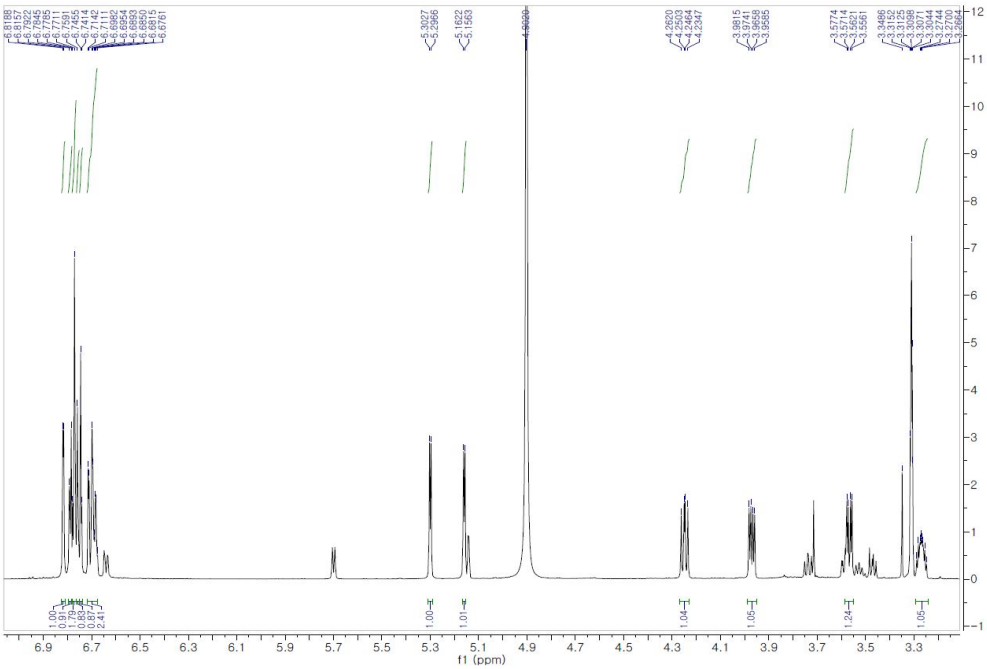

Figure 39: ^{1}H-NMR spectrum of compound **49** (600 MHz, MeOH-d_4)

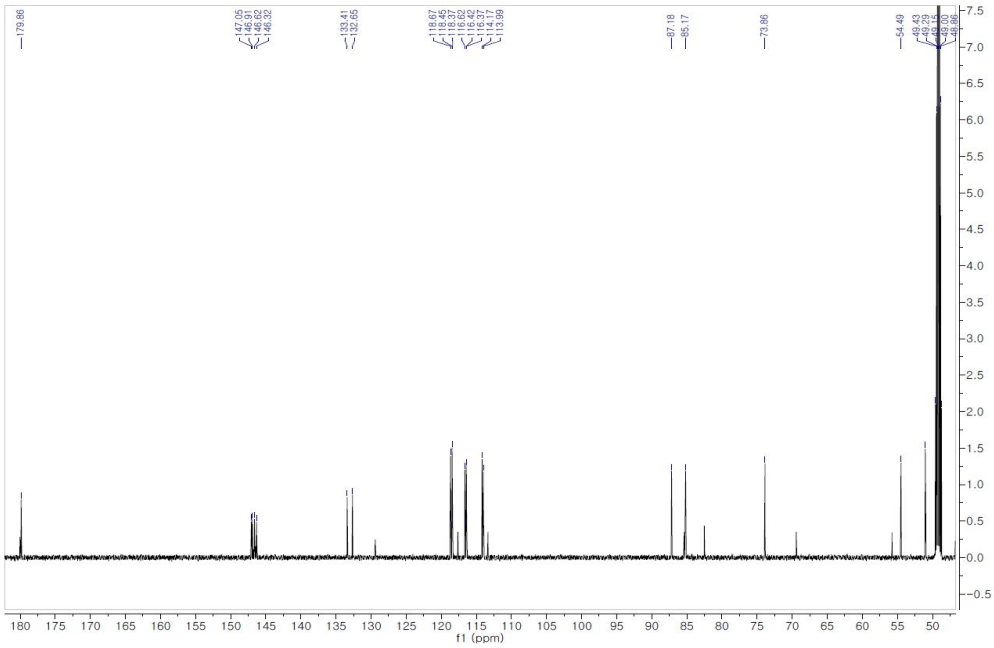

Figure 40: ^{13}C-NMR spectrum of compound **49** (150 MHz, MeOH-d_4)

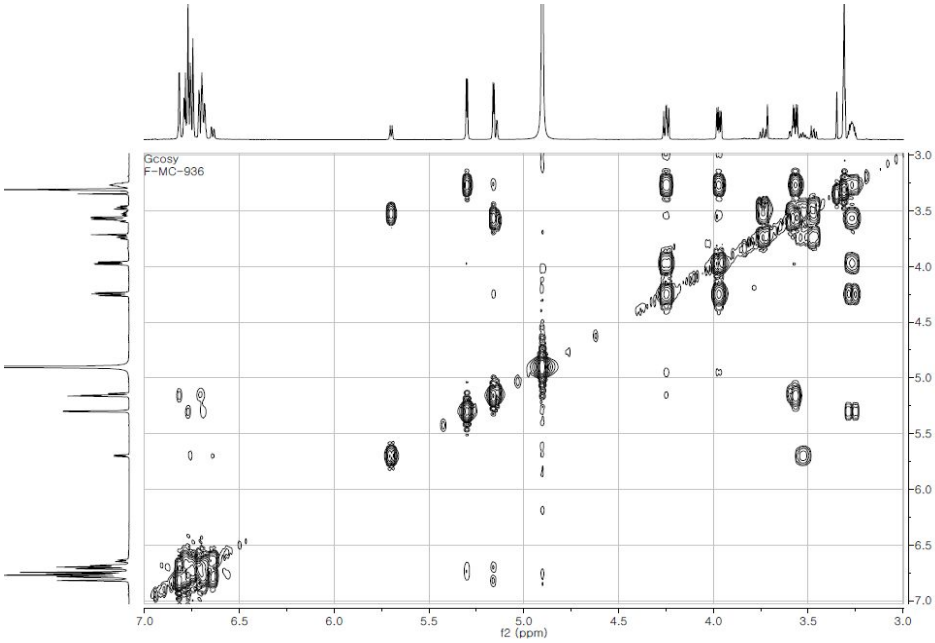

Figure 41: COSY NMR spectrum of compound **49** (600 MHz, MeOH-d_4)

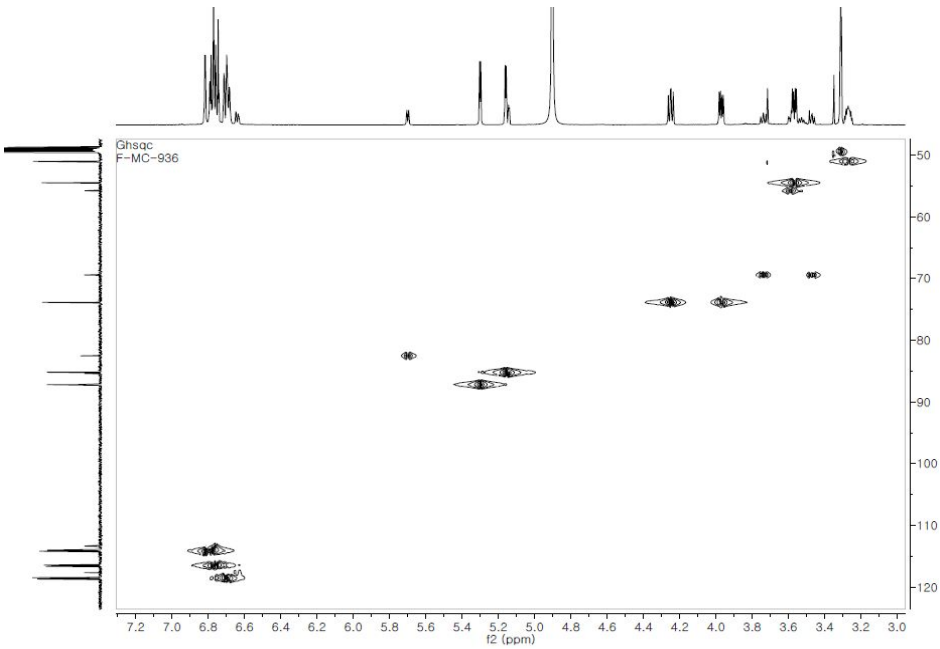

Figure 42: HSQC NMR spectra of compound **49** (600 MHz, MeOH-d_4)

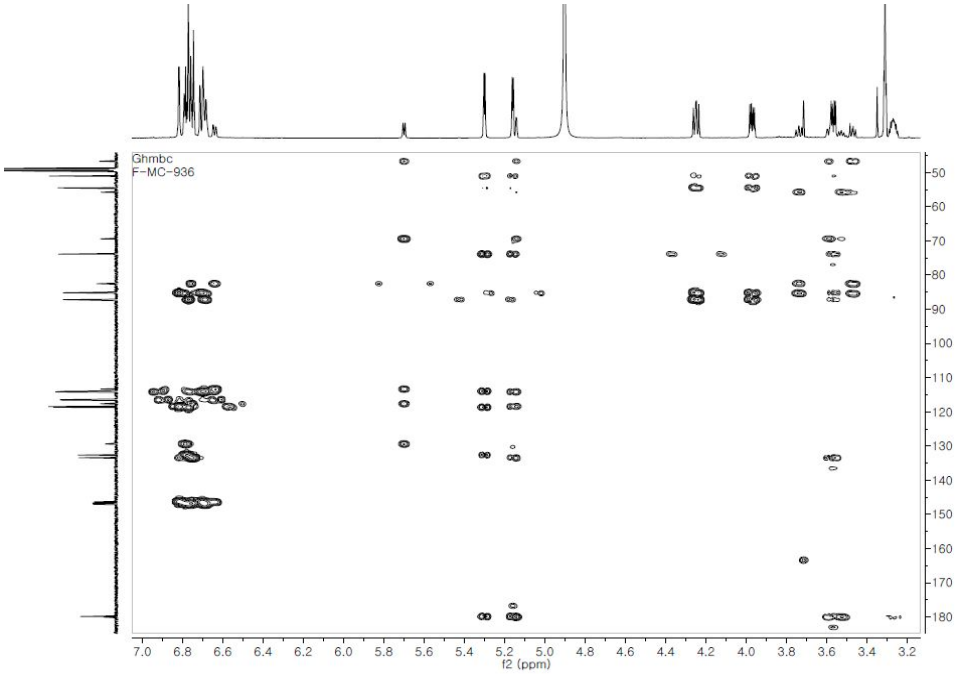

Figure 43: HMBC spectrum of compound **49** (600 MHz, MeOH-d_4)

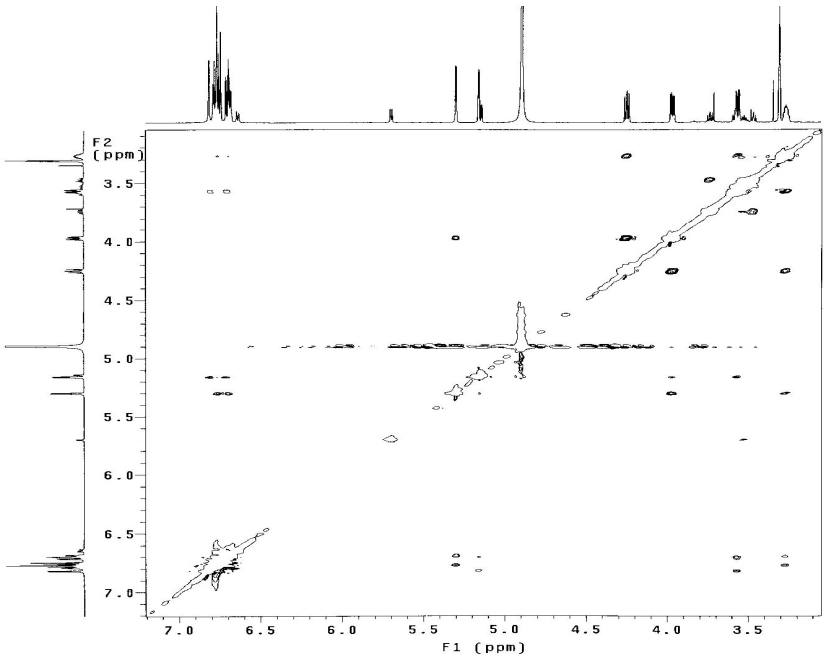

Figure 44: NOESY spectrum of compound **49** (600 MHz, MeOH-d_4)

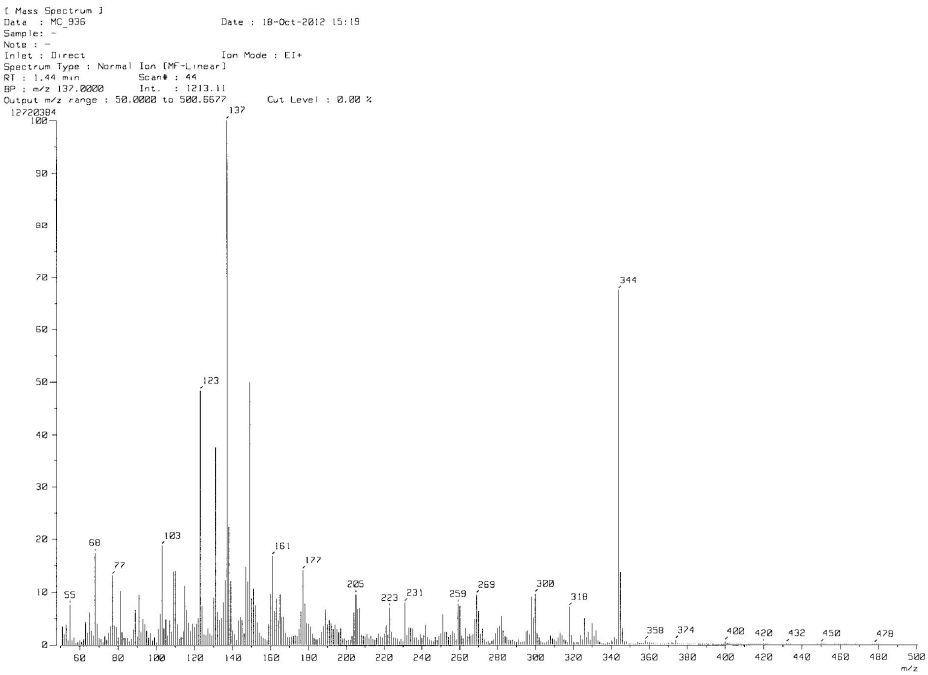

[Elemental Composition] Page: 1

Data : MC_936 Date : 01-Nov-2012 09:43

Sample: -

Note : -

Inlet : Direct Ion Mode : EI+

RT : 1.10 min Scan#: 23

Elements : C 100/1, H 100/1, O 10/1

Mass Tolerance : 3mmu

Unsaturation (U.S.) : 0.0 - 30.0

Observed m/z	Int%	Err[ppm / mmu]	U.S.	Composition
344.0894	100.0	-0.6 / -0.2	11.0	C 18 H 16 O 7

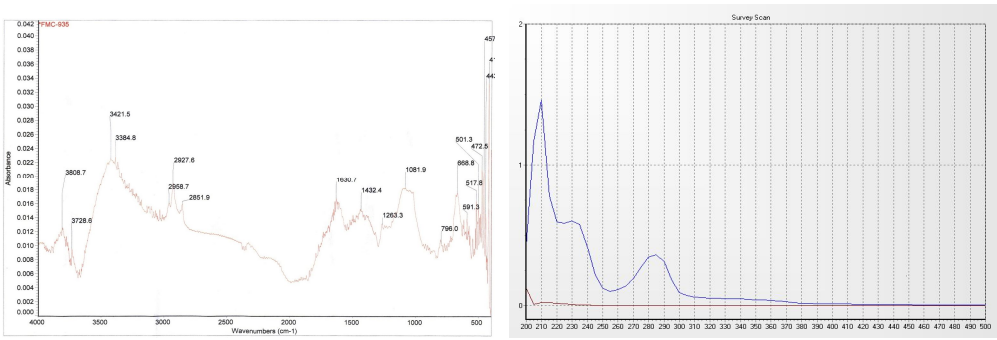

Figure 45: HREIMS, IR (KBr, left) and UV (c = 0.025, MeOH) spectra of compound **49**

3.2.5. Structural determination of new compound 50 and compound 52

Compound **52** was isolated as a brown yellowish amorphous powder with absorption bands at 3406 (OH), 2927(C–C), 1650 (CHO), 1418 (C-O), 1160-1042 cm^{-1} in the IR spectrum. Its UV spectrum (c 0.025, MeOH) showed absorption maxima at 210, 235, and 280 nm. The HR-EI-MS of compound **52** showed a molecular ion peak at *m/z* 302.0794 $[M]^+$ (calcd $C_{16}H_{14}O_6$ 302.0790).

The ^1H and ^{13}C NMR spectra of **52** showed pattern similar to those of compound **51**, except that the methoxy resonances were not present, but displayed signals for an aldehyde [δ_H 9.80 (1H, s), δ_C 192.9]. In the ^1H NMR spectrum, the presence of two 1,3,4-trisubstituted phenyl groups was indicated from the two ABX coupling systems [δ_H 6.79 (d, J = 8.1 Hz, H-5), 6.78 (dd, J = 8.1, 1.8 Hz, H-6), and 6.87 (d, J = 1.8 Hz); δ_H 7.13 (d, J = 8.4 Hz, H-5), 7.49 (dd, J = 8.4, 1.8 Hz, H-6), and 7.45 (d, J = 1.8 Hz, H-2)]. Moreover, we observed an oxymethine proton signal (δ_H 4.13, m), which was coupled to an oxymethine proton signal (δ_H 4.89, d, 7.8) and hydroxymethylene proton signals (δ_H 3.50 and 3.73). These observations were further supported by correlations found in the COSY experiment (Fig. 64). The proton-carbon long-range coupling correlations derived from the HMBC spectrum allowed us to determine the planar structure (Fig. 46). The oxymethine proton at δ_H 4.89 (H-7) was correlated with the 1,3,4-trisubstituted phenyl carbons at δ_C 115.6 (C-2) and 120.5 (C-6). In contrast, the aromatic protons at δ_H 7.45 (C-2) and 7.49 (C-6) were correlated with the aldehyde carbon at δ_C 192.9 (CHO). Further correlation was observed between the aldehyde proton at δ_H 9.80 (CHO) and the 1,3,4-trisubstituted phenyl carbons at δ_C 119.1 (C-2), 132.1 (C-1), and 125.5 (C-6). The

combination of all these data identified a 1,4-benzodioxan-type lignan.[48]

From the coupling constant of $J_{7,8}$ = 7.8 Hz, and the $[\alpha]_D^{25}$: +2.528 (c = 0.213, MeOH), the relative configuration of C-7 and C-8 in the dioxane ring was *trans*.[45] The absolute configuration of C-7 and C-8 was determined by the CD spectrum: the positive Cotton effect at 192 nm and the negative Cotton effect at 222 nm suggested a configuration of 7*R* and 8*R*.[66] Consequently, the structure of **52** was determined as (7*R*,8*R*)-3,4,9-trihydroxy-4′,7-epoxy-8,3′-oxyneoligna-1′-al, and named modafolia E.

The ^{1}H and ^{13}C NMR spectra of compound **50** were identical with **52**, and the $[\alpha]_D^{25}$: +0.235 (c = 0.213, MeOH). However, the additional *trans*-olefinic AB system at δ 7.56 and 6.00 (d, J = 15.9 Hz), with two corresponding carbons at δ_C 120.6 and 129.2 were further observed. Thus, compound **50** was elucidated as americanin A (Figure 46).[44]

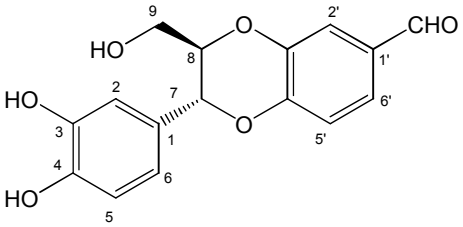

Chemical structure of compound **52**

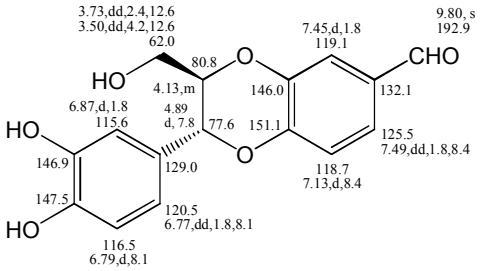

^{1}H and ^{13}C NMR data of compound **52**

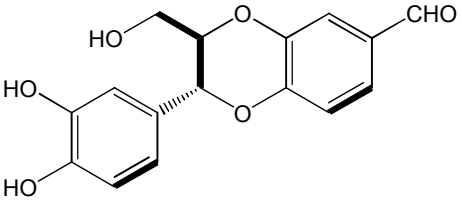

COSY correlations of compound **52**

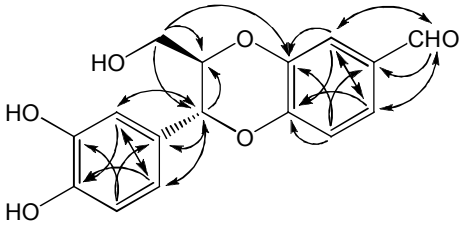

Total HMBC correlations of compound **52**

Figure 46: Chemical structure, 1D NMR, COSY, and HMBC of compound **52**

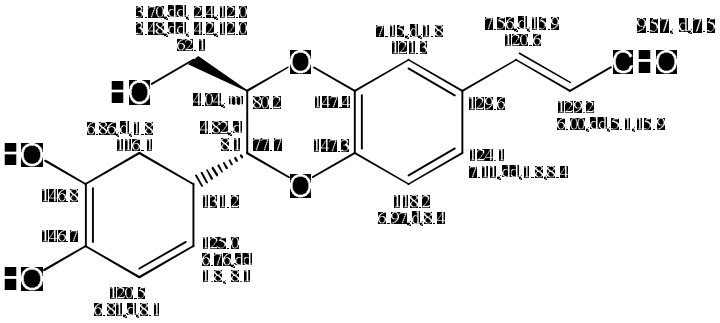

Figure 47: Chemical structure, 1D NMR (300/75 MHz, MeOH) of compound **50**

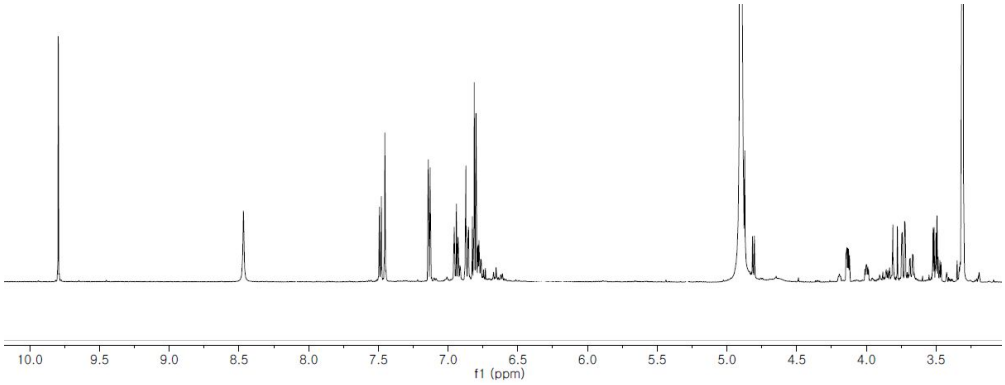

Figure 48: ^{1}H-NMR spectrum of compound **53** (600 MHz, MeOH-d_4)

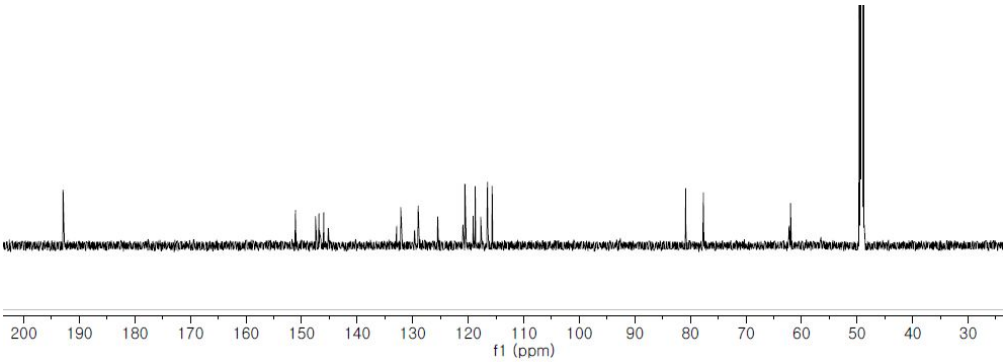

Figure 49: ^{13}C-NMR spectrum of compound **52** (150 MHz, MeOH-d_4)

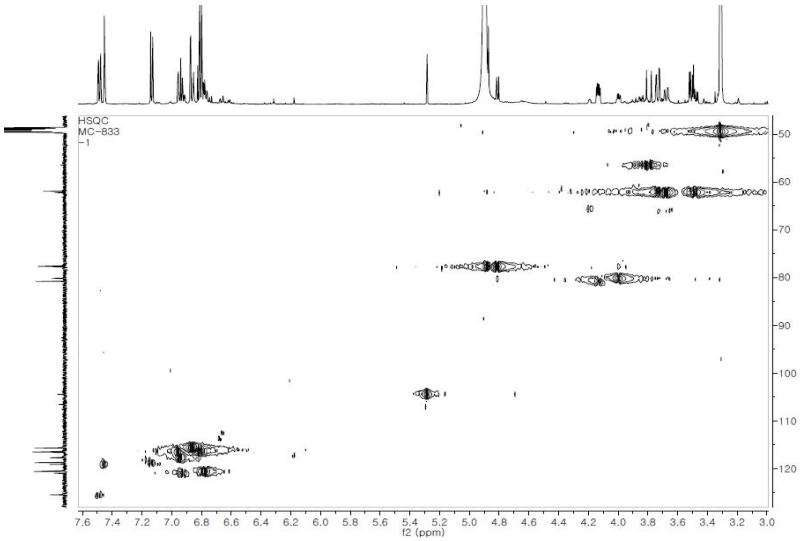

Figure 50: HSQC spectrum of compound **52** (600 MHz, MeOH-d_4)

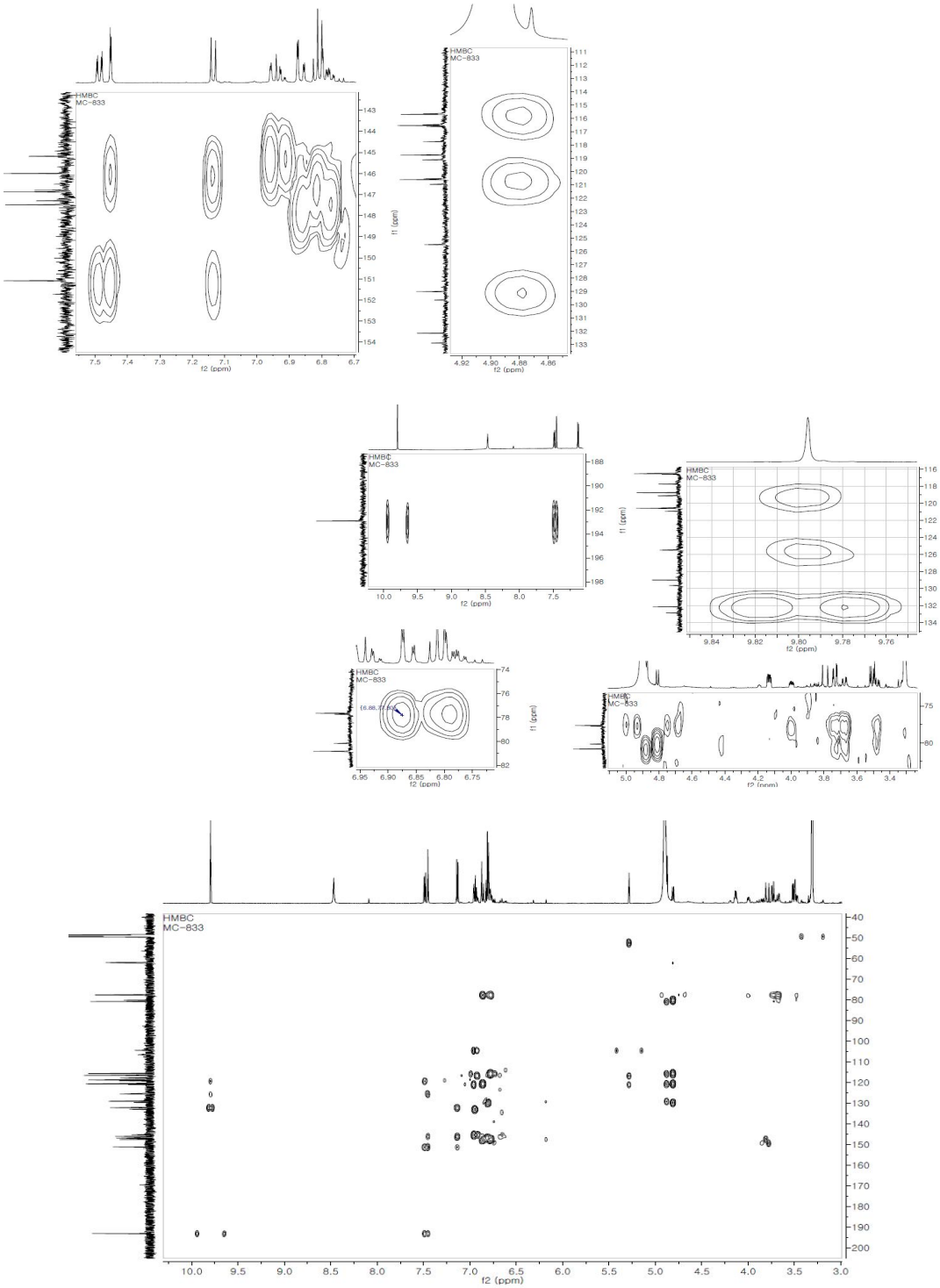

Figure 51: HMBC spectrum of compound **52** (600 MHz, MeOH-d_4)

3.2.6. Structural determination of new compound 51, and compound 54, 56

Compound **51** was also obtained as a light brown amorphous powder with absorption bands at 3406 (OH), 2927(C–C), 1606, 1468, 1374, 1279, 1142, and 1062 cm^{-1} in the IR spectrum. The HR-EI-MS of compound **51** showed a molecular ion peak at *m/z* 332.0898 $[M]^+$ (calcd $C_{20}H_{20}O_5$, 332.0896). The ^1H NMR spectrum of compound **52** showed characteristic signals for two sets of aromatic ABX-spin systems at δ_H 6.85 (1H, d, J = 7.8 Hz, H-5), 6.92 (1H, dd, J = 8.4, 1.8 Hz, H-6), 7.02 (1H, d, J = 1.8 Hz) for the ring A, and at δ_H 7.00 (1H, d, J = 8.4 Hz, H-5), 7.57 (1H, dd, J = 8.1, 1.8 Hz, H-6), 7.56 (1H, br, s, H-2) for the second ring B. Two oxymethine at δ_H 4.92 (d, J = 7.8 Hz, H-7) and δ_H 4.13 (m, H-8), and an oxymethylenes at δ_H 3.79 (1H, d, J = 2.4, 12.6 Hz, H-9ax) and 3.49 (1H, dd, J = 4.2, 12.6 Hz, H-9eq), with corresponding carbons at δ_C 77.5, 80.5, and 62.1, respectively. In addition, its ^1H and ^{13}C NMR spectra displayed a carboxylic group at δ_C 168.5, and a methoxy moiety at δ_H 3.88 (1H, s)/δ_C 56.6. All of these data resembled structure identical with arteminorin D.[45a] However, the *trans*-olefinic proton signals which assignable to aromatic AB system at δ 7.58 (d, J = 16.0 Hz, H-7) and 6.33 (d, J = 16.0 Hz, H-8), with two corresponding carbons at δ_C 146.1 and 117.4 in arteminorin D were disappeared at compound **51**.

The COSY spectrum of compound **51** showed the correlations between signal 4.92 (H-7) with 4.13 (H-8), and 4.13 (H-8) with 3.72, 3.49 (H_2-9). In HMBC experiment, correlations were observed from the H-2 (7.02) and H-6 (6.92) of the ring A to C-7 (77.7); H-2 (7.56) and H-6 (7.57) of the ring B to the carboxylic carbon (168.5); the proton signal of the methoxy moiety (3.88) to the oxygenated quaternary carbon at 149.4 (C-3).

Thus, compound **51** was elucidated as 3-methoxy-1′-carboxy-4′,7-epoxy-8,3′-oxyneoligna-4,9-diol,[48] a new novel natural neolignan from noni and named as modafolia D.

A large coupling constant between H-7 and H-8 ($J_{7,8}$ = 7.8 Hz), together with the $[\alpha]_D^{25}$: +4.68° (c = 0.167, MeOH) indicated that the two protons were in a *trans*-configuration.[45] The absolute configuration of C-7 and C-8 was determined by the CD spectrum: the positive Cotton effect near 192 and 208 nm and the negative Cotton effect at 220-226 nm suggested a configuration of 7*R* and 8*R*.[66]

Compound **54** was obtained as light brown amorphous powder, the molecular formula of compound **54** was tentatively determined as $C_{19}H_{18}O_7$ by EI-MS. Its ($[\alpha]_D^{25}$: –7.14 (c = 0.167, MeOH)) and CD data . Detailed comparison of the ^{1}H, ^{13}C NMR, and physicochemical data of compound **54** with published paper established compound **54** to be arteminorin D.[45a]

Compound **56** was obtained as brown amorphous gum and gave specific optical rotation value $[\alpha]_D^{25}$: +1.365 (c = 0.167) measured in MeOH. The molecular formula of compound **56** was determined as $C_{19}H_{22}O_6$ by EI-MS (*m/z* 346). The ^{1}H and ^{13}C NMR spectra of **56** gave a oxygenated propanoid chain at δ_H 3.55 (2H, t, J = 6.6 Hz, H-9)/δ_C 62.3 (C-9), 1.79 (2H, m)/δ_C 35.8 (C-8), and δ_H 2.58 (2H, t, J = 7.2 Hz, H-7)/δ_C 32.5 (C-7). Detailed comparison of its ^{1}H and ^{13}C NMR data with compound **54** and published data[45c] led to the identification of **56** to be rel-(7α,8β)-3-methoxy-4 ,7-epoxy-8,3 -oxyneolignan-4,9,9 -triol.

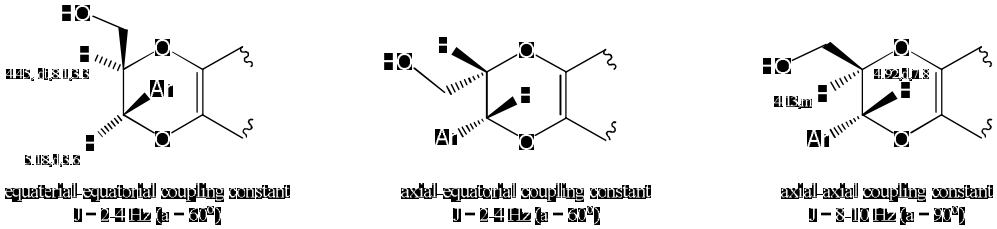

Figure 52: Relative stereochemistry proposed for compound **51**

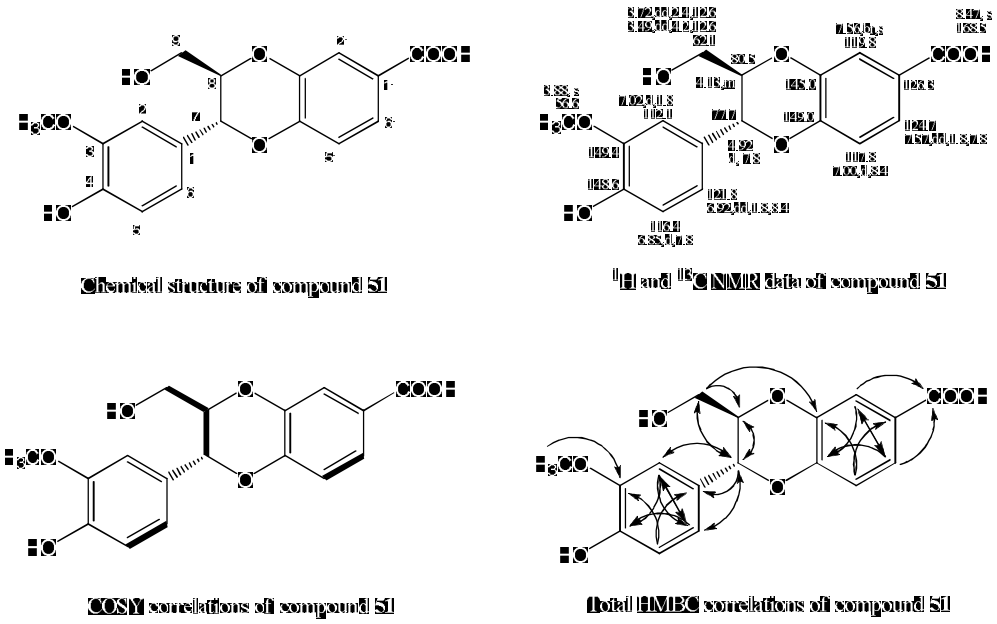

Figure 53: Chemical structure, 1D NMR, COSY, and HMBC of compound **51**

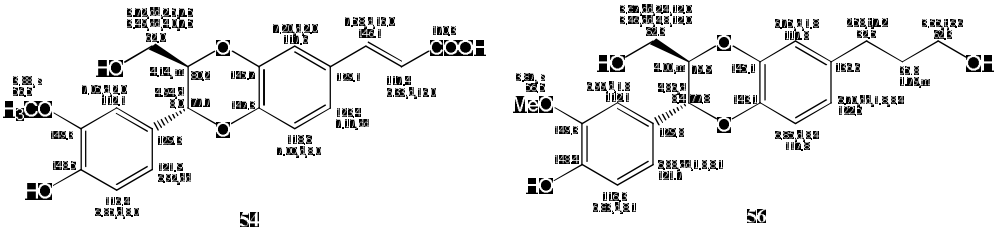

Figure 54: Chemical structure, ^{1}H- and ^{13}C NMR data of compounds **54** and **56**

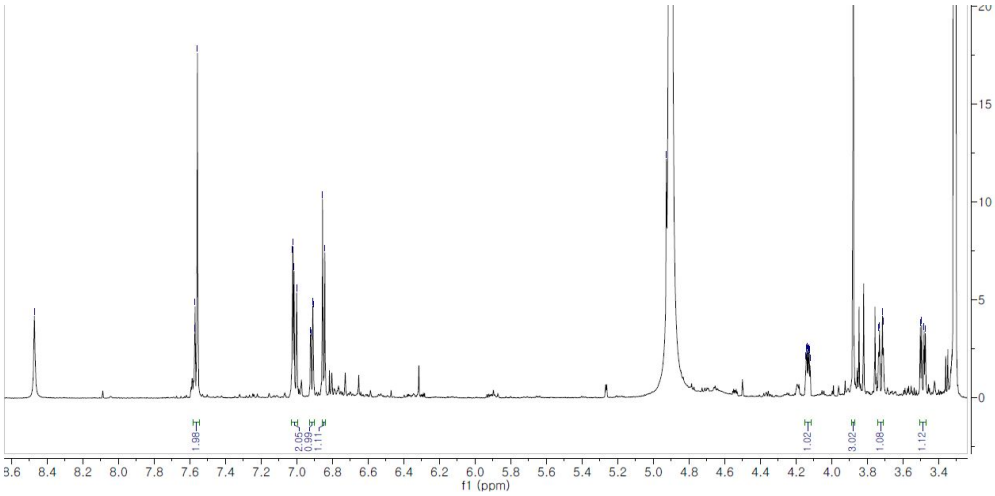

Figure 55: ^{1}H-NMR spectrum of compound **51** (600 MHz, MeOH-d_4)

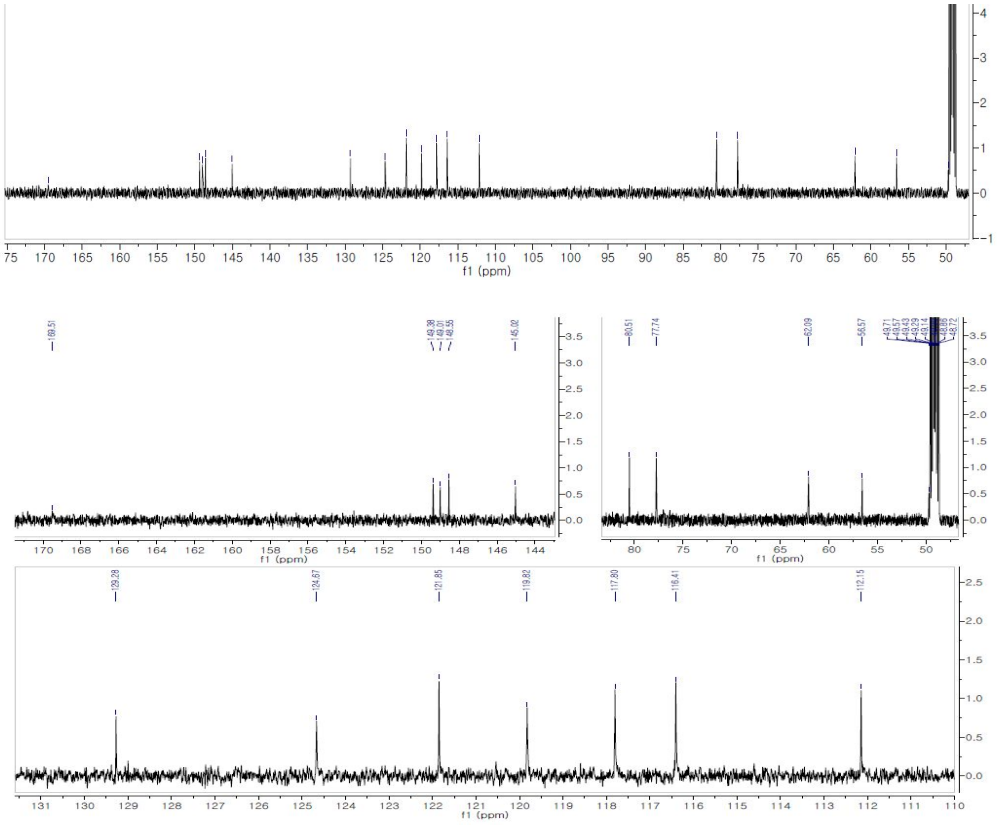

Figure 56: ^{13}C-NMR spectrum of compound **51** (150 MHz, MeOH-d_4)

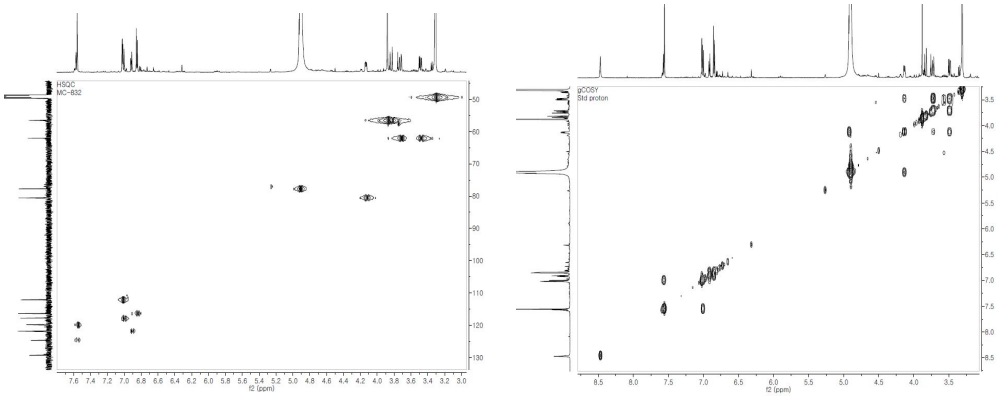

Figure 57: HSQC and COSY NMR spectra of compound **51** (600 MHz, MeOH-d_4)

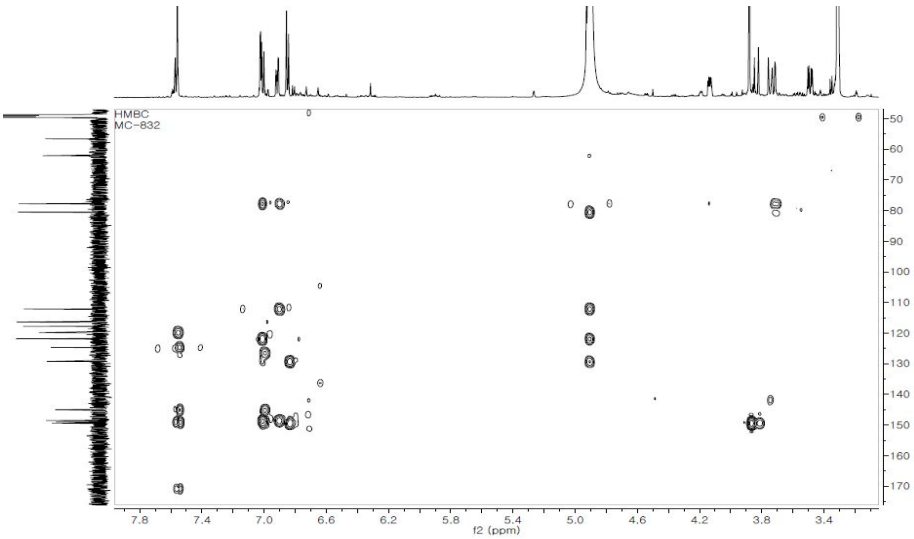

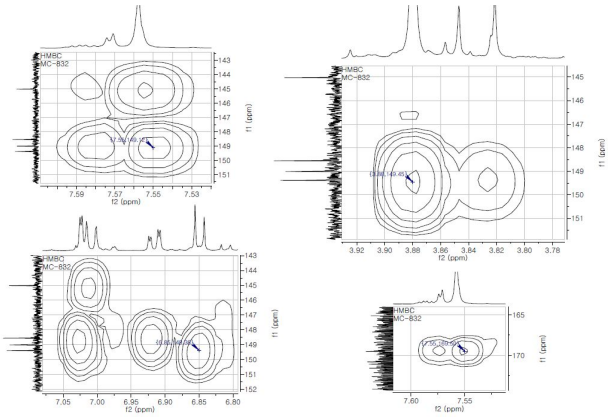

Figure 58: HMBC spectrum of compound **51** (600 MHz, MeOH-d_4)

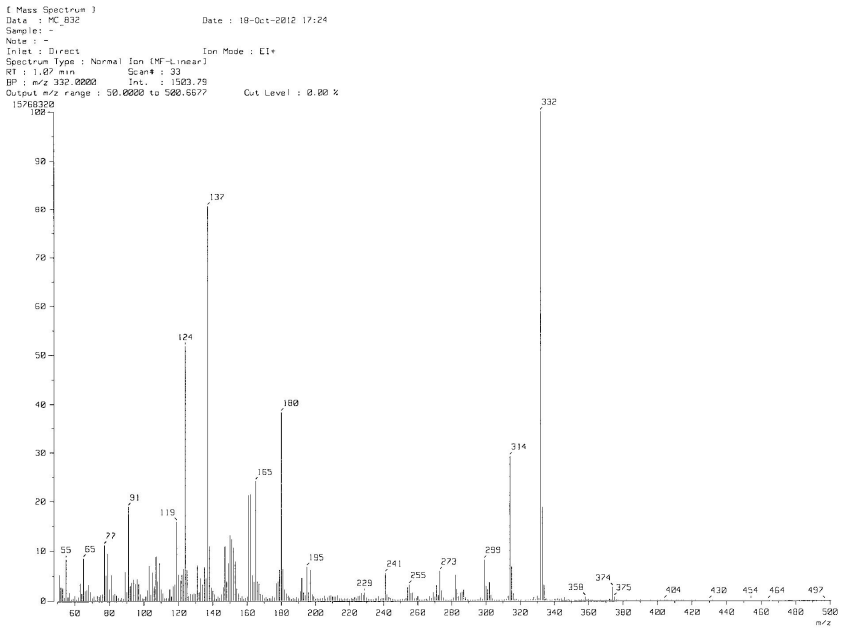

[Elemental Composition] Page: 1

Data : MC_832 Date : 31-Oct-2012 09:04
Sample: -
Note : -
Inlet : Direct Ion Mode : EI+
RT : 0.95 min Scan#: 20
Elements : C 100/1, H 100/1, O 10/1
Mass Tolerance : 3mmu
Unsaturation (U.S.) : 0.0 - 30.0

Observed m/z	Int%	Err[ppm / mmu]	U.S.	Composition
332.0898	93.2	+0.6 / +0.2	10.0	C 17 H 16 O 7

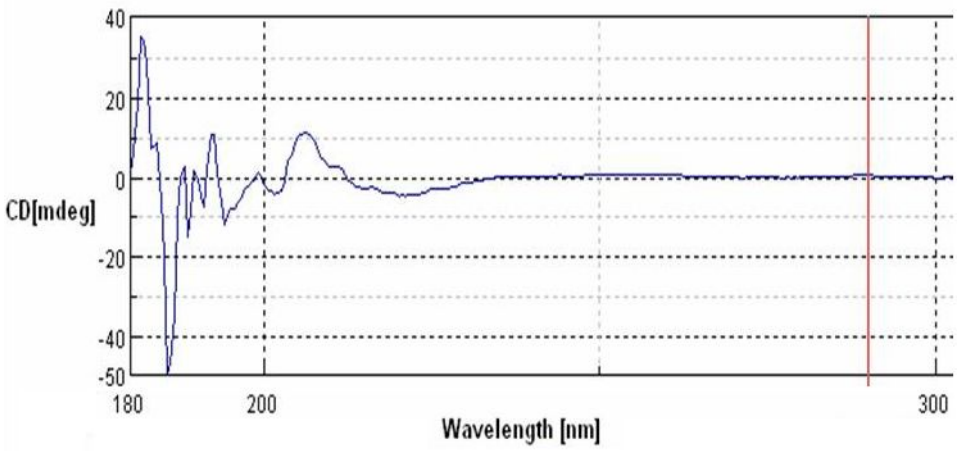

Figure 59: LR-EI-MS and HR-EI-MS and CD spectra of compound **51**

3.2.7. Structural determination of new compound 53 and compound 55

Compound **53** was also isolated as brown yellowish amorphous state and showed OH-functional group (3336 cm^{-1}), 1455 (C-O), 1142-1031 cm^{-1} in the IR spectrum. Its UV spectrum (c 0.025, MeOH) showed absorption maxima at 210, 235, and 280 nm. The molecular formula, $C_{16}H_{14}O_7$, was determined by a molecular peak at *m/z* 317 $[M-H]^+$ from HR-EI-MS. The ^1H and ^{13}C NMR spectra of **53** showed pattern similar with those of compound **52**, except that the aldehyde resonances were not present. Instead of that, a methyldioxiranyl signal was observed [δ_H 5.28 (1H, s), δ_C 104.4].

The ^1H NMR spectrum of **53** also presented two 1,3,4-trisubstituted phenyl groups [δ_H 6.82 (d, J = 8.1 Hz, H-5), 6.79 (dd, J = 8.1, 1.8 Hz, H-6), and 6.85 (d, J = 1.8 Hz); δ_H 6.95 (d, J = 8.4 Hz, H-5), 6.92 (dd, J = 8.4, 1.8 Hz, H-6), and 6.96 (d, J = 1.8 Hz, H-2)]. An oxymethine proton at δ_H 4.00 (H-8) which was coupled to the oxymethine proton at δ_H 4.89 (H-7) and the hydroxymethylene proton at δ_H 3.50 (H-9eq) and 3.73 (H-9ax). HMBC spectrum showed correlations between the oxymethine proton at δ_H 4.89 (H-7) and the 1,3,4-trisubstituted phenyl carbons at δ_C 115.6 (C-2) and 120.5 (C-6). While, the methyldioxiranyl proton at δ_H 5.28 were correlated with the other 1,3,4-trisubstituted phenyl carbons at δ_C 116.6 (C-2) and 120.9 (C-6). As compared with those of compound **52**, the $[\alpha]_D^{25}$ value +0.141 (c = 0.213) of **53** obtained in MeOH, and the coupling constant of $J_{7,8}$ = 7.8 Hz indicated the relative configuration of C-7 and C-8 in the dioxane ring as *trans*.[45] The absolute configuration of C-7 and C-8 was determined by a CD experiment, showing a positive Cotton effect at 187 nm and a negative Cotton effect near 222 nm evidenced a configuration of 7*R* and 8*R*.[44] From the above data analysis,

compound **53** was determined as (7α,8β)-3,4,9-trihydroxy-4′,7-epoxy-8,3′-oxyneoligna-1′-methyldioxiran, a novel natural neolignan appeared methyldioxane ring, and named modafolia F.

Compound 54 (modafolia F): Brown yellowish amorphous state; IR (KBr): v_{max} 3336 (OH), 2928 (C–C), 1455 (C-O), 1142-1031 cm^{-1}. UV (*c* 0.025, MeOH) λ_{max} nm: 210, 235, and 280 cm^{-1}; $[\alpha]_D^{25}$: +0.141° (c = 0.213, MeOH); HR-EI-MS *m/z* 317.0782 $[M-H]^+$, (calcd $C_{16}H_{13}O_7$, 317.0786).

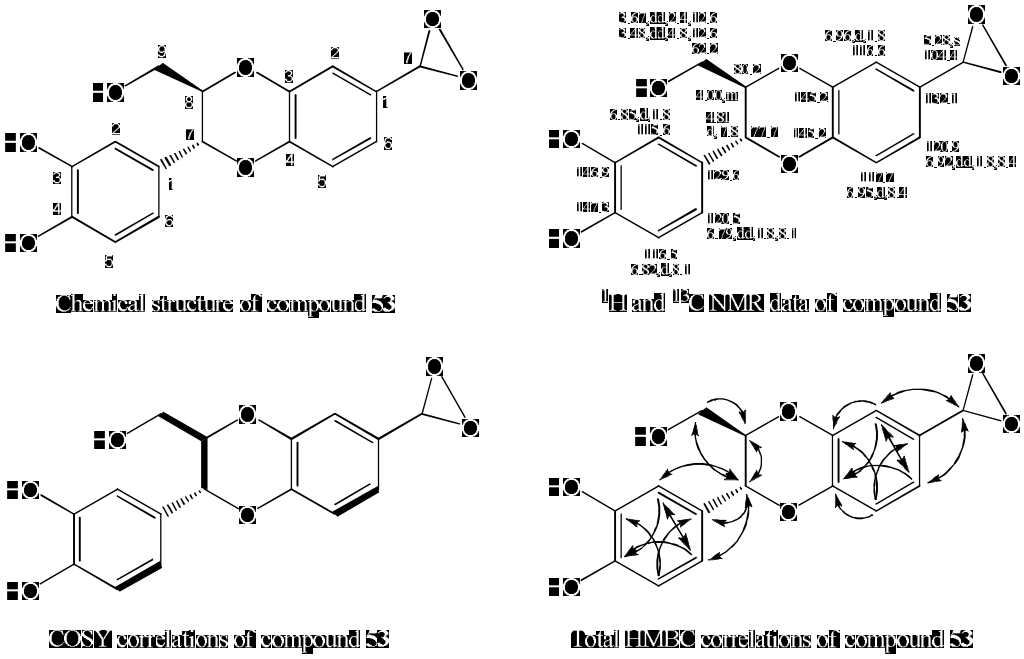

Figure 60: Chemical structure, 1D NMR, COSY, and HMBC of compound **53**

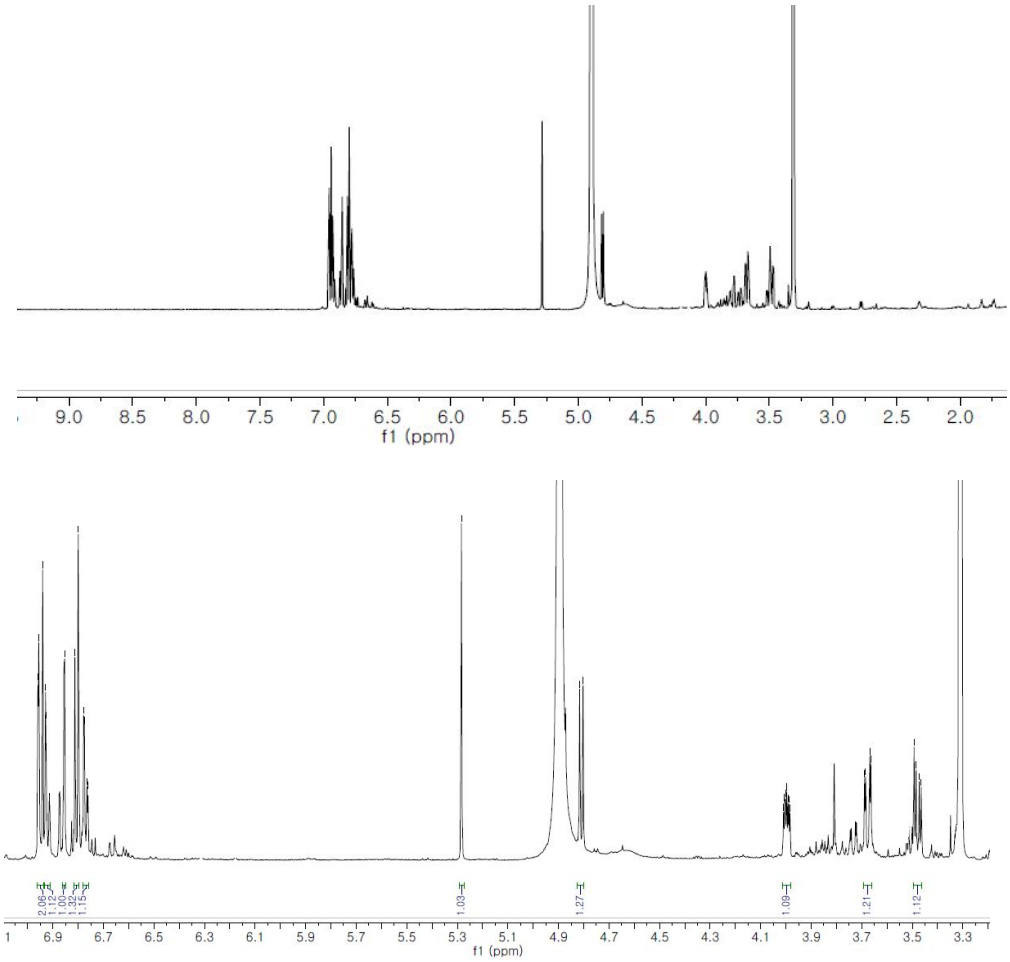

Figure 61: ^{1}H-NMR spectrum of compound **53** (600 MHz, MeOH-d_4)

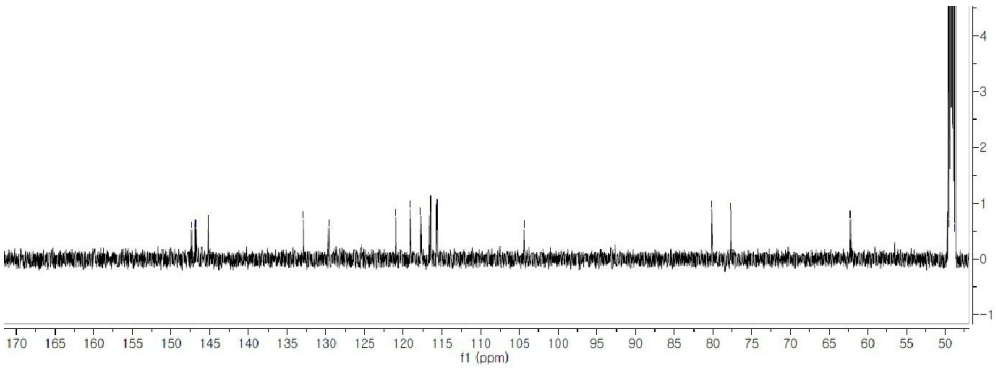

Figure 62: ^{13}C-NMR spectrum of compound **53** (150 MHz, MeOH-d_4)

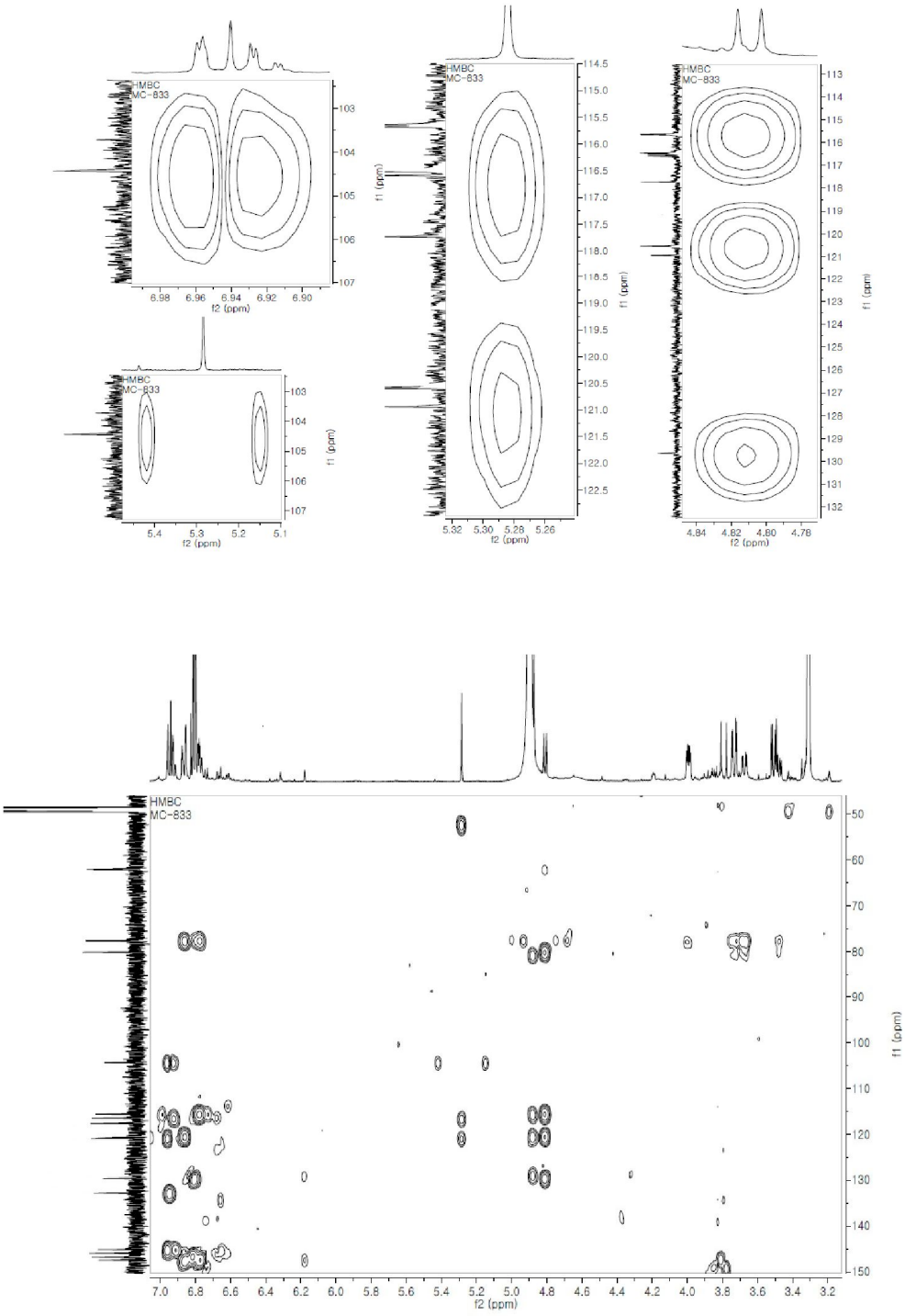

Figure 63: HMBC spectrum of compound **53** (600 MHz, MeOH-d_4)

Compound **55** was obtained as brownish amorphous showed absorption bands due to a conjugated carboxylic acid (1681 cm^{-1}) and a *trans* double bond (1660 and 979 cm^{-1}) in the IR (KBr) spectrum. The molecular formula, $C_{16}H_{14}O_7$, was deduced from EI-MS (m/z 344). The ^1H and ^{13}C NMR spectra of **55** were absolutely identical with morindolin.[44] Furthermore, in the aliphatic region of **55**, we observed *trans* double bond signals at δ_H 7.45 and 6.28 (d, J = 15.9 Hz) and an oxymethine signal at δ_H 5.50 and methylene signals at δ_H 3.77 and 3.82, which were coupled to a methine signal at δ_H 3.48. These data identified a benzofuran-type lignin for compound **55**. The coupling constant of $J_{7,8}$ = 6.0 Hz indicated that the relative configuration of C-7 and C-8 in the furan ring was *cis*.[44-45, 47] It is possible to revise the configuration at C-7 and C-8 of morindolin to be *cis*-form according to its coupling constants. The absolute configuration at C-7 and C-8 was deduced from the CD spectrum: a positive Cotton effect at 190 nm and the negative Cotton effect at 229 and 243 nm suggested a configuration of 7*R* and 8*R*. Thus, compound **55** was characterized as (7 *E*),(7α,8α)-3,3 ,4,9-tetrahydroxy-4 ,7-epoxy-8,5 -neolign-7 -en-9 -oic acid (morindolin).

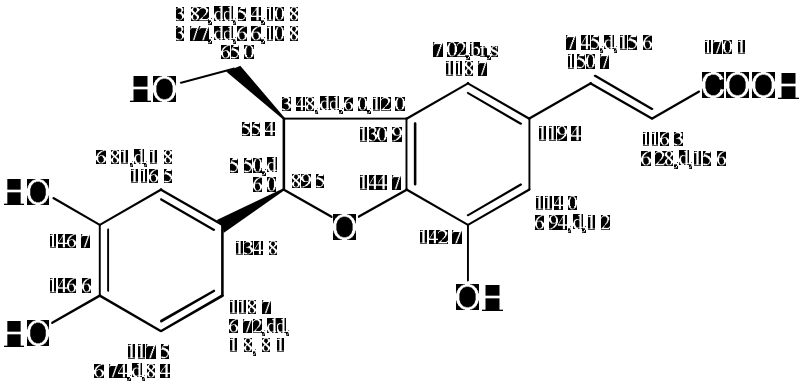

Figure 64: Chemical structure, ^1H and ^{13}C NMR data of compound **55**

3.2.8. Structural determination of new compound 57

Compound **57** was obtained as a brown-yellow amorphous powder. Its molecular formula, $C_{18}H_{16}O_7$, was deduced from a positive molecular ion peak at *m/z* 344.0896 $[M]^+$ (calcd for 344.0896) in the HR-EI-MS. The UV spectrum showed absorption bands at λ_{max} 210, 225, 234, 284, and 316 nm. IR spectrum suggested the presence of OH functional group (3405 cm^{-1}), C=O (1677-1631), 1510, and C–O stretching vibrations at 1159-1031 cm^{-1}.

The ^{1}H NMR displayed two ABX-type aromatic spin systems at δ_H 6.82 (1H, d, J = 1.8 Hz, H-2), 6.71 (1H, dd, J = 1.8, 8.4 Hz, H-6), and 6.76 (1H, d, J = 1.8 Hz, H-5), the other at δ_H 6.98 (1H, d, J = 8.4 Hz, H-5′), 7.12 (1H, dd, J = 1.8, 8.4 Hz, H-6′), and 7.16 (1H, d, J = 1.8 Hz, H-2′), and an AB-spin signals which assignable to a *trans*-olefinic protons at δ_H 7.48 (1H, d, J = 15.9 Hz, H-7′), 6.35 (1H, d, J = 15.9 Hz, H-8′), respectively. Furthermore, the ^{1}H and ^{13}C NMR spectra displayed an oxymethine proton at δ_H 4.45 (dt, J = 8.1, 3.3 Hz, H-8)/δ_C 80.4 which was coupled to the oxymethine proton at δ_H 5.18 (d, J = 3.6 Hz, H-7)δ_C 77.1 and the hydroxymethylene proton at δ_H 3.54 (dd, J = 8.4, 12.0 Hz, H-9ax) and 3.46 (dd, J = 3.6, 12.0 Hz, H-9eq)/δ_C 60.1, the COSY correlations in Figure 83 further supported this observation. In addition, ^{13}C NMR spectrum showed four oxygenated quaternary carbons at δ_C 146.7 (C-3), δ_C 144.0 (C-4), 145.4 (C-3), and 145.2 (C-4) and a carboxylic carbon at δ_C 172.9 (8-COOH). All of the above data resembled those of americanoic acid A (**58**),[44] the compound was also isolated in this study (see Scheme 3).

HMBC experiment of compound **57** indicated the correlations between the

oxymethine proton at δ_H 5.18 (H-7) and the 1,3,4-trisubstituted phenyl carbons at δ_C 130.4 (C-1), 114.6 (C-2), and 119.2 (C-6). While, the phenyl protons at δ_H 7.16 (H-2) and 7.12 (H-6) were correlated with the oxygenated aromatic carbon at δ_C 145.2 (C-4) and the olefinic carbon at 146.7 (C-7). Further correlations were observed between the olefinic proton at δ_H 7.48 (H-7) and the carboxyl carbon at δ_C 172.9 (C-9), and the quaternary carbon at δ_C 129.2 (C-1). The combination of all these data identified a 1,4-benzodioxan-type lignan.

From the coupling constant of $J_{7,8}$ = 3.6 Hz, the relative configuration of C-7 and C-8 in the dioxane ring was *cis*.[44-45, 47] The absolute configuration of C-7 and C-8 was deduced as 7*R* and 8*S* by the optical rotation value $[\alpha]_D^{25}$: –26.80° (c = 0.05, MeOH), and the positive Cotton effects near 190 nm and 212 nm. From the above data analysis, compound **57** was thus elucidated as (7′*E*),(7β,8β)-3,4,9-trihydroxy-4′,7-epoxy-8,3′-oxyneoligna-7′-en-8′-oic acid, and named modafolia G.

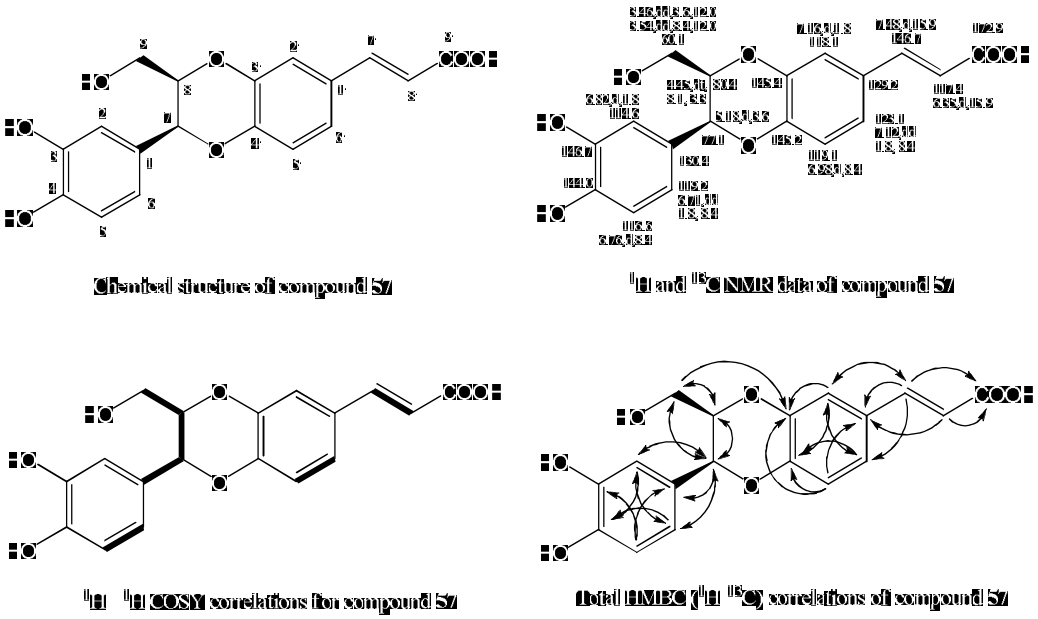

Figure 65: Chemical structure, 1D NMR, COSY, and HMBC data of compound **57**

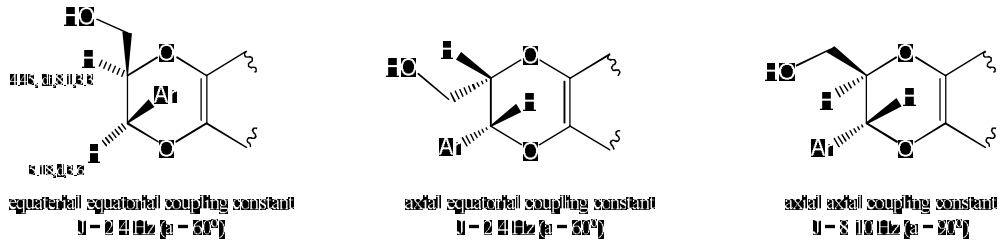

Fig. 66: Chemical shifts & coupling constants of the puran systems of compounds **57-59**

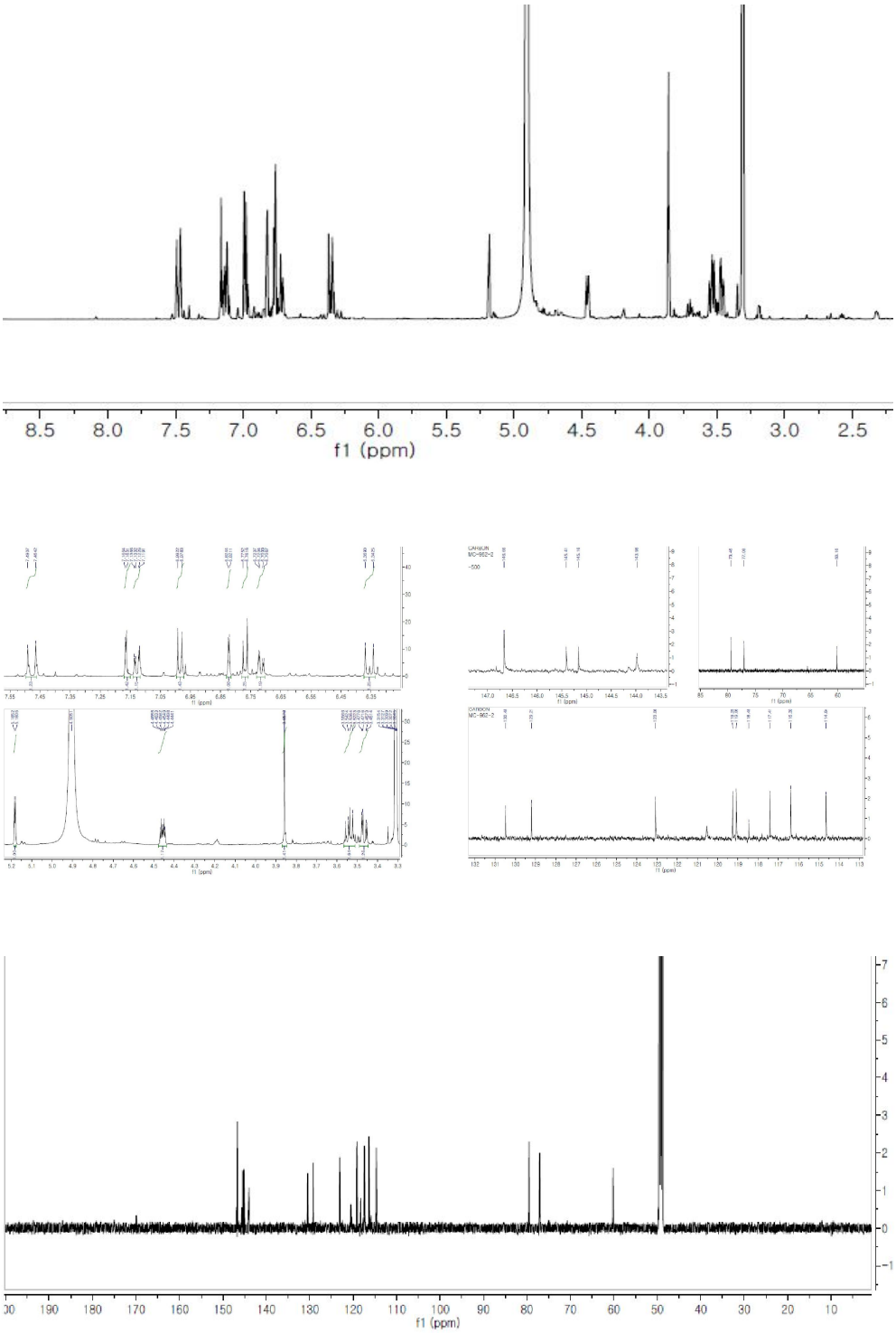

Figure 67: ^{1}H-NMR and ^{13}C-NMR spectra of compound **57** (600 MHz, MeOH-d_4)

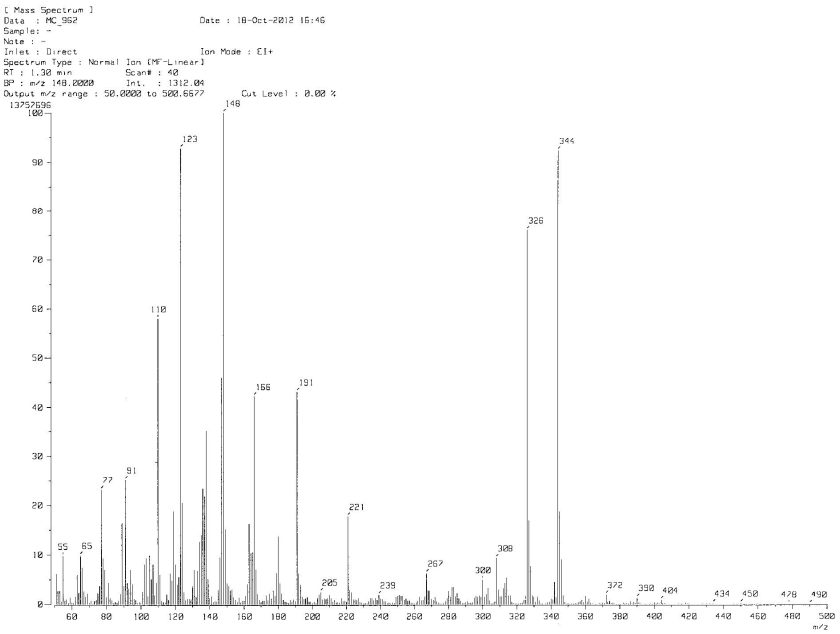

[Elemental Composition]

Page: 1

Data : MC_962

Date : 01-Nov-2012 09:18

Sample: -

Note : -

Inlet : Direct

Ion Mode : EI+

RT : 1.20 min

Scan#: 25

Elements : C 100/1, H 100/1, O 10/1

Mass Tolerance : 3mmu

Unsaturation (U.S.) : 0.0 - 30.0

Observed m/z	Int%	Err[ppm / mmu]	U.S.	Composition
344.0896	52.1	+0.0 / +0.0	11.0	C 18 H 16 O 7

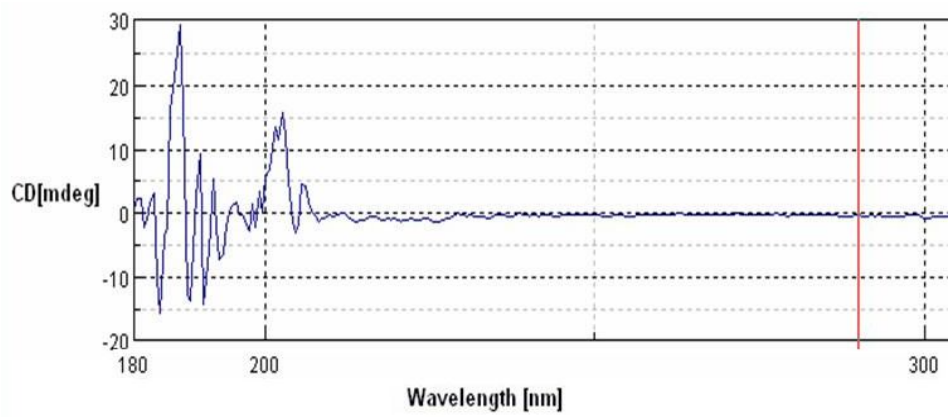

Figure 68: HR-EI-MS and HR-EI-MS and CD spectra of compound **57**

3.2.9. Structural determination of compound 58 and new compound 59

Compound **58** and **59** were obtained from a same sub-fraction by HPLC as a brown-yellow amorphous powder. Their retention times on RP-C18 column were 24.2 min and 28.5 min, respectively. The molecular formulas were deduced from a positive molecular ion peak at *m/z* 344.0896 $[M]^+$ (calcd for $C_{18}H_{16}O_7$, 344.0896) in their HR-EI-MS. The UV spectra showed absorption bands at λ_{max} 210, 225, 234, 284, and 316 nm. IR spectra suggested the presence of OH functional group (3405, 3219 cm^{-1}), conjugated C=O (1677, 1631), aromatic ring (1510), and C–O stretching vibrations at 1159-1031 cm^{-1}. Their ^1H and ^{13}C NMR were absolutely identical displaying two ABX-type aromatic spin systems at δ_H 6.81 (1H, d, J = 8.1 Hz, H-5), 6.71 (1H, dd, J = 1.8, 8.1 Hz, H-6), and 6.86 (1H, d, J = 1.8 Hz, H-2) for ring A, the other at δ_H 6.97 (1H, d, J = 8.4 Hz, H-5′), 7.11 (1H, dd, J = 1.8, 8.4 Hz, H-6′), and 7.15 (1H, d, J = 1.8 Hz, H-2′) for the B ring, and an AB-type spin signals which assignable to a *trans*-olefinic protons at δ_H 7.56 and 6.31 (each 1H, d, J = 15.9 Hz, H-7′). Furthermore, their ^1H and ^{13}C NMR spectra also displayed an oxymethine proton at δ_H 4.00-4.04 (1H, m, H-8)/δ_C 80.1-80.4 which were coupled to another oxygen-bearing methine proton at δ_H 4.82-4.85 (d, J = 8.1 Hz, H-7)/δ_C 77.7-78.1 and the hydroxymethylene proton at δ_H 3.47-3.48 (dd, J = 4.2, 12.0 Hz, H-9ax) and 3.69-3.70 (dd, J = 2.4, 12.0 Hz, H-9eq)/δ_C 62.1. A carboxylic carbon at δ_C 170.8 was found in their ^{13}C NMR spectra. The coupling constant of $J_{7,8}$ = 8.1 Hz indicated the relative configuration of C-7 and C-8 were *trans*.[44-45, 47]

Compound **58** was determined to be americanoic acid A by comparing its 1D NMR, optical rotation value $[\alpha]_D^{25}$: +2.24 (c = 0.87, MeOH), and CD data with published literature.

Similarly, the coupling constant of H-7 and H-8 of compound **59** was $J_{7,8}$ = 8.1 Hz, and its specific optical rotation value: $[\alpha]_D^{25}$: +1.36° (c = 0.78, MeOH), indicated the relative configuration of C-7 and C-8 in the dioxane ring was *trans*.[44-45, 47] The absolute configuration of C-7 and C-8 was deduced as 7*S* and 8*S* by the negative Cotton effects near 196, 210 nm and the positive Cotton effect at 202 nm from the circular dichroism experiments. Thus, chemical structure of compound **59** was established to be (7′*E*),(7β,8α)-3,4,9-trihydroxy-4′,7-epoxy-8,3′-oxyneoligna-7′-en-8′-oic acid, a new natural product named as modafolia H.

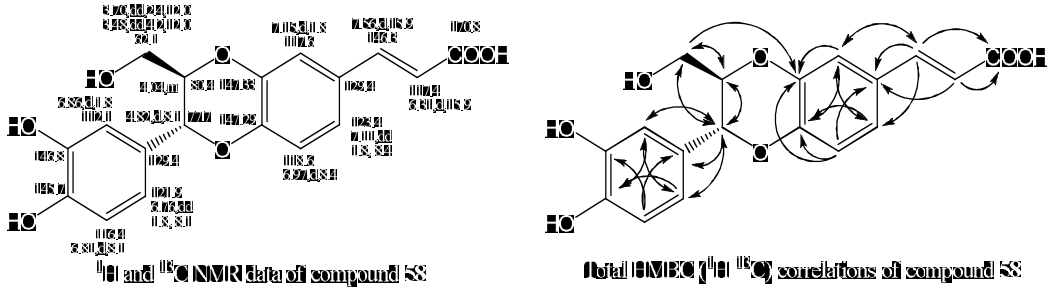

Figure 69: Chemical structure, 1D NMR, and HMBC data of compound **58**

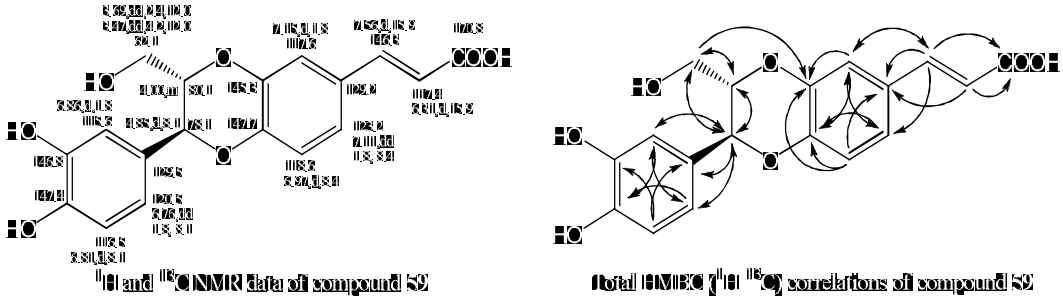

Figure 70: Chemical structure, 1D NMR, and HMBC correlation of compound **59**

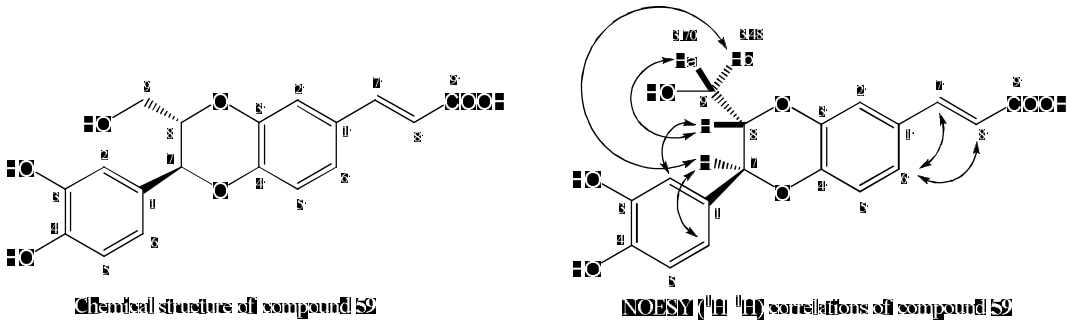

Figure 71: Chemical structure and NOESY correlations for compound **59**

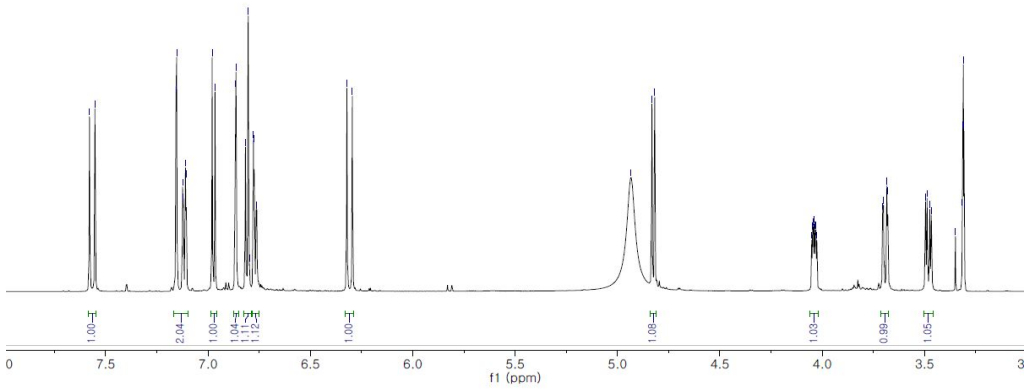

Figure 72: ^{1}H-NMR spectrum of compound **59** (600 MHz, MeOH-d_4)

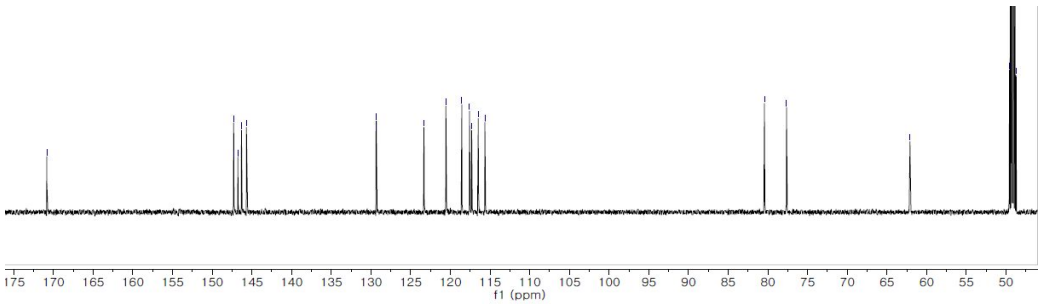

Figure 73: ^{13}C-NMR spectrum of compound **59** (150 MHz, MeOH-d_4)

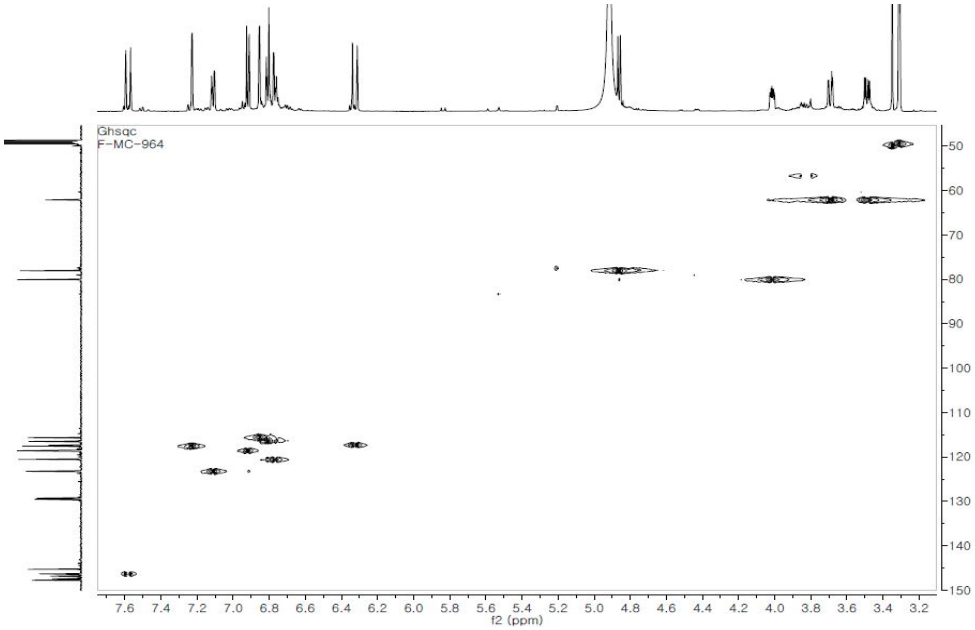

Figure 74: HSQC spectrum of compound **59** (600 MHz, MeOH-d_4)

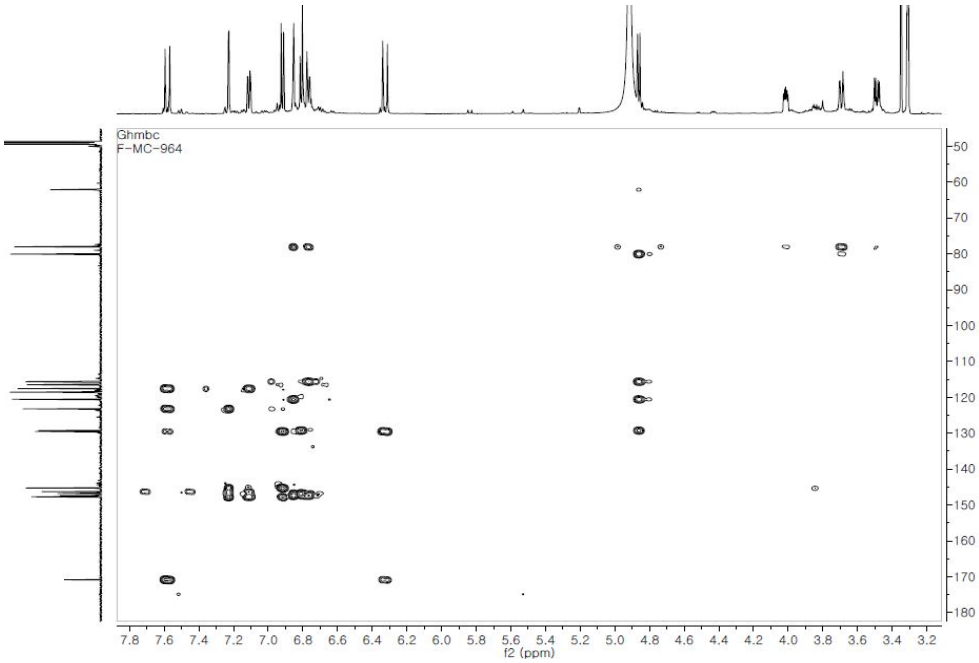

Figure 75: HMBC spectrum of compound **59** (600 MHz, MeOH-d_4)

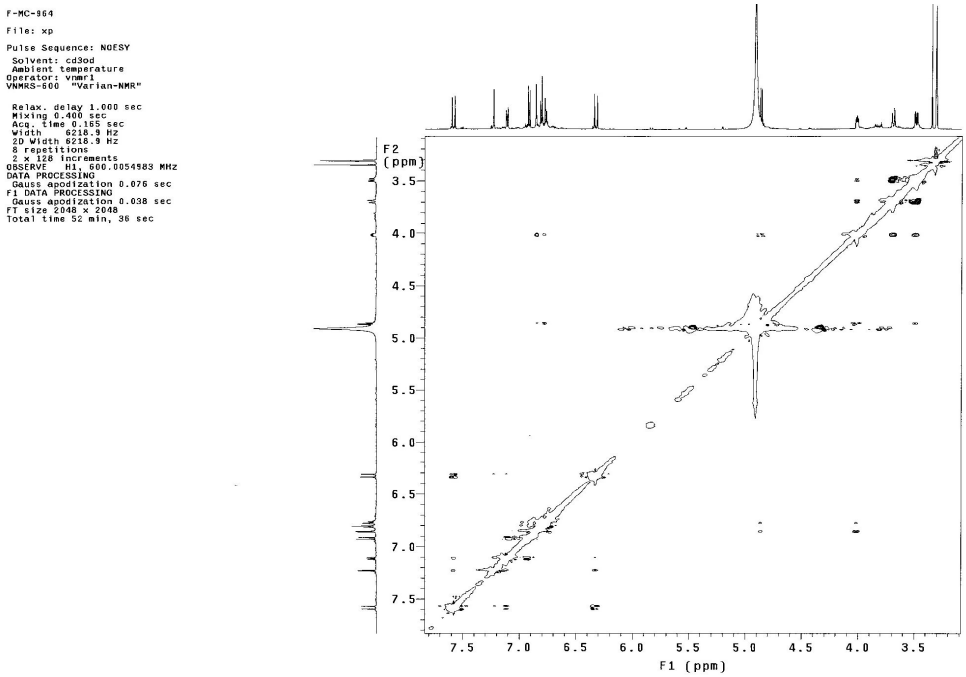

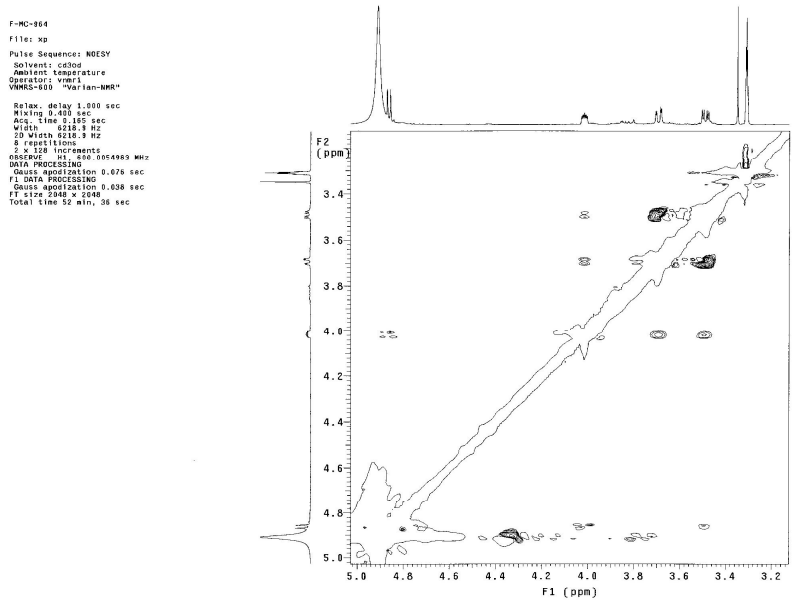

Figure 76: NOESY spectrum of compound **59** (600 MHz, MeOH-d_4)

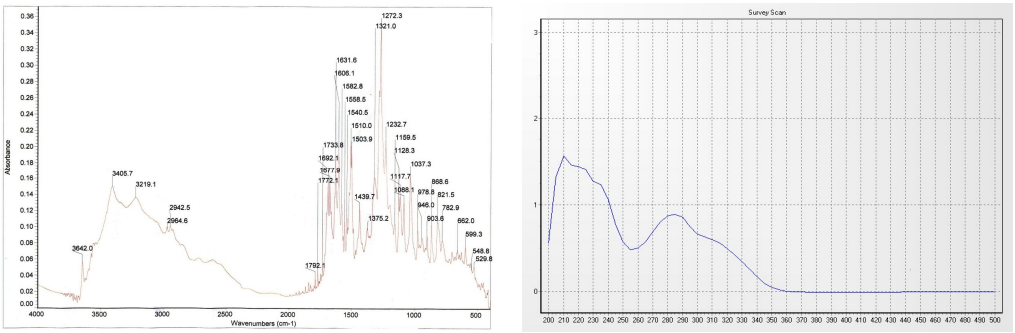

Figure 77: IR (KBr, left) and UV (c = 0.028, MeOH) spectra of compound **59**

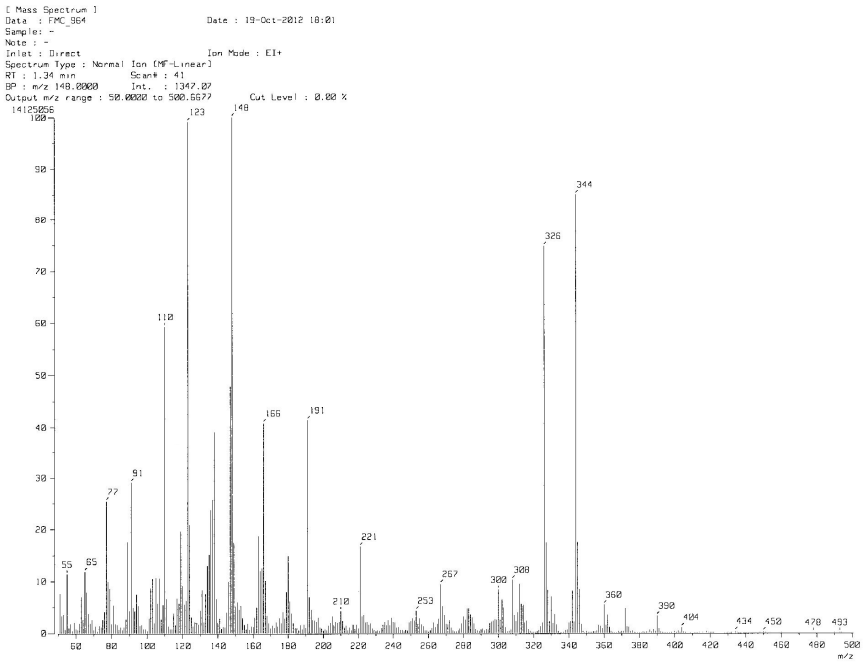

[Elemental Composition] Page: 1

Data : FMC_964 Date : 25-Oct-2012 17:36

Sample: -

Note : -

Inlet : Direct Ion Mode : EI+

RT : 0.30 min Scan#: 7

Elements : C 100/1, H 100/1, O 10/1

Mass Tolerance : 3mmu

Unsaturation (U.S.) : 0.0 - 30.0

Observed m/z	Int%	Err[ppm / mmu]	U.S.	Composition
344.0896	100.0	+0.1 / +0.0	11.0	C 18 H 16 O 7

Figure 78: LR-EI-MS and HR-EI-MS spectra of compound **59**

3.3. Assessment of anti-diabetes properties of the isolated compounds

3.3.1. Assessment of anti-diabetes properties of the isolated anthraquinones (1-21) from *Morinda longissima*

Repeated column chromatographies (including silica gel, RP-18, and semi-preparative HPLC) of the EtOH extract of the root of *M. longissima* resulted in the isolation of 21 anthraquinone analogues (**1-21**), comprising a new modasima A (**10**). In order to assess the potential activity of these compounds on glucose metabolism and insulin action, we first examined their stimulatory effects on the uptake of 2-NBDG, a fluorescents glucose analog widely used for monitoring glucose uptake in cells, using an *in vitro* assay[27] (2-NBDG assay) in 3T3-L1 adipocyte cells. The 3T3-L1 adipocytes was chosen for testing glucose uptake into cells, because fat represents one of the major body tissue types that are sensitive to the action of insulin. 3T3-L1 fibroblasts were induced to differentiate into adipocytes, and then each compound was treated to the differentiated 3T3-L1 adipocytes with 2-NBDG. As positive and negative controls, insulin at concentration of 2 μg/mL and DMSO were also added to the cells. As shown in figure 70, all the isolated anthraquinones enhanced 2-NBDG uptake into the cells at concentration of 10 μM. Among them, compounds **2**, **8-10**, and **17-18** were most potency showing stronger effects than insulin (positive control), while compounds **7**, **9**, **13**, **14**, **17**, and **21** were strong effect as insulin. Detailed investigation of the structure and activity relationship reveal that compounds which possess the hydrophobic functional groups at C-2 position displayed strong activity, while compounds bearing more electronegative atoms (more hydrophilic) showed weaker effects on glucose uptake.

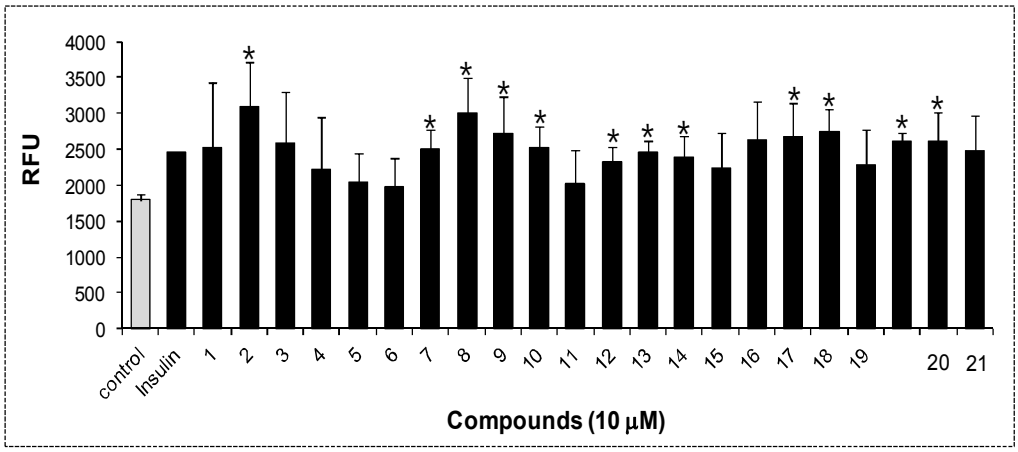

Figure 79: Stimulatory effects of isolated anthraquinones (**1-21**) on 2-NBDG uptake in 3T3-L1 adipocyte cells (* $p<0.05$) were measured using a fluorescent glucose probe (2-NBDG) assay with drug treatment. The tested compounds (**1-21**) were treated at a concentration of 10 μM to the cells for 90 min. DMSO and Insulin (2 μg/mL) were also treated to the cells as negative and positive controls.

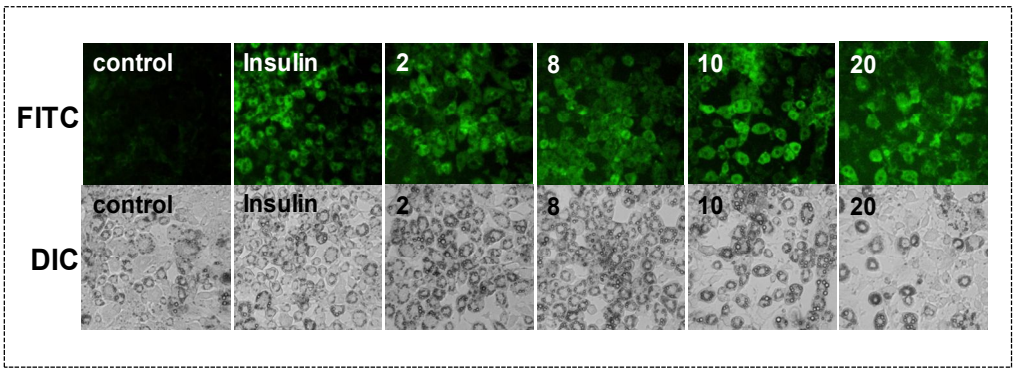

Figure 80: Increment of 2-NBDG uptake in 3T3 L1-adipocyte cells by compounds **2**, **8**, **10**, and **20**. Representative pictures were taken after drug treatment. Increased green fluorescent signals in the cells were observed by the drug treatment indicating that 2-NBDG was transported in to the cells.

Indeed, compounds **1** and **2** which are basic 9,10-anthraquinone skeleton showed opposite effects. Compound **1** with a hydroxy group attached at C-1 is more polar than **2** with a methyl group at C-2, however, compound **1** possessed weaker activity (2500 RFU, see fig. 94) than **2** (3000 RFU). In turn, compounds **3-5**, **11-12**, **14**, **19**, and **20-21**, which possess two hydroxyl and/or methoxy groups at C-1 and C-3, displayed weaker activities than **1** and **2**, while compound **6** with two hydroxy and one methoxy moieties at C-1, C-2, and C-3, showed worst effect on 2-NBDG uptake. This observation indicated that being more electronegative atom in the structure may responsible for decreasing activity of the 9,10-anthraquinones on 2-NBDG uptake. In contrast, compounds **7-10**, **13**, and **16**, which have more hydropholic groups (ethyl ether, butyl ether, hexyls ether) attached at C-2, showed potential effects even thought hydroxy and/or methoxy groups are presented. The above data obtained suggest that substitution of a hydrophobic moiety in B ring, especially at C-2 position, such as the substitution of methyl (compound **2**), ethyl ether (compounds **7**, **13**, **16**), and/or butyl ether (compound **9**) could be inducible 2-NBDG uptake. However, bearing groups with more electronegative atoms (OH and OCH_3) in their structure may responsible for the suppression of their effect on the uptake of 2-NBDG into adipocytes.

To further confirm the transportation efficacy of 2-NBDG into the cells by compounds **2**, **8**, **10**, and **20**, we measured fluorescent signals induce from adipocytes after drug treatment using fluorescence microscopy. As shown in figure 79, comparing to control group (treated with DMSO only), compounds **2**, **8**, **10**, and **20** showed higher level of fluorescent signals from the adipocytes representing the enhancement of 2-NBDG uptake into adipocytes. At the concentration of 10 μM, all treated compounds were significant

induced green fluorescence intensity as much as insulin or more. This result suggests that our compounds could be considered as new natural insulin mimickers, and it should be further progressed *in vivo* with animal model to investigate their insulin mimic property.

The glucose transport GLUT4 translocation is an essential step for inducible glucose uptake into to the plasma membrane in muscle and adipocyte cells. This translocation is mainly regulated by two independent pathways: the insulin signaling pathway and the AMP-activated protein kinase (AMPK) pathway.[49] It is suggested that to investigate the mechanism responsible for the stimulation of 2-NBDG uptake in to the cells by the isolated anthraquinones, we should examine their effects on the cellular signaling pathways that are known to mediate these processes. Thus, we further investigated whether the AMPK pathway is involved because this pathway is a major regulator of glucose uptake during exercise or in response to some anti-diabetic agents such as AICAR and metformin.[49]

According to this biological aspect, we first investigated whether these 2-NBDG uptake inducers activate AMPK. In differentiated C2C12 myotubes, we observed increased phosphorylation (Thr^{172}) of AMPK with compounds **2**, **8**, **10**, and **20** at the concentration of 10 μM (Figure 72) to a level comparable with the well-described AMPK agonist AICAR (as positive control, treated at 1 mM for 1 h). This observation suggests that the AMPK signaling pathway is likely responsible for the improvement of glucose uptake by these anthraquinones. The identification of the AMPK pathway as a likely mechanism for the stimulation of GLUT4 translocation by anthraquinones from *M. longsissima* is particularly interesting in relation to diabetes and obesity because activation of AMPK increases fatty

acid oxidation, inhibits lipid synthesis, and can improve insulin action.[50] Based on a number of studies showing that AMPK regulates a variety of different metabolic pathways, it is widely recognized as a useful and safe target for the treatment of metabolic disorders such as T2D and dyslipidemia.[50] Hence, our findings of the activation of the AMPK pathway by these compounds may implicate these 9,10-anthraquinones as a novel class of molecules with therapeutic potential for insulin resistance by targeting AMPK.

It is intriguing that many compounds that appear to have beneficial effects in the treatment of insulin resistance do so at least in part via activating AMPK activity. In particular, metformin and berberine,[51] two plant-derived compounds that have been described to increase insulin sensitivity and reduce body weight, both activate AMPK. In view of the potency of the 9,10-anthraquinones on glucose metabolism, it will be of great interest to determine the primary targets of these compounds leading to the activation of AMPK. One possibility might be that they act at intracellular target(s) after entering cells by some active transport system as the structural features of anthraquinones may render them as substrates for naturally occurring transporters. Alternatively, these anthraquinones may bind to cell surface receptors, initiating an intracellular signaling pathway analogous to that seen with other biological molecules such as leptin and adiponectin. Future studies should be required to distinguish between these possibilities.

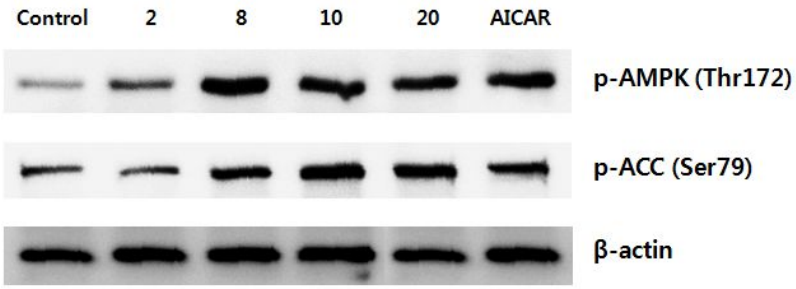

Figure 81: Stimulation effects of compounds **2**, **8**, and the new compounds **10** and **20** on AMPK in differentiated C2C12 cells. C2C12 cells were exposed to treated compounds for 2 h or positive control (AICAR, 1 mM) for 1 h, and phosphorylation of AMPK at Thr172 and ACC at Ser79 were analyzed by Western blotting. DMSO was also added to the cells as a negative control.

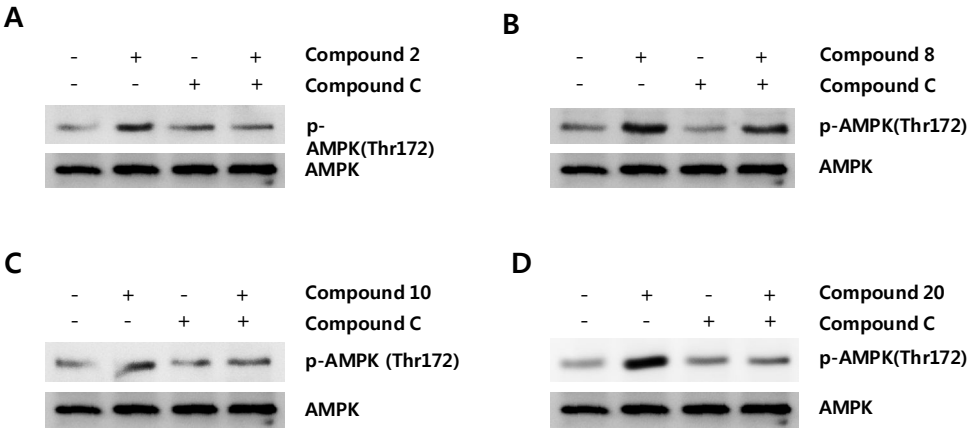

Figure 82: C2C12 cells were exposed to treated compounds for 2 h and phosphorylation of AMPK was analyzed by Western blotting. Compounds **2** (**A**), **8** (**B**), **10** (**C**), and **20** (**D**) increased phosphorylation of AMPK at Thr172 and ACC at Ser79. Increased phosphorylation of AMPK induced by 10 μM of compounds **2**, **8**, **10**, and **20** were abrogated by pretreatment with compound C (an AMPK inhibitor) at 10 μM for 10 min.

3.3.2. Assessment of anti-diabetes properties in cells of the isolated compounds (22-59) from *Morinda citrifolia*

Repeated column chromatographies (including silica gel, RP-18, MPLC, and semi-preparative HPLC) of the MeOH-soluble extract of the fermented dried powder of the fruits of *M. citrifolia* (Noni) resulted in the isolation of 38 natural products (**22-59**), comprising two new phenyl propanoids (**24** and **25**), 3 new 7,9':7',9-diepoxylignanes (Enantiomers **42**, **47**, and **49**), and 5 new 3',7-epoxy-8,4'-oxyneolignanes (**51-53**, **57**, and **59**). The stimulatory effects of 2-NBDG uptake on 3T3-L1 adipocyte cells of these isolates (**22–59**) were tested *in vitro* according to a published method.[27]

In this assay we used Rosiglitazone (Rosi) as positive control at concentration of 400 μM. Rosi showed improving glucose uptake in adipocytes almost twice as compared with control (DMSO). All our compounds were treated at concentration of 40 μM (10 times less than Rosi), however, compounds **42**, **45**, **47**, and **51** were treated at 20 μM (20 times less than Rosi). As shown in figure 74, all isolates possessed stimulatory effects on glucose uptake except for compounds **22**, **24**, **26**, and **37**. At concentration of 40 μM, ursolic acid (**39**) possessed stronger effect than Rosi at 400 μM. At 20 μM (20 times less than Rosi), however new compound **42** (modafolia A), compound **45** (lirioresinol B), and compound **48** showed stimulatory effect as strong as Rosi. This is suggested that compounds **42**, **45**, and **48** may possess stronger activity than positive control. Compounds **44** (pinoresinol) and **56** are ranked at third active group among the potential stimulators. The above observations indicate that triterpenoid (**39**) and the 7,9':9,7'-diepoxylignanes (**42-49**) have stronger stimulatory effects on 2-NBDG uptake than the 3',7-epoxy-8,4'-oxyneolignanes (compounds **50-59**) which in turn possessed higher effects than phenylpropanoids (**22-35**),

iridoids (**36-38**), and flavonoids (**40-41**) (See Fig. 17-20, and 82). In 7,9':9,7'-diepoxylignane type, compound **42** is (+)-(7α,7'β,8α,8'α)-3,3',4,4'-tetrahydroxy-7,9':7',9-diepoxylignane, an isomer of **43** (+)-(7α,7'α,8α,8'α)-3,3',4,4'-tetrahydroxy-7,9':7',9-diepoxylignane, but compound **42** showed stronger activity than **43**. Compounds **44** and **45** are isomers of **43** bearing two and four methoxyl moieties showed increasing activity, respectively. This is indicated that the 7α,7'β,8α,8'α skeleton is importance in response to the 2-NBDG uptake of the 7,9':7',9-diepoxylignanes, and substitution of hydroxyl group by methoxyl moiety may also responsible for enhancing effect of these lignans. However, opposite result was observed for the 7,9'-epoxylignano-9,7'-lactone (Compounds **48** and **49**). (+)-3,4,3',4'-tetrahydroxy-9,7'α-epoxylignano-7α,9'-lactone (**48**) displayed stronger activity than new compound **49** [(+)-3,4,3',4'-tetrahydroxy-9,7'β-epoxylignano-7β,9'-lactone] (see Fig. 19 and 82). Similar aspects were also observed for the 3',7-epoxy-8,4'-oxyneolignanes (compounds **50-59**). Indeed, the known compound **58**, (7′*E*),(7α,8β)-3,4,9-trihydroxy-4′,7-epoxy-8,3′-oxyneoligna-7′-en-8′-oic acid, displayed stronger activity than two new isomers **57** [(7′*E*),(7β,8β)] and **59** [(7′*E*),(7β,8)] (Fig. 20 and 82 for more detail). Moreover, attachment of methoxyl moiety at C-3 also increased the activity of these 3',7-epoxy-8,4'-oxyneolignanes (Compounds **54** and **56**). However, new compound **51** even borne a methoxyl group at C-3, but showed no effect on 2-NBDG uptake. It may be explained by the substitution of the (*E*)-propenoic moiety (compounds **50**, **54**, and **58**) by the COOH functional group. This observation has evidenced why new compounds **51**, **52**, and **53** possessed weaker activity than compounds **50**, **54**, **56**, and **58** in this 2-NBDG assay. In addition to the SAR, the iridoids **36-38** and flavonoids **40-41** were found to possess moderate activity. Except for compound **40**, both these type of compounds

possessed β-D-glucose moiety in their structures which may suppressed the transportation of 2-NBDG into the cells (Fig. 18 and 82). Finally, the courmarinoids (Compounds **23** and **26**), the benzoic acid derivatives (Compounds **29-34**), and the phenylpropanoid analogues (Compounds **22**, **24-25**, **27-28**, and **35**) displayed weak or no activity in stimulating 2-NBDG uptake in 3T3-L1 adipocytes (Fig. 17 and 82).

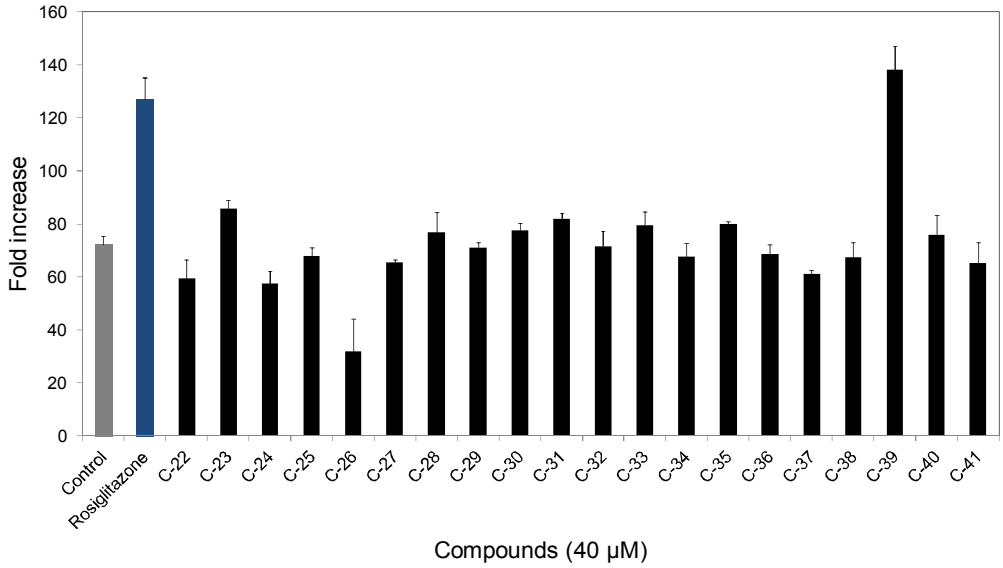

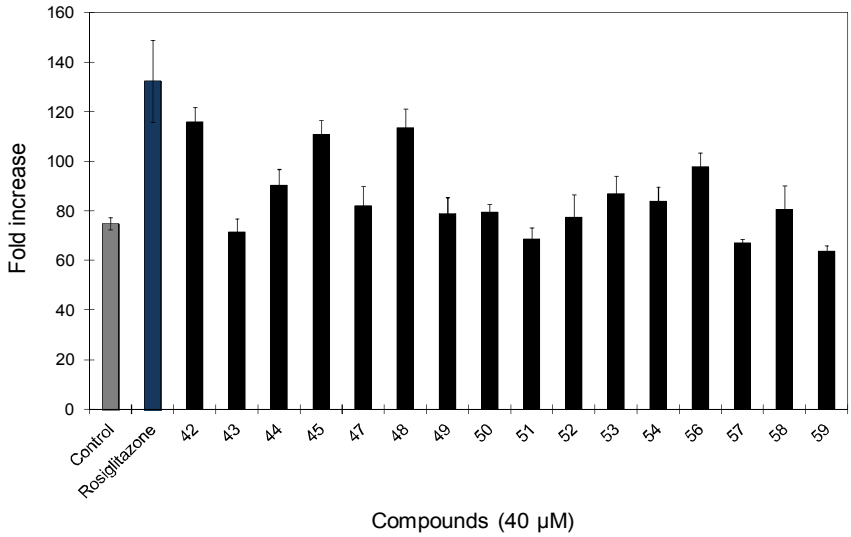

Figure 83: Stimulatory effects of isolated compounds (**22-59**) on 2-NBDG uptake in 3T3-L1 adipocyte cells. The tested compounds (**22-59**), DMSO (vehicle), and Rosiglitazone (positive control, 400 μM) were treated to the cells for 90 min. Compounds **42**, **45**, **47**, and **51** were treated as 20 μM.

The identification of the AMPK pathway as a likely mechanism for the stimulation of 2-NBDG uptake by triterpenoid **39** and 7,9':9,7'-diepoxylignanes **42-49** from *M. citrifolia* is particularly interesting in relation to diabetes and obesity because activation of AMPK increases fatty acid oxidation, inhibits lipid synthesis, and can improve insulin action. Thus, western blot was carried out for measuring phosphorylation of AMPK and its downstream target ACCs in cultured skeleton cells. As shown in figure below, all compounds possessed stimulatory effect on AMPK activity at concentration of 10 μM. Of them, compound **48** (7,9'-epoxylignano-9,7'-lactone) showed the most potential activation, followed by the unsymmetrical (+)-(7α,7'β,8α,8'α)-3,3',4,4'-tetrahydroxy-7,9':7',9-diepoxylignane (**42**), and then the symmetrical (+)-(7α,7'α,8α,8'α)-3,3',4,4'-tetrahydroxy-7,9':7',9-diepoxylignane (**44** and **45**).

Based on a number of studies showing that AMPK regulates a variety of different metabolic pathways, it is widely recognized as a useful and safe target for the treatment of metabolic disorders such as T2D and dyslipidemia. Hence, our findings of the activation of the AMPK pathway by these compounds may implicate these 7,9':9,7'-diepoxylignanes, especially the 7,9'-epoxylignano-9,7'-lactone, as novel classes of molecules with therapeutic potential for insulin resistant states by targeting AMPK.

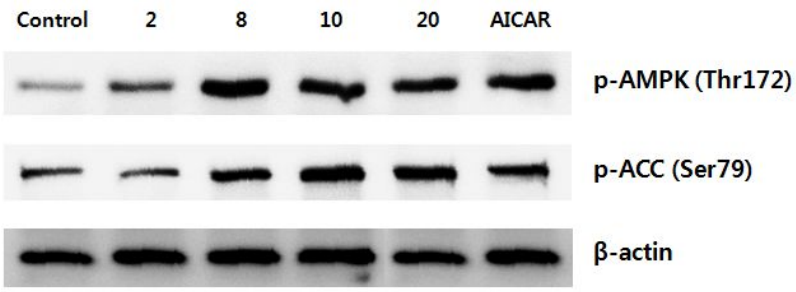

Figure 84: Activation of AMPK by compounds **39**, **42**, **44**, **45**, and **48** in differentiated C2C12 cells. C2C12 cells were exposed to treated compounds for 2 h or positive control (AICAR, 1 mM) for 1 h, and phosphorylation of AMPK at Thr172 and ACC at Ser79 were analyzed by Western blotting. DMSO was also added to the cells as a negative control.

IV. CONCLUSIONS

A diabetes epidemic is underway. An estimated 30 million people world-wide had diabetes in 1985. By 1995, this number had shot up to 135 million. The latest WHO (World Health Organization) estimate (for the number of people with diabetes, world-wide, in 2011) is 366 million. This will increase to at least 522 million by 2030. Diabetes caused 4.6 million deaths and caused at least USD 465 billion dollars in healthcare expenditures in 2011. Insulin resistance is one of the characteristic pathogenic signs of type-2 diabetes, and several drugs that increase the insulin sensitivity are currently in clinical trial. However, these drugs have a number of limitations, which include adverse effects and high rates of secondary failure. Thus, there is still a need to search for new natural products which can act as insulin mimics and/or insulin sensitizers for stimulating glucose uptake in cells.

It has been known for over two decades that a short time after exercise insulin works much better at stimulating glucose transport into muscle. Recently, evidence has emerged that AMPK may responsible for increasing insulin sensitivity and indirectly inhibit pre-adipocyte differentiation by improving insulin action. Because AMPK plays an important role in mediating the whole-body glucose and lipid homeostasis and regulating food intake and energy expenditure, AMPK activators are considered promising candidates for the discovery of anti-obesity and anti-diabetes agents as well as drugs for the treatment of other metabolic diseases.

As part of our ongoing investigation for discovering new anti-diabetes agents from medicinal plants, we found that the total extracts of two *Morinda* species (*M. longissima*

and *M. citrifolia*) showed *in vitro* glucose uptake effects on 3T3-L1 adipocytes. Thus, phytochemical investigation of these medicinal plants using chromatographic methods (silica gel, RP-C_{18}, MPLC, and preparative HPLC system) led to the isolation of 59 natural products, comprising of 9 new compounds (**10**, **42**, **47**, **49**, **51-53**, **57**, and **59**) as active constituents. Their chemical structures were elucidated on the basis of spectroscopic (including ^{1}H, ^{13}C, COSY, HSQC, HMBC, NOESY, and MS) data interpretation and physicochemical (IR, UV, CD, and $[\alpha]_D$) data analyses, as well as comparison with those published in literatures. According to the structural skeleton, their structures were characterized to be 21 anthraquinones (**1-21**), 2 coumarinoids (**23** and **26**), 12 phenylpropanoid and caffeic acid derivatives (**22-35**), 2 flavonol and flavonol glucoside (**40** and **41**), 3 iridoids (**36-38**), one triterpenoid (**39**), and 18 lignans and neolignans (**42-59**).

In order to assess the anti-diabetes properties of these natural products, we first examined their stimulatory effects on glucose uptake using an *in vitro* assay with 2-NBDG as substrate in 3T3-L1 adipocyte cells.[27] At the concentration of 10 μM, all isolates showed potential stimulatory effects on 2-NBDG uptake with a level comparable with insulin and rosiglitazone, the positive controls used in this assay. Among the isolated anthraquinones, compounds **2**, **8**, **10**, and **20** were found to be the most potency showing stronger effect than insulin (Fig. 78). Among the compounds isolated from Noni (**22-59**), we found that the 7,9':7',9-diepoxylignan and 3',7-epoxy-8,4'-oxyneolignan possessed strongest activity, and the most major compound **39** (ursolic acid, at 20 μM) showed stronger activity than rosiglitazone, the positive control used at 400 μM. The others showed moderate to weak

effect.

In addition, to confirm the transportation efficacy of 2-NBDG into the cells by isolated anthraquinones **2**, **8**, **10**, and **20**, we further measured fluorescent signals induced in the cells after drugs treatment. As shown in figure 79, we found that green fluorescent signals were increased in the cells after treatment of insulin and our compounds **2**, **8**, **10**, and **20**. This observation indicates that the transportation of 2-NBDG into cells was increased by our compounds.

In progress, we investigated whether these 2-NBDG uptake inducers activate AMPK pathway or not. In differentiated C2C12 cells, we observed increased phosphorylation of AMPK (Thr^{172}) by our compounds at the concentration of 10 μM (Fig. 80 and 83) to a level comparable with AICAR, a positive control used at 1 mM. Anthraquinones **8** showed strongest activation, followed by compounds **10** and **20**. Among the lignan type, 9,7'α-epoxylignano-7α,9'-lactone (**48**) and triterpenoid (**39**) showed strongest activation. These observation suggest that the AMPK signaling pathway is likely responsible for the improvement of glucose uptake by these compounds (**2**, **8**, **10**, **20**, **39**, **42**, **44**, **45**, and **48**). Taken together, our results indicated that anthraquinones, ursolic acid, and 7,9':7',9-diepoxylignans, especially the 9,7'α-epoxylignano-7α,9'-lactone, may be important for 2-NBDG uptake activity *in* v*itro*. Additionally, 2-NBDG uptake effects by members of anthraquinones and neolignans have not been previously reported. Further confirmation of the anti-diabetes effects of these natural products and evaluation of their potential *in vivo* efficacy in a diabetic model are necessary.

V. REFERENCES AND NOTES

1. UK prospective diabetes study (UKPDS) group 33. Intensive blood glucose control with sulphonylureas or insulin compared with conventional treatment and risk of complications with type-2 diabetes. *Lancet*, **1998**, *352*, 837-853.

2. Kumar S., Boulton AJ., Beck-Nielsen H., Berthezene F., Muggeo M., Persson B., Spinas G.A., Donoghue S., Lettis S., Stewart-Long P. Troglitazone, an insulin action enhancer, improves metabolic control in NIDDM patients. Troglitazone Study Group. *Diabetologia* **1996**, *39*, 701-709.

3. Moller DE. New drug targets for type 2 diabetes and the metabolic syndrome. *Nature* **2001**, *414*, 821-827.

4. (a) Miller DE., Flier JS. Insulin resistance-Mechanism, syndromes, and implications. *N Engl J Med*, 1991. 325, 938-948. (b) Reaven GM., Banting lecture 1998, Role of insulin resistance in human disease. *Diabetes*, **1988**, *37*, 1595-1607.

5. (a) Berg, J.M.; Tymoczko, J.L.; Stryer, L. *Biochemistry: International Edition*, 6th ed.; W.H. Freeman: New York, NY, USA, 2006. (b) Clark, D.; Sokoloff, L. *Basic Neurochemistry: Molecular, Cellular and Medical Aspects*; Lippincott: Boston, MA, USA, 1999.

6. (a) Speizer, L.; Haugland, R.; Kutchai, H. Asymmetric transport of a fluorescent glucose analogue by human erythrocytes. *Biochim. Biophys. Acta* **1985**, *815*, 75–84. (b) Yoshioka, K.; Takahashi, H.; Homma, T.; Saito, M.; Oh, K.B.; Nemoto, Y.; Matsuoka, H. A novel fluorescent derivative of glucose applicable to the assessment

of glucose uptake activity of Escherichia coli. *Biochim. Biophys. Acta* **1996**, *1289*, 5–9. (c) Yamada, K.; Saito, M.; Matsuoka, H.; Inagaki, N. A real-time method of imaging glucose uptake in single, living mammalian cells. *Nat. Protoc.* **2007**, *2*, 753–762.

7. (a) Yoshioka, K.; Saito, M.; Oh, K.B.; Nemoto, Y.; Matsuoka, H.; Natsume, M.; Abe, H. Intracellular fate of 2-NBDG, a fluorescent probe for glucose uptake activity, in Escherichia coli cells. *Biosci. Biotechnol. Biochem.* **1996**, *60*, 1899–1901. (b) Louzao, M.C.; Espina, B.; Vieytes, M.R.; Vega, F.V.; Rubiolo, J.A.; Baba, O.; Terashima, T.; Botana, L.M. "Fluorescent glycogen" formation with sensibility for *in vivo* and *in vitro* detection. *Glycoconj. J.* **2008**, *25*, 503–510. (b) Yoshioka, K.; Oh, K.B.; Saito, M.; Nemoto, Y.; Matsuoka, H. Evaluation of 2-[N-(7-nitrobenz-2-oxa-1,3-diazol-4-yl)amino]-2-deoxy-D-glucose, a new fluorescent derivative of glucose, for viability assessment of yeast Candida albicans. *Appl. Microbiol. Biotechnol.* **1996**, *46*, 400–404.

8. (a) Wang, M. Y.; West, B. J.; Jensen, C. J.; Nowicki, D.; Chen, S.; Palu, A. K.; Anderson, G. *Acta. Pharmacol. Sin.* **2002**, 23, 1127–1141. (b) Xie, Z. W. *Compilation of Chinese Traditional Herbal Drugs. 2nd ed.* People's Sanitation Publishing House: Beijing, 2000; Vol. 1. p 332. and Vol. 2. p 211.

9. Alison D. Pawlus and A. Douglas Kinghorn. Review of the ethnobotany, chemistry, biological activity and safety of the botanical dietary supplement *Morinda citrifolia* (noni). *J. Pharm. Pharmacology* **2007**, *59*, 1587–1609.

10. (a) McClatchey, W. C. (2002) Diversity of growth forms and uses in the *Morinda citrifolia* L. complex. Proceedings of the 2002 Hawai'i Noni Conference. University

of Hawaii at Manoa, College of Tropical Agriculture and Human Resources, pp 5–10. (b) Nelson, S. C. (2003) Morinda citrifolia L. Rubiaceae (Rubioideae) coffee family. Permanent Agriculture Resources. Holualoa, HI.

11. (a) Nguyen, V. D. (**1990**) *Medicinal plants in Vietnam*. World Health Organization, Regional Office for the Western Pacific, Hanoi, North Vietnam. (b) Morton, J. F. The ocean-going noni, or Indian mulberry (*Morinda citrifolia*, Rubiaceae) and some of its "colorful" relatives. *Econ. Bot*. **1992**, *46*, 241–256.

12. (a) Chang, P.; Lee, K. H. *Phytochemistry* **1984**, *23*, 1733–1736. (b) Xiang, W.; Song, Q. S.; Zhang, H. J.; Guo, S. P. *Fitoterapia* **2008**, *79*, 501–504.

13. (a) Pham, M. H.; Nguyen, D. T.; Do, T. D.; Nguyen, K. P. Hepatoprotective effect of the roots of Morinda longissima Y.Z. Ruan Rubiaceae tree. *TC Dược liệu*. **2004**, *9*, 95–98. (b) Nguyen, D. T.; Do, T. D.; Pham, M. H. Isolation and identification of emodin from roots of nho dong (Morinda longissima Y.Z.Ruan Rubiaceae). *TC Thông tin y dược học*. **2004**, *7*, 27–28.

14. Carling, D. The AMP-activated protein kinase cascade - a unifying system for energy control. *TRENDS in Biochemical Sciences*. **2004**, *29*(1), 18-24.

15. Kim, M. S.; Lee, K. U. Role of hypothalamic 5′-AMP-activated protein kinase in the regulation of food intake and energy homeostasis. *J. Mol. Med*. **2005**, *83*, 514–520.

16. (a) Ewart, M. A.; Kennedy, S. AMPK and vasculoprotection. *Pharmacology & Therapeutics* **2011**, *131*, 242–253. (b) Viollet, B.; Mounier, R.; Leclerc, J.; Yazigic, A.; Foretz, M.; Andreelli, F. Targeting AMP-activated protein kinase as a novel

therapeutic approach for the treatment of metabolic disorders. *Diabetes & Metabolism* **2007**, *33*, 395–402.

17. (a) Klaus, S.; Keipert, S.; Rossmeis, M..; Kopecky, J. Augmenting energy expenditure by mitochondrial uncoupling: a role of AMP-activated protein kinase. *Genes Nutr*. **2012**, *7*, 369–386. (b) Kahn, B. B.; Alquier, T.; Carling, D.; Hardie, D. G. AMP-activated protein kinase: Ancient energy Review gauge provides clues to modern understanding of metabolism. *Cell Metabolism* **2005**, *1*, 15-25.

18. (a) Miller, E. J.; Russell, R. R.; Li, J.; Young, L. H. AMPK – A pivotal rheostat in the control of cardiac metabolism. *Drug Discovery Today: Disease Mechanisms* **2005**, *2*(1), 93-100. (b) Zhang, B. B.; Zhou, G.; Li, C. AMPK: An Emerging Drug Target for Diabetes and the Metabolic Syndrome. *Cell Metabolism* **2009**, *9*, 407-416. (c) Winder, W. W.; Thomson, D. M. Cellular energy sensing and signaling by AMP-activated protein Kinase. *Cell Biochem. Biophys*. **2007**, 47, 332–347.

19. (a) Zhou, G.; Myers, R.; Li, Y.; Chen, Y.; Shen, X.; Fenyk-Melody, J.; Wu, M.; Ventre, J.; Doebber, T.; Fujii, N. et al. Role of AMP-activated protein kinase in mechanism of metformin action. *J. Clin. Invest*. **2008**, *108*, 1167–1174. (b) Shaw, R. J.; Lamia, K. A.; Vasquez, D.; Koo, S. H.; Bardeesy, N.; Depinho, R. A.; Montminy, M.; and Cantley, L. C. The kinase LKB1 mediates glucose homeostasis in liver and therapeutic effects of metformin. Science **2005**, *310*, 1642–1646. (c) Musi, N.; Hirshman, M. F.; Nygren, J.; Svanfeldt, M.; Bavenholm, P.; Rooyackers, O.; Zhou, G.; Williamson, J. M.; Ljunqvist, O.; Efendic, S.; et al. Metformin increases AMP-activated protein kinase activity in skeletal muscle of subjects with type-2 diabetes. *Diabetes* **2002**, *51*,

2074–2081.

20. (a) LeBrasseur, N. K.; Kelly, M.; Tsao, T. S.; Farmer, S. R.; Saha, A. K.; Ruderman, N. B.; and Tomas, E. Thiazolidinediones can rapidly activate AMP-activated protein kinase in mammalian tissues. *Am. J. Physiol. Endocrinol. Metab.* **2006**, *291*, E175–E181. (b) Ye, J. M.; Dzamko, N.; Hoy, A. J.; Iglesias, M. A.; Kemp, B.; and Kraegen, E. Rosiglitazone treatment enhances acute AMP-activated protein kinase-mediated muscle and adipose tissue glucose uptake in high-fat-fed rats. Diabetes **2006**, *55*, 2797–2804. (c) Kubota, N.;Yano, W.; Kubota, T.; Yamauchi, T.; Itoh, S.; Kumagai, H.; Kozono, H.; Takamoto, I.; Okamoto, S.; Shiuchi, T.; et al. Adiponectin stimulates AMP activated protein kinase in the hypothalamus and increases food intake. *Cell Metab*. **2007**, *6*, 55–68.

21. (a) Minokoshi, Y.; Kim, Y. B.; Peroni, O. D.; Fryer, L. G.; Muller, C.; Carling, D.; and Kahn, B. B. Leptin stimulates fatty-acid oxidation by activating AMP-activated protein kinase. *Nature* **2002**, *415*, 339–343. (b) Suzuki, A.; Okamoto, S.; Lee, S.; Saito, K.; Shiuchi, T.; and Minokoshi, Y. Leptin stimulates fatty acid oxidation and peroxisome proliferator-activated receptor alpha gene expression in mouse C2C12 myoblasts by changing the subcellular localization of the alpha2 form of AMP-activated protein kinase. *Mol. Cell. Biol*. **2007**, *27*, 4317–4327.

22. (a) Kola, B.; Hubina, E.; Tucci, S. A.; Kirkham, T. C.; Garcia, E. A.; Mitchell, S. E.; Williams, L. M., Hawley, S. A.; Hardie, D. G.; Grossman, A. B., et al. Cannabinoids and ghrelin have both central and peripheral metabolic and cardiac effects via AMP-activated protein kinase. *J. Biol. Chem*. **2005**, *280*, 25196–25201. (b) Lopez, M.; Lage,

R.; Saha, A. K.; Perez-Tilve, D.; Vazquez, M. J.; Varela, L.; Sangiao-Alvarellos, S.; Tovar, S.; Raghay, K.; Rodriguez-Cuenca, S.; et al. Hypothalamic fatty acid metabolism mediates the orexigenic action of ghrelin. *Cell Metab*. **2008**, *7*, 389–399. (c) Kola, B.; Farkas, I.; Christ-Crain, M.; Wittmann, G.; Lolli, F.; Amin, F.; Harvey-White, J.; Liposits, Z.; Kunos, G.; Grossman, A. B.; et al. The orexigenic effect of ghrelin is mediated through central activation of the endogenous cannabinoid system. *PLoS ONE* **2008**, *3*, e1797.

23. (a) Collins, Q. F.; Liu, H. Y.; Pi, J.; Liu, Z.; Quon, M. J.; and Cao, W. Epigallocatechin-3-gallate (EGCG), a green tea polyphenol, suppresses hepatic gluconeogenesis through 50-AMP-activated protein kinase. *J. Biol. Chem*. **2007**, *282*, 30143–30149. (b) Yin, J.; Gao, Z.; Liu, D.; Liu, Z.; and Ye, J. Berberine improves glucose metabolism through induction of glycolysis. *Am. J. Physiol. Endocrinol. Metab*. **2008**, *294*, E148–E156.

24. (a) Kim, M. S.; Park, J. Y.; Namkoong, C.; Jang, P. G.; Ryu, J. W.; Song, H. S.; Yun, J. Y.; Namgoong, I. S.; Ha, J.; Park, I. S.; et al. Anti-obesity effects of alpha-lipoic acid mediated by suppression of hypothalamic AMP-activated protein kinase. *Nat. Med*. **2004**, *10*, 727–733. (b) Lee, W. J.; Lee, I. K.; Kim, H. S.; Kim, Y. M.; Koh, E. H.; Won, J. C.; Han, S. M.; Kim, M. S.; Jo, I.; Oh, G. T.; et al. Alpha-lipoic acid prevents endothelial dysfunction in obese rats via activation of AMP-activated protein kinase. *Arterioscler. Thromb. Vasc. Biol*. **2005**, *25*, 2488–2494. (c) Onay-Besikci, A.; Wagg, C.; Lopaschuk, T. P.; Keung, W.; and Lopaschuk, G. D. Alpha-lipoic acid increases cardiac glucose oxidation independent of AMP-activated protein kinase in isolated

working rat hearts. *Basic Res. Cardiol*. **2007**, *102*, 436–444.

25. (a) Cool, B.; Zinker, B.; Chiou, W.; Kifle, L.; Cao, N.; Perham, M.; Dickinson, R.; Adler, A.; Gagne, G.; Iyengar, R.; et al. Identification and characterization of a small molecule AMPK activator that treats key components of type 2 diabetes and the metabolic syndrome. *Cell Metab*. **2006**, *3*, 403–416. (b) Scott, J. W.; van Denderen, B. J. W.; Jorgensen, S. B.; Honeyman, J. E.; Steinberg, G. R.; Oakhill, J. S.; Iseli, T. J.; Koay, A.; Gooley, P. R.; Stapleton, D.; and Kemp, B. E. Thienopyridone drugs are selective activators of AMP-activated protein kinase [beta]1-containingcomplexes. *Chem. Biol*. **2008**, *15*, 1220–1230.

26. Pang, T.; Zhang, Z. S.; Gu, M.; Qiu, B. Y.; Yu, L. F.; Cao, P. R.; Shao, W.; Su, M. B.; Li, J. Y.; Nan, F. J.; et al. Small molecule antagonizes autoinhibition and activates AMP-activated protein kinase in cells. *J. Biol.Chem*. **2008**, *283*, 16051–16060.

27. (a) 2-NBDG as a fluorescent indicator for direct glucose uptake measurement. *J. Biochem. Biophys. Methods* **2005**, *64*, 207–215. (b) Molecular imaging of glucose uptake in oral neoplasia following topical application of fluorescently labeled deoxy-glucose. *Int. J. Cancer* **2009**, *124*, 2634–2642. (c) Novel use of fluorescent glucose analogues to identify a new class of triazine-based insulin mimetics possessing useful secondary effects. *Mol. BioSyst.* **2011**, *7*, 346–358. (d) Uptake of 2-NBDG as a method to monitor therapy response in breast cancer cell lines. *Breast Cancer Res. Treat.* **2011**, *126*, 55–62.

28. (a) Cui, L.; Ndinteh, D. T.; Na, M. K.; Thuong, P. T.; Muruumu, J. S.; Njamen, D.; Mbafor, J. T.; Fomum, Z. T.; Ahn, J. S.; Oh, W. K. *J. Nat. Prod.* **2007**, *70*(6), 1039–

1042. (b) Nguyen, P. H.; Le, T. V. T.; Thuong, P. T.; Dao, T. T.; Njamen, D.; Mbafor, J. T.; Fomum, Z. T.; Kang, K. W.; Oh, W. K. *Bio. Med. Chem. Lett.* **2009**, *19*, 6745−6749. (c) Cui, L.; Thuong, P. T.; Lee, H. S.; Ndinteh, D. T.; Mbafor, J. T.; Fomum, Z. T.; Oh, W. K. *Bio. Med. Chem*. **2008**, *16*, 10356–10362. (d) Chiang, L.; Abdullah, M. A. *Process Biochemistry* **2007**, *42*, 757–763.

29. Addition compounds between phenols and ammonia. IV. Ammoniations of naphthols, diphenols, hydroxybenzoic acids, hydroxyanthraquinones and o-nitrophenols; heats of ammoniation. *Helvetica Chimica Acta* **1928**, *11,* 926-944.

30. (a) Anthraquinones from Natural and Transformed Roots of *Plocama pendula*. *Chemistry & Biodiversity* **2009**, *6*, 182-192. (b) New Anthracene Derivatives from *Coussarea macrophylla*. *Journal of Natural Products* **2003**, *66*(7), 905-909.

31. (a) Coloring matters of Australian plants. IX. Anthraquinones from *Morinda species*. *Australian Journal of Chemistry* **1962**, *15*, 332-335. (b) Antimicrobial anthraquinones from Morinda angustifolia. *Fitoterapia* **2008**, *79*(7), 501-504.

32. (a) Anthraquinones from *Ophiorrhiza pumila* tieesue and cell cultures. *Phytochemistry* **1998**, *48*(1), 107-111. (b) Anthraquinone and anthrone series. XVIII. A synthesis of lucidin. *Journal of Scientific & Industrial Research* **1955**, *14*B, 87-92.

33. (a) Anthraquinones from *Isoplexis isabelliana* cell suspension cultures. *Phytochemistry* **1999**, *52*(7), 1283-1286. (b) New pyranonaphthoquinone and pyranonaphthohydroquinone from the roots of *Pentas longiflora*. *Journal of Natural Products* **2002**, *65*(9), 1377-1379.

34. (a) Inhibitory effect of anthraquinones isolated from the Noni (*Morinda citrifolia*) root on animal A-, B- and Y-families of DNA polymerases and human cancer cell proliferation. *Food Chemistry* **2010**, *118*(3), 725–730. (b) Anthraquinones with antibacterial activities from *Crucianella maritima* L. growing in Egypt. *Natural Product Sciences* **2004**, *10*(2), 63-68.

35. Anthraquinones from Natural and Transformed Roots of *Plocama pendula. Chem. Biodivers.* **2009**, *6*, 182–192.

36. (a) Thallium in organic synthesis. 61. Intramolecular capture of radical cations from thallium (III) trifluoroacetate oxidation of arylalkanoic acids and arylalkanols. New routes to oxygen heterocycles. *J. Am. Chem. Soc.*, **1981**, *103*(23), 6856–6863. (b) Chestnut (*Castanea crenata*) inner shell extract inhibits development of hepatic steatosis in C57BL/6 mice fed a high-fat diet. *Food Chemistry* 2010, 121, 437–442. (c) Synthesis of a New Spirolactone: 7,10-Dimethoxy-1-oxaspiro[4,5]deca-6,9-diene-2,8-dione. *International Journal of Chemistry* **2012**, *4*(1), 2-6. (d) Pyrolysis-gas chromatography-mass spectrometry of isolated, synthetic and degraded lignins. *Org. Geochem*. 1984, *6*, 417-422.

37. (a) Two new phenylpropanoids and one propanoate from Morinda citrifolia. *Journal of Asian Natural Products Research* **2011**, *13*(3), 238-241. (b) Enantioselective Syntheses of Isoaltholactone, 3-*epi*-Altholactone, and 5-Hydroxygoniothalamin. *Org. Lett.* 2000, *2*(19), 2983-2992. (c) The queen recognition pheromone of solenopsis invicta preparation of (*E*)-6-(1-phenyl)-2H-pyran-2-one. Tetrahedron Letters **1983**, *24*(18), 1889-1892.

38. (a) Evaluation of the Potential Hypoglycemic and Beta-Cell Protective Constituents Isolated from *Corni Fructus* To Tackle Insulin-Dependent Diabetes Mellitus. *J. Agric. Food Chem*. **2011**, 59, 7743–7751. (b) 4-Hydroxy-3-Methoxybenzoic Acid Methyl Ester: A Curcumin Derivative Targets Akt/NFKB Cell Survival Signaling Pathway: Potential for Prostate Cancer Management. *Neoplasia*. **2003**, *5*(3), 255 – 266. (c) Synthesis, spectral and electrochemical behaviour of α-diimine complexes of platinum (II) and palladium (II) with 3,4-dihydroxybenzoic acid. *Polyhedron* **1994**, *13*(2), *291-299*. (d) Esters of 3,4-dihydroxybenzoic acid, highly effective inhibitors of the *sn*glycerol-3-phosphate oxidase of *Trypanosoma brucei brucei. Molecular and Biochemical Parasitology* **1986**, *21*, 55-63.

39. In Vitro and in Vivo Metabolism of Verproside in Rats. *Molecules* **2012**, *17*, 11990-12002.

40. (a) Hepato-protective effects of loganin, iridoid glycoside from *Corni Fructus*, against hyperglycemia-activated signaling pathway in liver of type 2 diabetic db/db mice. *Toxicology* **2011**, *290*, 14– 21. (b) Novel Trisaccharide Fatty Acid Ester Identified from the Fruits of *Morinda citrifolia* (Noni). *J. Agric. Food Chem.* **1999**, *47,* 4880-4882. (c) The structure of loganin. *Tetrahedron Letters*. **1961**, *2*(12), 394-397.

41. Spectral Assignments and Reference Data. *Magn. Reson. Chem.* **2003**, *41*, 636–638.

42. (a) Triterpenoid, flavonoids and sterols from Lagenaria siceraria fruits. *Der Pharmacia Lettre*, **2010**, *2*(1), 307-317. (b) Isolation and Tyrosinase Inhibitory Effects of Polyphenols from the Leaves of Persimmon, Diospyros kaki. *J. Agric. Food Chem*. **2011**, *59*, 6011–6017.

43. (a) Novel Antioxidative Metabolites in Rat Liver with Ingested Sesamin. *J. Agric. Food Chem.* **2003,** *51,* 1666-1670. (b) Lignans of *Forsythia intermedia*. *Phytochemistry* **1990**, *29*(6), 1971-1980. (c) Lipoxygenase Inhibitory Constituents of the Fruits of Noni (*Morinda citrifolia*) Collected in Tahiti. *J. Nat. Prod.* **2007,** *70*(5), 859-862.

44. Chemical Constituents of *Morinda citrifolia* Fruits Inhibit Copper-Induced Low-Density Lipoprotein Oxidation. *J. Agric. Food Chem.* **2004**, *52,* 5843-5848.

45. (a) Chemical Constituents from the Aerial Parts of *Artemisia minor*. *J. Nat. Prod.* **2009,** *72,* 1198–1201. (b) Cleomiscosin D, a coumarino-lignan from seeds of *Cleome viscose*. *Phytochemistry,* **1988**, *27*(2), 636-638. (c) A new 4 ,7-epoxy-8,3 -oxyneolignan from the acetone extract of *Juniperus brevifolia* leaves. *Phytochemistry Letters* **2010**, *3*, 126–128.

46. (a) Phellinsin A, a Novel Chitin Synthases Inhibitor Produced by *Phellinus sp*. PL3. *J. Antibio*. **2000**, *53*(9), 903-911. (b) Biotransformation of caffeic acid by *Momordica charantia* peroxidase. *Can. J. Chem*. **2008**, *86*, 821–830.

47. Spectrometric identification of organic compounds (7th edition), State University of New York, USA, **2005**, pp, 171-172.

48. Moss, G. P. Nomenclature of lignans and neolignans. *Pure Appl. Chem.* **2000**, *72*(8), 1493–1523.

49. Huang, S.; Czech, M. P. The GLUT4 glucose transporter. *Cell Metab*. **2007**, *5*, 237–252.

50. (a) Ye, J. M.; Ruderman, N. B.; and Kraegen, E. W. AMP-activated protein kinase and malonyl-CoA: Targets for treating insulin resistance? *Drug Disc. Today: Ther. Strateg.* **2005**, *2*, 157–163. (b) Iglesias, M.A., Ye, J.M., Frangioudakis, G., Saha, A.K., Tomas, E., Ruderman, N.B., Cooney, G.J., and Kraegen, E.W. AICAR administration causes an apparent enhancement of muscle and liver insulin action in insulin-resistant high-fat-fed rats. *Diabetes* **2002**, *51*, 2886–2894. (c) Musi, N. AMP-activated protein kinase and type 2 diabetes. *Curr. Med. Chem*. **2006**, *13*, 583–589.

51. (a) Lee, Y. S.; Kim, W. S.; Kim, K. H.; Yoon, M. J.; Cho, H. J.; Shen, Y.; Ye, J. M.; Lee, C. H.; Oh, W. K.; Kim, C. T.; Hohnen-Behrens, H.; Gosby, A.; Kraegen, A. W.; James, D. E.; Kim, J. B. Berberine, a natural plant product, activates AMP-activated protein kinase with beneficial metabolic effects in diabetic and insulin-resistant states. *Diabetes* **2006**, 55, 2256–2264. (b) Zhou, G.; Myers, R.; Li, Y.; Chen, Y.; Shen, X.; Fenyk-Melody, J.; Wu, M.; Ventre, J.; Doebber, T.; Fujii, N. et al. Role of AMP-activated protein kinase in mechanism of metformin action. *J. Clin. Invest.* **2001**, *108*, 1167–1174.

ACKNOWLEDGEMENTS

Foremost, I would like to express my sincerest gratitude to my supervisor, Prof. Oh Won-Keun, who first brought me into the world of research and with whom I began to learn about bioassay guided-isolation and structural elucidation of natural products. His encouragement, enthusiasm and perpetual demand for excellence, both scientifically and professionally, have been the mainstay of my inspiration throughout my work and stay in Korea. It is a great privilege for me, and I believe, for all of those who have ever had an opportunity to work under his guidance. I cannot figure out appropriate words to express how thankful and admirable I am to my great mentor.

In completing the course I have also been particularly impressive with the boundless helps of our lab members, Trong-Tuan Dao, Ja-Yeon Kim, Hu-Won Kang, Thi Ngoc Anh Nguyen, Thi Van Thu Le, Thanh-Tung Bui, Thai-Trung Dang, Tien-Lam Tran, Tuan-Phong Do, Mohammed Narsi Uddin, and Govinda Sharma with whom I have shared the hardship, daunting difficulties and excitements during the working time. I am thankful to them for their excellent assistance and significant contribution.

I wish to express my sincere gratitude to all professors at College of Pharmacy, Chosun University for their invaluable mentoring, support and emotional encouragement during my graduate training. I also thank to all my Korean friends who have shared and help me a lot in solving my difficulties during the time I stay in Korea.

Finally, my work would not have been possible without the unfailing support of my family and especially my wife, Pham Thi Thanh Tuyen. I would like to give this great achievement to my mother and express my special thanks to her for her constant encouragement. I wanna give special thanks and express my permanent love to my wife for her undiminished enthusiasm, patience of wait, and a constant love which have sustained my endeavor to complete my work.

Korea, Jan 10th, 2013